Final Report

Bicyclist Longitudinal Motion Modeling

Hesham Rakha
Virginia Tech Transportation Institute
Charles E. Via, Jr. Department of Civil and Environmental Engineering
Virginia Polytechnic Institute and State University
Phone: (540) 231-1505; Email: hrakha@vt.edu

Karim Fadhloun
Virginia Tech Transportation Institute
Phone: (540) 231-1500; Email: karim198@vt.edu

Mansoureh Jeihani
Department of Transportation and Urban Infrastructure Studies,
Morgan State University
Phone: (443) 885-1873; Email: mansoureh.jeihani@morgan.edu

Alireza Ansariyar
Email: alans2@morgan.edu

Eazaz Vaziri
Email: eazaz.sadeghvaziri@morgan.edu

Anam Ardeshiri
Email: anam.ardeshiri@morgan.edu
Department of Transportation and Urban Infrastructure Studies,
Morgan State University

Date
December 15, 2022

Prepared for the Urban Mobility & Equity Center, Morgan State University, CBEIS 327, 1700 E Coldspring Ln, Baltimore, MD 21251

ACKNOWLEDGMENT

This research was supported by the Urban Mobility & Equity Center at Morgan State University and the University Transportation Center(s) Program of the U.S. Department of Transportation.

Disclaimer

The contents of this report reflect the views of the authors, who are responsible for the facts and the accuracy of the information presented herein. This document is disseminated under the sponsorship of the U.S. Department of Transportation's University Transportation Centers Program, in the interest of information exchange. The U.S. Government assumes no liability for the contents or use thereof.

1. Report No. UMEC-035	2. Government Accession No.	3. Recipient's Catalog No.
4. Title and Subtitle Bicyclist Longitudinal Motion Modeling		**5. Report Date** November 2022 **6. Performing Organization Code**
7. Author(s) Karim Fadhloun (VT) https://orcid.org/0000-0002-0442-3727 Hesham Rakha (VT) https://orcid.org/0000-0002-5845-2929 Mansoureh Jeihani (MSU) https://orcid.org/0000-0002-5845-2929 Alireza Ansariyar (MSU) https://orcid.org/0000-0002-5704-6347 Eazaz Vaziri (MSU) https://orcid.org/0000-0003-1002-237X Anam Ardeshiri (MSU) https://orcid.org/0000-0002-2497-3443		**8. Performing Organization Report No.**
9. Performing Organization Name and Address Virginia Tech Transportation Institute 3500 Transportation Research Road Blacksburg, VA 24060		**10. Work Unit No.** **11. Contract or Grant No.** 69A43551747123
12. Sponsoring Agency Name and Address US Department of Transportation Office of the Secretary-Research UTC Program, RDT-30 1200 New Jersey Ave., SE Washington, DC 20590		**13. Type of Report and Period Covered** Final January 2021 - November 2022 **14. Sponsoring Agency Code**

15. Supplementary Notes

16. Abstract

Bike is a promising, human-powered and emission-free transportation mode that is being increasingly advocated as a sustainable mode of transportation due to its significant positive impacts on congestion and the environment. Cities in the United States have experienced a rapid increase in bicycle ridership over the past decade. However, despite the growing popularity of bicycles for short-distance commuting and even for mid-distance recreational trips, researchers have generally ignored the investigation of bicycle traffic flow dynamics. Due to the shared space and frequent interactions among heterogeneous road users, bicycle flow dynamics should be evaluated to determine the tendency of lateral dispersion and its effects on traffic efficiency and safety. Therefore, this research effort proposes to model bicyclist longitudinal motion while accounting for bicycle interactions using vehicular traffic flow techniques. From the comparison of different states of motion for these two transport modes, we assumed there is no major differences between vehicular and bicyclist traffic characteristics. The study adapts aspects of the Fadhloun-Rakha car-following model previously developed by the research team to make it representative of bicycle traffic flow dynamics. Initially, two naturalistic cycling datasets obtained from similar ring-road experiments are used in the re-parameterization process of the Fadhloun-Rakha model to ensure the development of a good descriptor for bicycle acceleration and deceleration behavior. Using German and Chinese experimental data, the model performance is assessed by quantifying its ability to generate trajectories that are highly consistent with empirically observed behavior and comparing it to that of other models that were specifically designed to simulate bicycle longitudinal motion dynamics. Next, the research team recruited 33 participants to operate a bike simulator and a car simulator in order to acquire data to validate the proposed model under realistic traffic conditions. Six scenarios that were categorized based on the initial position of the bike and car were developed. Using the collected data to validate both the original Fadhloun-Rakha car-following model as well as the variant developed for modeling bicycle longitudinal motion, both model variants are demonstrated to be good descriptors for speed, acceleration and deceleration behaviors by analyzing their goodness of fit to the empirical behavior using the Root Mean Squared Error as a performance metric.

17. Key Words: Longitudinal motion, Bicyclists, Bicycle traffic flow dynamics, Bike Simulator (BS.), Traffic efficiency and safety	18. Distribution Statement No restrictions.		
19. Security Classif. (of this report): Unclassified	**20. Security Classif. (of this page)** Unclassified	**21. No. of Pages** 73	**22. Price**

TABLE OF CONTENTS

LIST OF TABLES

LIST OF FIGURES

ABSTRACT

Bike is a promising, human-powered and emission-free transportation mode that is being increasingly advocated as a sustainable mode of transportation due to its significant positive impacts on congestion and the environment. Cities in the United States have experienced a rapid increase in bicycle ridership over the past decade. However, despite the growing popularity of bicycles for short-distance commuting and even for mid-distance recreational trips, researchers have generally ignored the investigation of bicycle traffic flow dynamics. Due to the shared space and frequent interactions among heterogeneous road users, bicycle flow dynamics should be evaluated to determine the tendency of lateral dispersion and its effects on traffic efficiency and safety. Therefore, this research effort proposes to model bicyclist longitudinal motion while accounting for bicycle interactions using vehicular traffic flow techniques. From the comparison of different states of motion for these two transport modes, we assumed there is no major differences between vehicular and bicyclist traffic characteristics. The study adapts aspects of the Fadhloun-Rakha car-following model previously developed by the research team to make it representative of bicycle traffic flow dynamics. Initially, two naturalistic cycling datasets obtained from similar ring-road experiments are used in the re-parameterization process of the Fadhloun-Rakha model to ensure the development of a good descriptor for bicycle acceleration and deceleration behavior. Using German and Chinese experimental data, the model performance is assessed by quantifying its ability to generate trajectories that are highly consistent with empirically observed behavior and comparing it to that of other models that were specifically designed to simulate bicycle longitudinal motion dynamics. Next, the research team recruited 33 participants to operate a bike simulator and a car simulator in order to acquire data to validate the proposed model under realistic traffic conditions. Six scenarios that were categorized based on the initial position of the bike and car were developed. Using the collected data to validate both the original Fadhloun-Rakha car-following model as well as the variant developed for modeling bicycle longitudinal motion, both model variants are demonstrated to be good descriptors for speed, acceleration and deceleration behaviors by analyzing their goodness of fit to the empirical behavior using the Root Mean Squared Error as a performance metric.

Key words: Longitudinal motion, Bicyclists, Bicycle traffic flow dynamics, Bike Simulator (BS.), Traffic efficiency and safety

1. INTRODUCTION

The last decade has seen cycling emerge as a sustainable mode of transportation with growing popularity among both users and governments. As cities have invested in non-motorized transportation infrastructure, bicycling has become a meaningful alternative mode of transportation for those commuting to activities such as school, work, shopping, and recreation (Pucher and Buehler, 2016). Bikes improve other modes of transportation by reducing traffic congestion, emissions, pollution, and delays in central downtown areas. They also connect more people to public transportation and provide a low-cost mode of transportation that requires minimal federal investment. For these reasons, the popularity of bike commuting, bike-sharing systems, and electric bikes in general has increased the desirability of safe and efficient bicycle infrastructure like protected bike lanes. According to one questionnaire exploring bicycle usage patterns in the United States, 47% of Americans say they would be more likely to ride a bike if pathways were physically separated from motor vehicles, 52.4% of Americans worry about being hit by a motor vehicle when riding a bicycle, and only 0.6% percent of American employees include biking in their commute to work (People for bikes participation study, 2016).

Despite the urgent need to develop models and planning techniques for bicycle traffic operation, traffic researchers have neglected the traffic flow dynamics of bicycles relative to vehicular traffic flow. The observed gap between vehicular and bicycle traffic flow dynamics models can be justified by the scarcity of naturalistic and experimental cycling data. Using two new experimental cycling datasets in this study is one of the important, heuristically-added values of this research.

Our research aims to provide a comprehensive investigation of the traffic flow dynamics of bicycles. The research develops a model that captures the characteristics of the longitudinal motion of bicyclists while accounting for their interactions and the variability of their behavior. It is worth mentioning that this study hypothesizes that there are no significant similarities between car-following behavior and bicycle-following behavior and therefore applies vehicular traffic flow modeling techniques to effectively simulate bicyclists' behavior. The assumption is partly justified by the fact that existing cycling data comes from single-file ring-road experiments in which overtaking was not allowed. The team thus redesigned the existing car-following model to make it representative of a bike/bicyclist system rather than a vehicle/driver system. In that regard, two cycling datasets from German and Chinese experiments are used to re-parametrize the Fadhloun-Rakha (FR) car-following model [7] to make it representative of bicyclist acceleration/deceleration behaviour. The FR car-following model was chosen for its ability to model the human-in-the-loop explicitly and separately from vehicle dynamics. That aspect is anticipated to increase the model's chances of capturing bicyclist variability, which is more influential than driver variability in car-following theory. The model's performance is then assessed by quantifying its ability to generate trajectories that are highly consistent with empirically observed behavior and comparing it to that of other models that were specifically designed to simulate bicycle longitudinal motion dynamics. Finally, in order to validate the proposed model, the research team recruited participants to operate a bike-simulator and a car-simulator under realistic traffic conditions and collected the resulting data. The collected simulator data is then used to further investigate and confirm the validity of

the proposed bicycle-following model as well as the original Fadhloun-Rakha car-following model.

1.1. Scope of work

The proposed research aims to provide a comprehensive investigation of the traffic flow dynamics of bicycles. Specifically, the research team developed a model that captures the characteristics of the longitudinal motion of bicyclists while accounting for their interactions and the variability of their behavior. To achieve that, the study starts by hypothesizing that significant similarities exist between car-following behavior and bicycle-following behavior. Based on that assumption, the proposed research applied vehicular traffic flow modeling techniques to simulate bicyclist behavior, thus circumventing the challenges associated with modeling a very complex phenomenon from scratch. In that regard, the team first worked on deriving a formulation for the proposed bike-following model from the newly developed FR car-following model [7]. That was achieved through the re-parameterization of vehicle-related input variables along with the potential integration of necessary new parameters such that the characteristics and fundamentals of the bicycle/bicyclist system are fully captured. The research team then assessed the adequacy of the proposed formulation as a descriptor of bicycle longitudinal motion by estimating its quality of fit using an experimental dataset collected on a circular track in Germany [5]. Thereafter, for validation purposes, the team validated the model using data from a Chinese ring-road bicycle experiment [8]. The performance of the model is assessed by comparing its predictive power against that of models that are specifically designed for bicyclist behavior simulation. Given the controlled environment in which the aforementioned ring-road experiments were conducted, certain important factors that impact bicyclists in real traffic situations were ignored. To address that, the team conducted an experiment in which recruited participants operated a bike simulator and a car simulator under different traffic conditions and scenarios. The final task of this study involved using the collected simulator data to assess the effectiveness of the proposed model as well as the original car-following model in a realistic environment.

1.2. Goal

This research models bicyclist longitudinal motion while accounting for interactions with other vehicles using vehicular traffic flow techniques. There is a need for methods that provide a better understanding of bicyclists' behavior and preferences on currently unavailable and unknown bicycle facilities. Different survey methods have been used to study bicyclists' behavior, experiences, and preferences, all ranging from verbally described facilities to surveys including images and videos (Nazemi et al, 2021). Bicyclist longitudinal motion has not been modeled in previous studies. The main achievement of this research is the modeling of bicyclist longitudinal motion while accounting for bicycle interactions using vehicular traffic flow techniques. The second achievement is revamping an appropriate car-following model previously developed by the research team to make it representative of bicycle traffic flow dynamics. The third achievement is using an accurate, naturalistic dataset to develop a good descriptor for bicycle speed, acceleration, and deceleration behavior. Finally, the last achievement is using the bike simulator to provide a realistic environment for bicyclists (Jiang et al, 2017). The BS determines the bicyclist's behavior

under different scenarios, and the interaction of the car-following model with bicyclists and the proximity of the behavior of car drivers and bicyclists appear through the bike simulator.

2. LITERATURE REVIEW

Our research is multi-faceted, covering "bicyclist's behavior and bike flow dynamics," "bicycle interactions using vehicular traffic flow techniques," "BS applications studies," and "usage of car-following models for bicyclists." These topics are addressed in this section.

2.1. Bicyclist's behavior and bike flow dynamics

(Gavrilidou et al, 2019) defined the cyclist's operational level in terms of decision-making factors, arguing that it consists of two intertwined processes, a mental one and a physical one. They also argued that it consists of two intertwined processes, a mental and a physical process. The mental process refers to path choices made within a route and the physical process refers to the bicycle control dynamics through pedaling and steering. A novel two-layer framework was proposed where each layer captured the tasks of one of the processes within the operational level. A discrete choice theory was proposed to model each layer, and mathematical models were estimated for the two layers using cyclist trajectory data collected at a signalized intersection in Amsterdam, the Netherlands.

Unsafe bicyclist-overtaking behavior based on social or psychological factors was studied by (Goddard, 2020). Their research explored the impact of implicit and explicit attitudes on drivers' behavior in interactions with bicyclists. In a driving simulator, various objective measures of safety (e.g., speed, passing distance, crash occurrence) were collected in an overtaking scenario. Participants' self-reported attitudes about driving and bicyclists were collected via a survey instrument and an online test of subconscious attitudes called an "Implicit Association Test." The results provided potential avenues for infrastructure and education interventions to improve pedestrian and bicyclist safety. One of the best models to determine bicyclist's behavior is cellular automata. A cellular automaton consists of a regular grid of cells, each in one of a finite number of states.

An improved multi-value cellular automata that modeled heterogeneous bicycle traffic flow by taking the higher maximum speed of electric bicycles was developed by (Jin et al, 2015). The study proposed an improved multi-value cellular automata (MCA) model that introduces the maximum speeds of two and three cells(s) for Regular Bicycles (RBS) or Electric Bicycles (EBS). The numerical simulation results and fundamental diagrams for bicycle traffic were analyzed and discussed. Three parameters consisting of the slowdown probability, the percentage of EBS, and the number of bicycle lanes were analyzed in both the deterministic and stochastic cases. The results determined that the proposed model matches the field bicycle data better than previous models. Understanding bicyclist's behaviors on real-world roads has been a pertinent topic in transportation research for some time, but the modeling and simulation of heterogeneous bicycle traffic flow is becoming increasingly important for bicycle path planning, management, and operation.

Investigating bicycle flow dynamics on wide roads by using a wide track model was proposed by (Guo et al, 2019). By studying the weight density of the radial locations of cyclists,

their research argued that bicycle flow rates remain nearly constant across a wide range of densities. This behavior arises from the formation of additional lanes with the increase of global density. The extra lanes prevent the longitudinal density from increasing as quickly as in a single-file bicycle flow. When the density is larger than 0.5 bicycles/m2, the flow rate begins to decrease, and stop-and-go traffic emerges (Guo et al, 2019).

Studies on bicyclist's behaviors at signalized intersections based on real-world data were conducted by (Twaddle, 2017). Behavioral models were calibrated and validated in a microscopic traffic simulation. Video data were collected at four intersections that differed from one another in their geometry and traffic volume. Automated video analysis was used to extract trajectories, which quantify the spatial progression of road users in a subset of the video data. Distortion in the trajectory data resulting from a wide-angle lens was corrected, and the maneuver (right turn, left turn or traveling straight across the intersection) of each bicyclist was identified. The resulting behavioral models were integrated with the microscopic traffic simulation software SUMO to evaluate the overall ability of the models to realistically simulate bicycle traffic. Results indicated that the proposed integrated modeling approach is capable of realistically simulating the flexible behavior of bicyclists at signalized intersections.

As the number of bicyclists in urban areas continues to increase, the need to realistically model the movement and interactions of bicyclists in mixed urban traffic is rapidly gaining importance. In response to this need, (Twaddle et al, 2014) modeled and evaluated bicyclist behavior on "uninfluenced operational and tactical behavior" and "influenced operational and tactical behavior" levels. The ability to model bicyclist behavior on each of these levels was evaluated based on the results of an extensive literature review. The results of the assessment indicated that it is possible to model the majority of bicyclist's behaviors on an "uninfluenced operational and tactical behavior" level. It is worth mentioning that the uninfluenced and influenced tactical behaviors of bicyclists are important for accurate modeling as bicycle behavior is less constrained by road markings and traffic regulations.

Some studies have evaluated complex patterns of bicycling behavior, such as those conducted by (Thigpen et al, 2019) and (Thigpen, 2019). They considered the readiness for bicycling. The added-value of a categorization of bicyclists based on the stages of change feature of the Trans theoretical Model (TTM) was presented and examined how this new categorization can contribute unique insights for practice through novel behavioral information. Spatial statistical techniques were conducted using survey data from a sample of 2398 individuals from three medium-sized Canadian cities were presented. The results suggested that categorizing people as a function of readiness for change allows for populations to be characterized by their likelihood of being beneficially impacted by policies that support bicycling.

Another study was conducted by (Chuang, 2013) that scrutinized how motorized vehicle-related factors, road-related factors, and bicyclist-related factors influenced motorists' decisions about initial passing distances and bicyclists' behaviors after the motorists started to pass. A quasi-naturalistic riding method was used for thirty-four participating bicyclists riding an instrumented bicycle in real traffic.

Another study included 1,380 incidents of left-side passing by motorists. It revealed the main factors influencing motorists' initial passing distance and bicyclists' positions (lateral

distance from the passing motorists), wheel angle, and speed control behaviors while the motorists passed. They also found that bicyclists avoided road surface hazards and reduced initial passing distances that the motorists had chosen (Piatkowski et al, 2017). Furthermore, the presence of behavioral norms while riding a bicycle in mixed-traffic conditions was examined. They studied car and bicycle on-street interactions by asking bicyclists to consider how they would respond when driving a car while encountering a bicyclist behaving in ways that might be perceived as reckless, rude, and/or illegal.

The behavior of bicyclists when they were biking and using instrumental devices such as mobiles, MP3 players etc. was studied by (Nygårdhs et al, 2018). The aims of this study were to explore how cyclists adapt when texting and listening to music in a complex urban environment and whether they compensate sufficiently to maintain safe traffic behavior. Forty-one cyclists participated in a semi-controlled study, using their own bikes and smartphones in real traffic. They were equipped with eye-tracking glasses and traveled two laps, completing a total of 6 km divided into six segments. The results showed that listening to music while cycling did not affect workload, speed, SMS interaction or attention.

This section examined studies evaluating bicyclist path choice behaviors (path planning, management, and operation), bicycle control dynamics, bicyclist overtaking behaviors in different real-world segments such intersections, and the adaptation of cyclist's behaviors when they are not limited to a certain set of behaviors. To the best of the authors' knowledge, simulations bicyclist longitudinal motions along specific segments were not performed in prior studies. This research proposes the bicyclist longitudinal motion while accounting for bicycle interactions using vehicular traffic flow techniques and considers the behavioral and physical aspects of bike motion on different roads.

2.2. Bicycle interactions using vehicular traffic flow techniques

There is a need to better understand bicyclists' interactions with vehicles and to build models and to evaluate multimodal transportation infrastructure with respect to cycling safety, accessibility, and other aspects. This section reviews the previous studies in terms of bicyclists and other road user's interaction under different traffic conditions based on traffic flow techniques.

A framework for modeling the bicyclist's comfort zone and interactions was provided by (Lee et al, 2020). Unlike the driver's comfort zone, little was previously known about that of the cyclist. They modeled the braking and steering maneuvers of cyclists by using obstacle avoidance data. Their results determined that when cyclists avoid obstacles by braking, they kept a constant rate of deceleration; as their speed increased, they started to break earlier, farther from the obstacle, while maintaining a nearly constant time to collision zone. When cyclists avoid obstacles by steering, they maintain a constant distance from the object, independent of speed. Overall, the higher the speed, the more the steering maneuvers were temporally delayed compared to braking maneuvers.

Another way to address cyclist's interactions with their surrounding environment is to construct bike-friendly environments. Bike-friendly environments can be evaluated in such a way whether associations between environmental characteristics and cycling are context-specific. Furthermore, bike-friendly environments may improve natural environment characteristics'

contribution to cycling duration. The viability of constructing bike-friendly environments to increase the use of bicycles as a significant transportation mode was investigated by (Joo and Oh, 2013). Evaluating the performance of bicycling environments remains a significant technical challenge for researchers, and this study proposed a novel method of doing so that evaluates bicycle performance in terms of safety and mobility. An Instrumented Probe Bicycle (IPB) equipped with a Global Positioning Systems (GPS) receiver, accelerometer, and gyro sensor was used to develop the proposed method. The IPB provides useful bicycle maneuvering data for identifying longitudinal, lateral, and vertical maneuverings of the bicycle, which are affected by environmental factors such as heavy vehicle volume, surface conditions, grade, crossings, humps, and curbs.

Another way to monitor the interaction of bicyclists and motorized vehicles was explored by utilizing video data (Twaddle et al, 2014) collected at three busy urban intersections in Munich, Germany. In order to analyze the interaction of bicyclists and motorized vehicles through traffic flow techniques, large volumes of motor vehicles, bicycles, and pedestrians at intersections were tracked. The trajectories of cars, bicycles, or pedestrians were monitored. Then, their interaction was classified based on their dynamic characteristics. A classified structure for the maneuvers of different road users (as important interactions between cyclists and other vehicles) was also presented.

(Luo et al, 2013) proposed a cellular automata model to simulate heterogeneous traffic on urban roads. In the proposed model, the researchers adopted a novel occupancy rule to capture the complex interactions between cars and bicycles and consider the variable lateral distances of mixed vehicular traffic. Researchers devised fundamental diagrams under different bicycle densities before discussing the bicycles' spilling behavior. They then modeled the interference transformation from friction state to block state to reflect the interference of a bicycle on a car. Their results indicated that the constant and fixed occupancy rule adopted in the study might lead to overestimation of car flux in heterogeneous traffic flows with different bicycle densities.

The relevant factors impacting lateral spacing between bicycles and vehicles in mixed urban traffic (passing distance, PD) and their resulting effect on a bicyclists' comfort were examined based on a study of six sites performed by (Apasnore et al, 2017). The average distance of bicycles from the curb and parked vehicles, motor vehicle speed, lane width, and bicycle position from adjacent curb edge line, whiles inversely correlated to ambient traffic density and bicycle speed and Ambient Traffic Density (ATD), were found to be the most important factors to a Bicyclists' Comfort Perception (BCP).

The interaction of bicyclists and motor vehicle drivers was studied by (Klieger and Savage, 2020) and (Silva et al, 2019). They evaluated how well unprotected bicycle lanes function as dedicated travel lanes for bicyclists. Two types of bicycle lanes were included in this study, including on-street bicycle lanes demarcated with painted lines on the vehicular roadway and bicycle lanes at-grade with, and immediately adjacent to, the pedestrian sidewalk. More specifically, the research focused on how people behave and interact on street segments with these facilities in place.

2.3. BS Applications Studies

Various types of vehicle simulators – such as automobile, bicycle, flight, tank and ship simulators – have been developed and widely used for testing the design evaluation of environments, training for driving, entertainment, and so on (Guiso, 1995). Even though many studies have been conducted regarding various driving simulators, few are related to two-wheeled, human-powered simulators like a BS. A BS consists of a stationary bike, a monitor, analyzing software, and a VR-Design platform. It visualizes biking behavior on different roads in a realistic environment. A BS also includes of a frame, clamp to hold the bicycle securely, a roller that presses up against the rear wheel, and a mechanism that provides resistance when the pedals are turned (Curtis, 2014).

For bicycle dynamics calculation and real-time simulation, it is necessary to identify the control inputs from both the rider and the virtual environment (Shin and Lee, 2002). The virtual environments, such as the ground configuration and condition, can be generated and provided by a visual system. The steering, pedaling and braking torques can be measured directly by using torque sensors attached to the corresponding components. Given the significant application of BSs in previously published studies and the utility of applying simulators as an alternative to real bicycles, this study was designed to synthesize the lessons learned from existing studies that quantified the application of BSs. We implemented a scoping review to identify, screen, and review the existing literature on BS applications. The results of which we hope can assist researchers, policy makers, and practitioners with the selection of appropriate evaluation methods based on their objectives. This study can be a starting point for other researchers to explore more frequent objectives when applying BSs and present new studies with additional innovations.

After reviewing the literature, five approaches were identified: application of a BS to suggest a mathematical dynamic model for bicycle stability, incorporation of a BS with virtual reality (VR) technology, application of a BS in safety promotion studies, installing special sensors on the BS to measure specific datasets, and the application of a BS in medicine, psychology, sports management, and other branches of science.

2.4. Applications of BS in Modeling Bicycle Stability

A simulator is designed to create a virtual model of a real-life situation for the purpose of instruction or experiment in a laboratory environment. Studies that generate different prototypes for a bicycle product using a systematic concept generation method, describe the use of an instrumented bicycle and its computational model, and provide mathematical models for bicycle stability are reviewed in this section. Methods for data collection, analysis, modeling, and simulation of performance parameters by BSs were developed or evaluated are also discussed. BS is and efficient way to scrutinize the interaction of bicyclists with other road users in a real-world simulation environment. Hereupon, this section reviews the interaction of bike and motorized vehicles in terms of bike stability, and lateral and longitudinal movements. The degree-of-freedom (DOF) of BS affects its stability. The higher the DOF of the BS, the more it can obtain acceptable

results regarding the participant's behavior during interaction with motor vehicles. Hereupon, this section reviews previous studies in terms of conceptual designing of the BSs.

Scholars e.g., (Abagnale et al, 2016), (Arunachalam and Rajesh, 2014), (Beckmann et al, 2015), (Dahmen et al, 2011), (Escalona et al, 2018), and (Englund et al, 2016) proposed a series of new dynamic models and mathematical equations that use a BS for bike stability. A new dynamic model consisting of an electrical motor in the central position that, by means of a bevel gear, transmits the torque to the central hub to investigate the tracking errors was proposed by (Abagnale et al,2016). (Arunachalam & Rajesh, 2014) suggested a mathematical equation for investigating the stability of foldable bicycles. A method of mixed reality extended by modern industrial technologies to allow natural interaction with virtual prototypes of the BSs was proposed by (Beckmann-Dobrev et al, 2015). A mathematical model was implemented by (("<CAS_Readiness_of_the_road_network_April_2017.pdf>,")[1]Dahmen et al, 2011) for simulating rides on real courses, providing similar quality measures when comparing field and simulator measurements. (Escalona et al, 2018) proposed the mathematical equations to generate a simple computer graphics animation of bicycle riding. In another study, a mathematical model was suggested by (He et al (a), 2005) to investigate the bicyclist's stability and vibration behavior. A new dynamic model was suggested by (He et al (b), 2005) for BSs consisting of motion generation, and force reaction, dynamics simulation, and visual/audio systems. In addition to previous studies, a new rehabilitation training system (consisting of a dynamic model) was developed by (Jeong et al, 2005) to improve equilibrium sense control by combining virtual reality technology with a fixed exercise bicycle. A new dynamic model to validate the integrated power-assisted BS was proposed by (Kakutani & Furusho, 2004). They suggested an integrated prototype that was able to investigate power-assisted bicycle. (Kim et al, 2017) developed a heuristic dynamic model to evaluate the user experience of virtual systems. They modeled the user experience of virtual bikes by VR technology. In another research project, (Kooijman et al, 2008) suggested a model study to consider many physical aspects of a real bicycle such as the flexibility of the frame and wheels, play in the bearings, and precise tire characteristics. One of the first proposed BSs was introduced by (Kwon et al, 2001) KAIST Interactive BS (Korean BS) consists of a bicycle, a Stewart platform, magnetorheological handle, pedal, resistance system to generate motion feelings, real-time visual simulator, and a projection system, sub-controllers, and an integrating control network. A dynamic model that couples the bicycle roll and steer in a realistic manner was proposed by (Lee et al, 2017) and it also allowed studying the effect of balance on the rider's higher-level cognitive decisions. (Schwab & Recuero, 2013) described and used a BS prototype that can help understand the synergy among the parts intervening in the active stabilization process in cycling. An affordable BS prototype with proper longitudinal and lateral stability (Snapika et al, 2018) that simulates the form of indoor cycling was presented. To increase the efficiency of BSs, new methods were proposed by the following researchers. In all reviewed methods, a particular structure or architecture is presented that can increase the efficiency of the BS. This issue is clearly discussed in studies such as (Englund et al, 2016): (Ginters et al, 2014): (Jamin et al, 2019). (Shin and Lee, 2002) proposed the control inputs from the rider as well as the

virtual environments for the calculation of bicycle dynamics in a bicycle simulator. The impression of geometry and road surface characteristics – such as radius of curvature, road adhesion, and unevenness of road profile – was simulated by (Shoman & Imine, 2020), based on which a dynamic model was developed. Finally, a 6-degrees-of-freedom (DOF) platform that is controlled by linear actuators and a microcontroller was proposed by (Yap et al, 2016), who successfully formulated the kinematics equation. The aforementioned studies propose different physical concepts of the BS. In each of these studies, the degree of freedom and dynamic features of a BS have been changed to suggest the new structure for the BS.

After reviewing the aforementioned studies, we conclude that a BS can be used to model the physical motions of the human body. Therefore, spatial geometric equations have been defined to model the stability of bicyclists. To sum up, the first application of the BS is limited to the process of presenting such models or mathematical equations.

2.5. Incorporation of BS with Virtual Reality (VR) Technology

Virtual reality (VR) refers to a computer-generated simulation in which a person can interact with an artificial three-dimensional environment using electronic devices with a screen or gloves fitted with sensors (Mitchell, 2020). VR can be a 360-degree immersive experience, where computer-generated graphics help create things as close to reality as possible. Many researchers have attempted to integrate BSs with the VR technology to gain more realistic data. VR's most immediately recognizable component is the Head-mounted Display (HMD), which can be applied to simulate the performance of bike riders in different situations.

VR technology was used by (Bogacz et al, 2020) to contribute to a better understanding of the implications of the choice of the experimental setup by comparing the cycling behavior between two groups of participants. The first group controlled the maneuvers using a keyboard and the other group rode an instrumented bicycle. Some studies examined unique applications of a BS&VRT (Bottone et al, 2015): (Carraro et al, 1998): (Kikuchi, 2011): (Kakutani, 2004): (Katsigiannis et al, 2019): (Al-Kefagy, 2019): (Padmini et al, 2019): (Schulzyk et al, 2009). The two degree of freedom (2-DOF) mechanism on a dynamic platform driven by changing the cable length and its application to VR for bicyclists in virtual environments was presented by (Chen et al, 2007) Their prototype could interact between the bicycle and VR system and integrate exercise with entertainment. (Dahmen & Saupe, 2009) concentrated on the simulation of endurance sports with an emphasis on competitive cycling with BS&VRT. The goal of Gao et al.'s work was to provide a simulator system that enables race bikers to improve their performance in training (Gao et al, 2005). In another study, (Hernández–Melgarejo et al, 2020) integrated physical VR and control behavior systems to compose a virtual bicycle simulator. They designed and implemented a VR bicycle system based on a functional-based mechatronic design approach. An immersive bicycle simulation platform and VR technology for several applications in the areas of biomechanics, sports, traffic education, road safety, and entertainment was proposed by (Herpers et al, 2009) Their prototype consists of special immersive visualization systems to simulate biking

in a real-world environment. All the aforementioned studies were tested in a laboratory environment.

The following studies are instances of new integrated systems that have been suggested to promote the performance of BS&VRT. Studies like (Horne et al, 2018): (Jia et al, 2006) proposed new techniques to improve the performance of a BS&VRT. A calibration procedure was proposed by Horne et al. that uses general equations and techniques to calibrate speed measurements and improve the consistency of experimental data. (Jia et al, 2006) evaluated the role of the human-computer interaction system as the key technology of a virtual bicycle simulator.

Researchers, e.g., (Keler et al, 2020) and (Nazemi et al, 2018) used BS&VRT to evaluate novel traffic control strategies on existing transport infrastructure depicted in VR environments. In addition, (Nazemi et al, 2018) used BS&VRT to evaluate the effects of environmental properties and road infrastructure design on cyclists' perceived safety. This study investigated the combination of immersive VR and an instrumented cycling simulator for in-depth behavioral studies of cyclists. Researchers, e.g., (Ouden, 2011) used a BS for physical rehabilitation purposes. BS&VRT has been used to train children and help them get used to being on a bicycle. Children's cycling has been studied less than adult cycling. Therefore, additional studies should be conducted because children have been considered as one of the groups for whom education can positively affect their behavior in adulthood.

An example of a well-done study regarding the bicyclists' behavior on different pavements was performed by (Rakhmatov et al, 2018) They designed a data-collection bike that captures the vibrations induced at the handlebar and the cycling velocity for different tire pressures. The level of tire pressure, the weight of bicyclists, and the role of pavement in the reaction of bicyclists was investigated. By studying the behavior of cyclists, (Schramka et al, 2017) investigated how different street design configurations and traffic levels impact perceived cycling stress levels, cognitive reactions, and mobility behavior. The role of environmental elements to investigate how cyclists adapt their behavior (e.g., speed, safety, gaps, steering, etc.) was evaluated by (Shoman & Imine, 2021) They adjusted their riding practices as they interacted with other road users and anticipated risks in hazardous riding situations. In another study, (Ullmann et al, 2020) used the integration of BS&VRT to provide rare qualitative factors (such as stress, perception of time, and attractiveness of the environment). They utilized an audiovisual VR bicycle simulator to allow the user to ride in a virtual urban environment. The aforementioned studies were conducted with adult cyclists. Finally, the exercise and entertainment purposes of a BS&VRT were studied by (Tang et al, 2018) and (Yap et al, 2018) who investigated the entertainment role of BSs.

Overall, the number of studies regarding incorporating VR and BSs has risen in recent decades, reflecting increasing interest by researchers. Incorporating VR and BS provides a fairly realistic environment for the participants of the research, and they can efficiently adapt to the simulated environment when riding a BS. Riding a BS which is integrated with VR technology may improve the BS participant's understanding regarding the simulated environment and it effects positively on the bicyclist's behavior in interaction time intervals with other motorized vehicles.

2.6. Application of BS in Safety Promotion Studies

The popularity of biking has drawn researchers' attention to finding methods for protecting bicyclists on public roads. Bicyclists (and pedestrians) are frequently classified as "vulnerable road users." The biking community, however, is not comfortable regarding the safety of these two groups (Cynecki, 2012). Bicyclists are susceptible to serious injuries, and special attention should be paid to the safety of this group (Ragland, 2012). The elevated risk of injury to bicyclists when they encounter motor vehicles makes it important to identify and implement strategies to protect cyclists on the road. There is some evidence that bicycling has increased in recent years (Jacobsen et al, 2009). However, even with widespread encouragement, many will be deterred from biking if they do not feel safe.

When a crash occurs between a vehicle and a bike, it is the cyclist who is most likely to be injured. By law, bicycles on the roadway are vehicles with the same rights and responsibilities as motorized vehicles. Over 1,000 people were killed in bicycle crashes in 2018 and over 300,000 ended up in the emergency room. In the U.S. in 2017, over eight times more men were killed in bicycle crashes than women (Grover, 2020). One notable application of BSs is in safety promotion studies. Researchers have studied the interaction of bicycles with other vehicle types, plans to increase bicyclist's safety, and the most hazardous situations for bicyclists. Different cyclist's behaviors and cyclist-enhanced safety schemes can be evaluated when they interact with the road and other vehicle types. "The role of bicyclists under different conditions" and "the role of the road and its characteristics" are two critical properties involved in increasing or decreasing cyclist safety.

The following studies investigated the role of the bicyclist in the occurrence of crashes. A novel approach consisting of a unique bicycle simulator equipped with sensors capable of capturing the behavior of bicyclists was suggested by (Englund et al, 2016) to model the visual distraction of bicyclists. (Ghodrat Abadi et al, 2019) suggested a high-fidelity full-scale bicycling simulator that examined the interaction of bicyclists and trucks near Commercial Vehicle Loading Zones (CVLZ) in urban areas. They investigated the influence of engineering treatments on bicyclist performance.

Additionally, a factorial design with three levels of pavement markings (white lane marking, solid green, and dashed green), two levels of signage (no signs and warning signs), and three levels of truck maneuvers (no truck, parked trucked, and exiting truck) was developed by (Kaß et al, 2020) evaluated and investigated cyclists' behavior during dynamically evolving interactions. Furthermore, they measured the dynamic behavior patterns. The research focused on external human-machine interface (eHMI) as a communication interface of automated vehicles.

Researchers such as (Lindström et al, 2019) have evaluated how radar sensors and technologies common in automotive vehicles can be transferred for use on bicycles. A bicycle simulator was used for testing and evaluation. Moreover, high-risk scenarios and requirements were identified, followed by identified design challenges and design activities. To facilitate road safety for children, (Matviienko et al, 2018) explored the use of multimodal warning signals to

increase their awareness and prime action in critical situations. A BS linked to these signals and the results showed that the participants spent significantly more time perceiving visual than auditory cues. A better understanding of bicyclists' perceived safety and their preferences for currently unavailable and/or unknown facilities was studied by (Nazemi, 2020) who used different survey methods ranging from verbal descriptions of facilities to surveys including images and videos. There is evidence that some aspects of cyclist performance when interacting with the road environment can be investigated by using a BS. (O'Hern et al, 2017) concentrated on the cyclist spatial position measures to investigate the bicyclists' interaction. They assessed the validity of the participants' performance using a BS compared to riding on road. In line with former research, (O'Hern et al, 2018) examined how bicycle lane width and perceptual countermeasures can influence cyclist speed and position. Researchers such as (Powell, 2017) concentrated on the injuries caused by bicyclists and motor vehicle crashes. They used a particular BS to provide a virtual environment and reduce crashes by safely investigating the interaction between bicycle riders and traffic, particularly when bicyclists were crossing streets. (Sawitzky et al, 2020) studied the effects of new infrastructural concepts and technologies, such as a head-up display (HUD) for cyclists' potential crash possibilities brought by automated vehicles, and smart, connected traffic, on actual cyclist road safety. Some researchers studied the hazard of biking on sidewalks. (Suzuki, 2013) is a good example, concentrating on a particular BS that is available for analysis of the safety and influence on other transport modes.

Using BSs and VR technology for assessing bicyclists' safety was studied by (Tsuboi et al, 2018). They proposed methods to improve the awareness of bicycle riding safety by experiencing virtual accidents in a virtual space. The study helped the participants learn desirable and safe bicycle riding behavior. The role of bicyclists in injury or fatal crashes was assessed by (Warner et al, 2017). They concentrated on the right-hook crash, which is a crash between a right-turning motor vehicle and an adjacent by-moving bicycle. They evaluated driver behavior in collisions that occur during the latter green phase (the second portion of the green signal phase, after the initial vehicle queue has cleared) at signalized intersections with a bicycle lane and a shared right-turn lane.

Researchers like (Brown et al, 2017) and (Yamaguchi et al, 2018) investigated the role of the road and its characteristics on bicyclists' crashes. Alternative pavement markings were investigated by Brown et al. for bicycle wayfinding and proper bicycle placement at signalized intersections. Yamaguchi et al. proposed an innovative method to detect road hazards using sensors attached to a bicycle. The built-in sensors send the speed and front-wheel angle information to the control unit. The proposed system allows for dangerous situations to be easily and repeatedly created with no danger to the bicyclists.

Overall, in many studies a BS was used to simulate the behavior of bike riders under different environmental conditions and on different road types. As explained in this section, the application of BS in safety-related studies improved the adaptability of bicyclists in interaction time intervals. Furthermore, BS as an efficient instrument can be utilized in safety-related studies

to investigate the bicyclist's lateral and longitudinal movements which is not easy to measure in the real world.

2.7. Installing Various Sensors on the BS to Record Different Characteristics

The studies in this section installed specific sensors on the BS to record characteristics of the participant's body. (Alemeida et al, 2020), (Caro et al, 2015), (Dialynas et al, 2019), (Herpers et al, 2011), and (Rittenbruch et al, 2020) present the most important research conducted in this area. (Alemeida et al, 2020) presented a virtual BS (SimBike) that used non-conventional motor, sensors, sensorimotor devices to provide greater user involvement and comfort. They used special sensors to investigate how the devices in SimBike contributed to the user experience in the virtual simulator, including the level of immersion, realism, and cyber-sickness symptoms. The results suggested improvements to make the simulator more suitable for all types of users, regardless of characteristics such as weight and height. The role of the different sensory information available was determined by (Caro et al, 2015). They concentrated on the mechanisms of perception of the natural speed which affect the adopted speed. Natural speed defines the speed limits of vehicles specified on traffic signs while the adopted speed is defined as the adaptive speed of the driver during interaction with other road users. An experiment was carried out on a BS where three sensory datapoints were separately manipulated: the speed of the image, the resistance to pedaling, and the airflow. Based on this research, "airflow" had no effect. This indicator should be better evaluated by conducting more accurate models. A step-by-step guide (Dialynas et al, 2019) to building a BS was presented at TU Delft University, highlighting the mechanical and mechatronic aspects. They used special sensors in their proposed prototype to effectively simulate a mountain bike placed on top of rollers and later fitted with a haptic steering device. The FIVIS simulator system was constructed by (Herpers et al, 2011). It addressed the visual and acoustic cues as well as vestibular and physiological cues. Sensory feedback from skin, muscles, and joints was integrated within this VR visualization environment, allowing the BS to simulate otherwise dangerous traffic situations in a controlled laboratory environment. They developed a BS that was embedded into an immersive visualization environment, which provided visual cues to peripheral areas of the visual field of the trainee. A physical computing toolkit (Rittenbruch et al, 2020) was presented to support the rapid exploration and co-design of on-bicycle interfaces. Physical plug-and-play interaction modules controlled by an orchestration interface allowed participants to explore different tangible and ambient interaction approaches on a BS. Results revealed how this toolkit can combine with a lightweight bicycle simulator and simulate hazards to evaluate different designs and elicit rich feedback.

2.8. Usage of Car Following Models for Bicyclists

Bicycle traffic operations have become increasingly important, yet have been largely ignored in the traffic flow community until recently. Some researchers hypothesized that there is no qualitative difference between vehicular and bicycle traffic flow dynamics, so the latter can be described by re-parameterized car following models, such as those tested by (Kurtc and Treiber, 2020). They reproduced bicycle experiments on a ring with an Intelligent-Driver model and

compared its fit quality (calibration) and predictive power (validation) with that of a Necessary-Deceleration-Model specifically designed for bike traffic. The results showed that there are similar quality metrics for both models, so the above hypothesis of a qualitative equivalence cannot be rejected. Follow-the-leader is one of the fundamental behaviors in bicycle traffic that describes the longitudinal interactions between two consecutive bicycles. It plays a predominant role in the development of micro-simulation models, safety evaluation, and the capacity estimation of bicycle infrastructure. To understand bicycle-following movements, previous studies have either adopted car-following models or developed specialized bicycle-following models. However, these models were not calibrated and validated in a unified configuration using empirical data derived from realistic cycling behaviors.

(Xue et al, 2020) investigated the single-file dynamics of bicycle traffic from the perspective of car-following models. Using empirical datasets from a series of bicycle experiments, the proposed models were calibrated and validated. The results demonstrated that the assumptions, such as keeping a velocity-based distance from the leader, was a robust behavioral mechanism across all of the empirical datasets. The results could enhance the understanding of the behavioral dynamics of bicycle traffic, meanwhile providing deeper insights into the mechanisms of developing bicycle simulation models.

In order to develop traffic modeling, it is necessary to consider adapting these models to bicycle traffic and thus benefit from all of the research efforts in the field of traffic theory. Since, the objective function of a driver or cyclist is to control the vehicle's speed and direction while maintaining his/her desired speed and avoiding accidents, it is likely that despite the difference in vehicle type, the driving logic and driver behavior will be similar. (Abdelaziz and Gang, 2014) presented three aspects of traffic vehicle science adapted to bicycle traffic: car-following models, the fundamental relationships of traffic flow, and the action point model. The results obtained using car-following models were compared to empirical data collected with global positioning system devices installed on a pair of cyclists in a following situation with no opportunity to overtake. The fundamental relationships were examined using data collected by video at a fixed location at a bike facility. The results indicated that car-following models, fundamental relationships, and the action point model all have the potential to reproduce real-world data for bicycle traffic.

2.9. Summary of Literature Review

After reviewing the previous studies regarding the bicyclist traffic safety and interactions with vehicle traffic, it is clear that the proposed research effort will be the first of its kind to develop a dynamics-based model for the longitudinal motion of bicycles in both constrained and unconstrained conditions. Bicyclist behavior variability and bicyclists' motions are modeled during our manuscript. Furthermore, previous studies that investigated bicycle-following behavior were based solely on ring-road experimental data, which is not typically reflective of bicycle riding. For that reason, our study involves testing a developed model using collected bike simulator data. This review showed that previous studies carry certain shortcomings, and further investigation is required for a reliable evaluation of bicyclist safety research. Future research is

also required to better understand and evaluate bicyclists' motion while addressing the gaps in the existing methods and the challenges in the bicyclist behavior evaluation.

3. BICYCLE-FOLLOWING MODEL DEVELOPMENT

In this section, the research team proposes to use vehicular traffic flow techniques to model bicyclist longitudinal motion while accounting for bicycle interactions. Specifically, an existing car-following model, the Fadhloun-Rakha (FR) model is used as the basis for the proposed model. The performance of the proposed model formulation is evaluated using experimental datasets collected from two ring-road bicycle experiments; one conducted in Germany in 2012, and the second in China in 2016. The validation of the model is achieved by investigating and comparing the proposed model outputs against those obtained from two state-of-the-art models, namely: the Necessary Deceleration Model (NDM), which is a model specifically designed to capture the longitudinal motion of bicyclists; and the Intelligent Driver Model, which is a car-following model that was demonstrated to be suitable for single-file bicycle traffic. Through a quantitative and qualitative evaluation, the proposed model formulation is demonstrated to produce modeling errors that are consistent with the other two models. While all three models generate trajectories that are consistent with empirically observed bicycle-following behavior, only the proposed model allows for an explicit and straightforward tuning of the bicyclist physical characteristics and the road environment. A sensitivity analysis, demonstrates the effect of varying the different model parameters on the produced trajectories, highlighting the robustness and generality of the proposed model.

3.1. Background

Nowadays, the reliance of traffic engineering on computerized traffic simulations for planning, urbanization, and environmental purposes is increasing as a result of the continuous technological advancement and proliferation of microscopic simulation frameworks. While those computational tools allow for the evaluation of different potential scenarios in a fast and cost-effective manner without dealing with any real world challenges, their results remain directly correlated to the accuracy and precision of the different logics integrated in them. That is the main reason for which a significant portion of traffic flow theory is oriented towards developing good descriptors of real traffic situations and empirical behavior. Looking at most of the existing microscopic simulation software, one perceived shortcoming relates to their orientation towards modeling vehicular traffic only. Such an observation becomes quite understandable when the huge gap between the number of research studies addressing vehicular and non-vehicular transportation modes is considered.

A main area of traffic flow theory for which the aforementioned gap is quite evident is car-following theory. Car-following theory proposes mathematical models (Chandler et al., 1958; Drew, 1968; Fritzsche, 1994; D. C. Gazis et al., 1961; Jiang et al., 2001; Newell, 2002; Olstam et al., 2004; Treiber et al., 2000) that aim to predict the temporal and spatial longitudinal behavior of a follower when the trajectory of the leader is known. In relation to modeling the longitudinal motion of moving entities, non-vehicular transportation modes such as cycling received little

attention when compared to vehicular modes. The observed disparity is justified by the fact that the popularity of cycling as a sustainable commuting mode was minimal up until recently. Another potential reason relates to the lack of experimental and naturalistic data describing bicyclist behavior. In fact, it is only quite recently that datasets containing information about bicycle-following behavior became available to traffic researchers.

To illustrate the extent to which modeling the longitudinal motion of bicycles was ignored historically, there is no better argument than noting that the first model specifically designed to simulate the following behavior of bicyclists was only developed in 2012. The model in question is the Necessary Deceleration Model (NDM) (Andresen et al., 2014). The NDM is a discrete bicycle-following model that uses three components (*acc*, dec_1, dec_2) to compute the acceleration and the deceleration of a bicycle, as presented in Equations (1-5), using the following bicycle speed v_n, the spacing s_n, and the speed differential between the two bikes $\Delta v_n = v_n - v_{n-1}$.

$$a_{NDM} = acc - \min(dec_1 + dec_2, b_{max}) \tag{1}$$

$$acc = \begin{cases} 0 & s_n \le d(v_n) \\ \dfrac{v_f - v_n}{\tau} & s_n > d(v_n) \end{cases} \tag{2}$$

$$dec_1 = \begin{cases} min\left(\dfrac{(\Delta v_n)^2}{2(s_n - s_j)}, b_{max}\right) & \Delta v_n < 0 \\ 0 & \Delta v_n \ge 0 \end{cases} \tag{3}$$

$$dec_2 = \begin{cases} b_{max}\left(\dfrac{s_n - d(v_n)}{l_n - d(v_n)}\right)^2 & s_n \le d(v_n)\,, \Delta v_n \ge -\varepsilon \\ 0 & otherwise \end{cases} \tag{4}$$

$$d(v_n) = s_j + T.v_n \tag{5}$$

Besides the free-flow speed v_f and the spacing at jam density s_j, the NDM requires the calibration of three additional parameters, which are: a constant of proportionality *T*, a maximum deceleration level b_{max}, and a relaxation time τ that controls how fast a bicycle accelerates to the desired speed v_f. Furthermore, the model involves the use of the bicycle length l_n which is set equal to 1.73 m (average bicycle length) and a positive constant ε = 0.5 m/s.

Based on the observation that there are no major differences between the dynamics of single-file bicycle traffic and vehicular traffic, the researchers also investigated the possibility of adapting aspects of existing car-following models to emulate bicycle longitudinal motion and cyclists' behavior. That is the case of the Intelligent Driver Model (IDM) (Treiber et al., 2000) which, after a simple re-parameterization of its parameters, was proven to be a good descriptor of bicycle-following behavior (Kurtc et al., 2020). The IDM model, which requires the calibration of five parameters, computes the acceleration of the following bicycle as presented in Equations (6-7).

$$a_{IDM}(v_n, s_n, \Delta v_n) = a\left(1 - \left(\frac{v_n}{v_f}\right)^4 - \left(\frac{s^*(v_n, \Delta v_n)}{s_n}\right)^2\right) \tag{6}$$

With

$$s^*(v_n, \Delta v_n) = s_j + v_n T + \frac{v_n \Delta v_n}{2\sqrt{a.b}} \quad (7)$$

Where s^* denotes the steady state spacing, a is the maximum acceleration level, b is the maximum deceleration level, and T is the desired time headway.

3.2. Fadhloun-Rakha Car-Following Model

One of the simplest car-following strategies is to follow the lead vehicle at a constant headway, which is typically taken equal to the driver perception-reaction time T as illustrated in Equation 8. This model is also known as the Pipes or GM-1 model (D. Gazis et al., 1961; Pipes, 1953, 1967). This time headway ensures that the subject vehicle n follows its leader at a safe spacing in order to avoid a collision under steady-state conditions (i.e. when both vehicles are traveling at the same constant velocity and assuming that the subject vehicle's deceleration maneuver starts T seconds after the lead vehicle decelerates).

$$\tilde{s}_n = s_j + T v_n \quad (8)$$

In the context of car-following modeling, Van Aerde (M. Van Aerde, 1995) and Van Aerde and Rakha (Michel Van Aerde et al., 1995a) proposed a more general formulation that reflects empirical driver behavior better than other models. This formulation combines the Pipes (Equation 8) and the Greenshields models to generate a more general formulation (H. Rakha, 2009; Rakha et al., 2009; Wu et al., 2009), presented in Equation 9.

$$\tilde{s}_n = c_1 + \frac{c_2}{(v_f - v_n)} + c_3 v_n \quad (9)$$

Here, $c_1, c_2,$ and c_3 are model coefficients that can be computed using key roadway traffic stream parameters (Equation 10) (H. Rakha, 2009), namely: the free-flow speed, v_f; the speed-at-capacity, v_c; the roadway capacity, q_c; and the roadway jam density, k_j (the inverse of the jam density spacing, s_j).

$$\begin{aligned} c_1 &= \frac{v_f}{k_j v_c^2}(2v_c - v_f); \\ c_2 &= \frac{v_f}{k_j v_c^2}(v_f - v_c)^2; \\ c_3 &= \frac{1}{q_c} - \frac{v_f}{k_j v_c^2} \end{aligned} \quad (10)$$

A slight modification in the expression of the steady-state model presented in Equation 9 is implemented when the lead vehicle is traveling at a lower velocity than the following vehicle (non-steady-state conditions). In those specific scenarios, a safety distance margin is considered in addition to the steady-state spacing as shown in Equation 11. The additional term is computed as the braking distance needed for the follower to decrease its speed to that of the leader at a deceleration level d (d is positive in the equation). The purpose of the desired safe following

spacing is to allow the following driver to drive at a spacing longer than the steady-state spacing when the vehicle ahead of it is driving at a lower speed. It is noteworthy to mention that the additional term is formulated such that it is only active when the following vehicle is approaching the lead vehicle. Otherwise, it is equal to zero which leads back to Equation 9.

$$\tilde{s}_n = \max\left(c_1 + \frac{c_2}{(v_f - v_n)} + c_3 v_n + \frac{v_n^2 - v_{n-1}^2 + \sqrt{(v_n^2 - v_{n-1}^2)^2}}{4d}, s_j\right) \tag{11}$$

Finally, the vehicle acceleration behavior is governed by the vehicle dynamics, as demonstrated in Equation 12 to ensure that vehicle accelerations are realistic.

$$a_{max} = \frac{\min\left(\frac{\beta \eta_d P_n}{v_n}, m_{ta} g \mu\right) - \frac{\rho C_d C_h A_f v_n^2}{2} - mgC_{r0}(C_{r1} v_n + C_{r2}) - mgG}{m} \tag{12}$$

Rakha and Lucic (2001) introduced the β factor in order to account for the gearshift impacts at low traveling speeds when trucks are accelerating. This factor is set to 1.0 for light-duty vehicles (Rakha et al., 2004). Other parameter definitions are: η_d is the driveline efficiency (unitless); P is the vehicle power (W); m_{ta} is the mass of the vehicle on the tractive axle (kg); g is the gravitational acceleration (9.8067 m/s^2); μ is the coefficient of road adhesion or the coefficient of friction (unitless); ρ is the air density at sea level and a temperature of 15°C (1.2256 kg/m^3); C_d is the vehicle drag coefficient (unitless), typically 0.30; C_h is the altitude correction factor equal to 1-0.000085h, where h is the altitude in meters (unitless); A_f is the vehicle frontal area (m^2), typically 0.85 multiplied by the height and width of the vehicle; C_{r0} is a rolling resistance constant that varies as a function of the pavement type and condition (unitless); C_{r1} is the second rolling resistance constant (h/km); C_{r2} is the third rolling resistance constant (unitless); m is the total vehicle mass (kg); and G is the roadway grade (unitless).

To capture the driver input the f_p factor is introduced, which ranges between 0.0 and 1.0. The final FR model formulation, which considers the deceleration necessary to avoid a collision with a slower traveling leader, is cast using Equation 13. This equation includes two terms. The first is the acceleration term while the second is the deceleration term. Both terms ensure that the following vehicle does not collide with its leader.

$$a_n = f_p a_{max} - \frac{\left[v_n^2 - v_{n-1}^2 + \sqrt{(v_n^2 - v_{n-1}^2)^2}\right]^2}{16(d_{des} - gG)(s_n - s_j)^2} \tag{13}$$

Here f_p is computed using Equation 14 where X_n is calculated using Equation 15.

$$f_p = e^{-g_1 X_n}\left(1 - X_n^{g_2} e^{g_2(1-X_n)}\right)^{g_3} \tag{14}$$

$$X_n = \frac{\min(\tilde{s}_n, \tilde{s}_n((1-\alpha)v_f))}{\min(s_n, \tilde{s}_n((1-\alpha)v_f))} \cdot \frac{v_n}{\tilde{v}_n} \tag{15}$$

Here $\tilde{s}_n$ is the desired spacing for the current speed (computed using Equation 11); $\tilde{v}_n$ is the desired speed for the current spacing (which is computed by solving for the driver's desired speed based on its current spacing using Equation 11); α is the percentile off v_f (suggested to be 2.5%); d_{des} is the desired deceleration level; g_1, g_2 and g_3 are model parameters that are calibrated to a specific driver and model the driver power input through the application of the gas pedal.

In order to ensure that the parameters (g_1, g_2 and g_3) result in a minimal maximum value of f_p in the deceleration domain, an iterative procedure was developed. The iterative procedure, presented in Equation 16, is only approximate and converges relatively fast (within four to five iterations) to the location of the maximum of f_p, which is then verified to be below a threshold ε (for instance, $\varepsilon = 0.1$). By doing so, it is decided whether the chosen values for the g_1, g_2 and g_3 parameters are accepted or rejected. Of course, this procedure was only adopted after ensuring that the number of different combinations of (g_1, g_2 and g_3) that would result in $f_p\left(X_{k\to inf}\right) < \varepsilon$ was significant. It is worth clarifying the reason for which this additional step was needed given that a simple binary function would have been sufficient. In fact, this step is necessary in order to make the model computationally friendly as it significantly reduces the feasible region for the model parameters without major repercussions on the model performance. In fact, the defined feasible region for the variables is big enough to allow the model to possess flexibility and adaptability under different scenarios.

$$\begin{cases} X_0 = 3\left(-1+\sqrt{2\ln(3)}\right) \\ X_{k+1} = 3\left[-1+\sqrt{2\ln\left(3\left[1+\frac{g_2 g_3}{g_1}\left(1-\frac{1}{X_k}\right)\right]^{1/g_2}\right)}\right] \end{cases} \tag{16}$$

Finally, three noise variables are added to the model formulation in order to capture the perception and control inaccuracies of the drivers. The first two signals attempt to model the perception errors in estimating the leader's speed and the gap distance separating the two vehicles. They consist of two Wiener processes that are incorporated in the model formulation as presented in Equations 17 and 18. Equation 17 emulates the driver's inability to have an exact estimation of the speed of the leading vehicle while Equation 18 simulates the driver's error in estimating the spacing separating them. Additionally, a white noise signal, presented in Equation 19, is added to the model to capture the control errors during the acceleration and deceleration maneuvers. The compounding effect of these three signals makes the model output more representative of human behavior. The model output is computed as the sum of Equation 19 and Equation 13 in which $\widetilde{v_n}(t)$ and $\widetilde{s_{n+1}}(t)$ are used instead of u_n and s_{n+1}.

$$\begin{cases} \widetilde{v_{n-1}}(t) = u_{n-1}(t-\Delta t) - 0.01\left(s_n - s_j\right)\left(e^{-0.01}.W_l(t-\Delta t) + \sqrt{0.02}.N(0,1)\right) \\ W_l(1) = N(0,1) \end{cases} \tag{17}$$

$$\begin{cases} \tilde{s_n}(t) = s_n(t-\Delta t) \times e^{0.1\left(e^{-0.01}.W_s(t-\Delta t)+\sqrt{0.02}.N(0,1)\right)} \\ W_s(1) = N(0,1) \end{cases} \quad (18)$$

$$\breve{a}_n(t) = N(0, 0.25) \quad (19)$$

3.3. Model Formulation

For the most part, the car-following strategy of the FR model remains valid for modeling the longitudinal single-file motion of bicycles. Specifically, the functions governing collision avoidance, steady state behavior, and human behavior modeling would have the same functional forms. For the aforementioned functions, the differences between vehicular traffic and bicycle traffic would be expressed at the level of the adopted values of their different parameters. The latter is not the case for the vehicle dynamics model (H. Rakha, Pasumarthy, P., and Adjerid, S. , 2009), which requires the implementation of structural modifications in order to make it descriptive of the maximum acceleration behavior of bicycles.

The biggest challenge the research team faced in this phase related to choosing an adequate expression for the tractive force. Having a good approximation of the traction as a result of pedaling significantly impacts the precision and the accuracy of the bicycle trajectories generated by the model as it defines the maximum acceleration profile a_{max}. The proposed expression for the tractive force was achieved by modeling the cyclist as a motor generating power. In order to account for the cyclist output variability over time, we opted to estimate power as the product of the cyclist's weight and the highest average power that could be sustained over a certain period of time, commonly known as functional threshold power (FTP factor in W/kg). Understandably, the FTP factor depends on several variables, such as gender, stamina, and the time interval as shown in Table 1. For instance, a healthy male cyclist in a good shape is able to generate an average of 3.91 W/kg over an hour period and a higher average of 8.28 W/kg over a 1-minute period. For a healthy female cyclist, these values decrease slightly to 3.39 W/kg and 6.75 W/kg over the same time periods. Finally, in order to account for the losses incurred while the pedaling power is transmitted to the rear wheel, several efficiency factors were applied. These factors attempt to model the effect of the bicycle gears and the friction of the bicycle chain.

Table 2 presents a summary of the needed changes to account for the differences between bicycles and vehicles.

Table 1 Maximal power outputs for different cyclist categories (https://zwiftinsider.com/rider-categorization-based-on-ftp-how-do-you-rank/, 2016)

Bicyclist Condition	Male			Female		
	1 min	5 min	1 hour	1 min	5 min	1 hour
World Class	11.50	7.60	6.40	9.29	6.61	5.69
Exceptional	10.35	6.57	5.51	8.38	5.68	4.87
Excellent	9.66	5.95	4.98	7.84	5.13	4.38
Very good	8.97	5.33	4.44	7.3	4.57	3.88
Good	8.28	4.70	3.91	6.75	4.02	3.39
Moderate	7.48	3.98	3.29	6.12	3.37	2.82
Fair	6.79	3.36	2.75	5.57	2.82	2.32
Untrained	5.87	2.53	2.04	4.85	2.07	1.67

Table 2 Summary of the dynamics model for bicycles and cars(Soden et al., 1979)

	Bicycles	Cars
Tractive Force	$\min\left(\eta_{eff}\eta_{gears}\frac{m_{cyclist}P_{ftp}}{v_n}, m_{ta}g\mu\right)$ η_{eff} depends on bicycle chain η_{gears} depends on gears and bike geometry m_{ta} depends on center of gravity position	$\min\left(\frac{\beta\eta_d P_n}{v_n}, m_{ta}g\mu\right)$
Rolling Resistance	mgC_{rr} C_{rr} depends on road type	$mgC_{r0}(C_{r1}v_n + C_{r2})$
Aerodynamic Resistance	Same formulation except: C_dA_f depends on cyclist physique and posture on bike	C_dA_f depends on car shape
Grade Resistance	Same formulation	

3.4. Analysis

In this section, we propose to evaluate the performance of the proposed model formulation against the NDM and the IDM models using the German and Chinese datasets. The choice of these two specific models is not arbitrary. In fact, both models were used in previous studies to investigate bicycle-following behavior based solely on ring-road experimental data. That makes them the perfect candidates for investigating the suitability of the reparametrized FR model for simulating bicycle traffic flow and following behavior.

3.4.1. Experimental Data

The bicycle trajectory data used in this study is the result of two controlled ring-road experiments. The first experiment was carried out by the University of Wuppertal in conjunction with the Julich Supercomputing Center in May, 2012 (Andresen et al., 2014). Participants from different age groups were instructed to follow one another without overtaking on an 86-meter circular track. The experiments were conducted with 5, 7, 10, 18, 22 and 33 cyclists, allowing them to capture the effects of different density levels. Through the use of two cameras overlooking the road, the cyclists' trajectories were captured along a 20 m long straight section of the test track. As a side remark, it is worth mentioning that the experiments were mainly performed for the sake of calibration and validation of the NDM model, which is the first model designed to simulate the longitudinal motion of bicycles.

The second dataset originates from a 2016 Chinese experiment that was conducted on a 146-meter circular track. Like the German experiments, the experimental runs were performed with 39, 48 and 63 cyclists for the purpose of reproducing different global densities. Using a video camera that was mounted on the top of a high building, the researchers were able to extract the full trajectories of the bicycles.

The original datasets, which were collected with a sampling frequency of 10 Hz and 15 Hz respectively, captured the bicycle positions using a multi-dimensional coordinate system and manifested significant noise levels that resulted during the data extraction process from the recorded videos. As a result, we had to pre-process the data by expressing the bicycle trajectories in a radial coordinate system and applying exponential smoothing in order to eliminate the observed noise.

The aggregated data for the different runs can be visualized in Figure 1 and Figure 2, which show the data in different domains of the fundamental diagram. The dispersion of the data confirms a similar behavior to that originating from vehicular traffic. The macroscopic data points presented in the figure are obtained from the microscopic bicycle trajectories through the use of virtual loop detectors located at the entrance and the exit of the 20 m section on which the different trips occurred for the German experiment, and on a 50 m section of the circular track for the Chinese experiment.

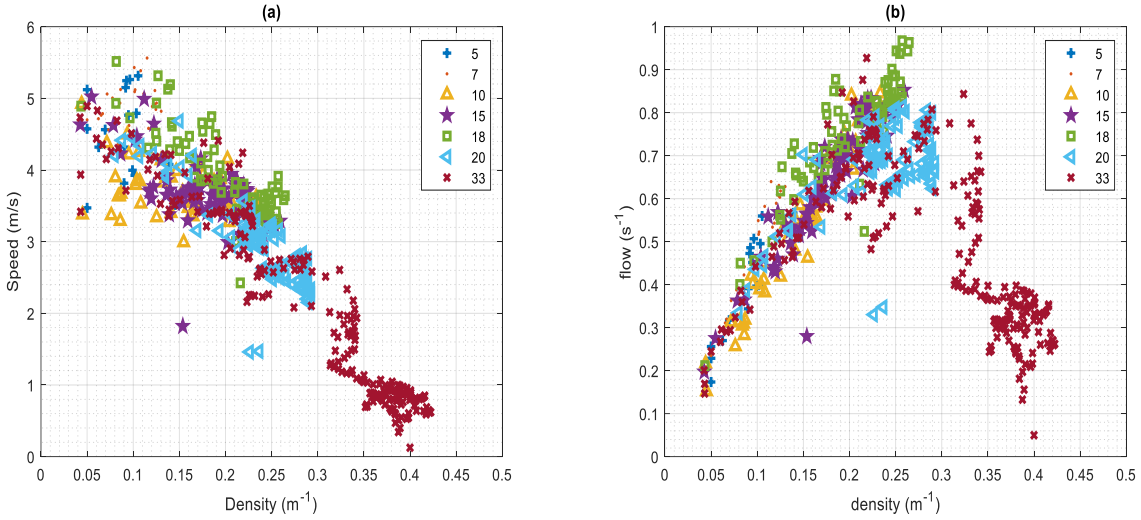

Figure 1 German experiment a) Speed-density relationship; b) Flow-density relationship

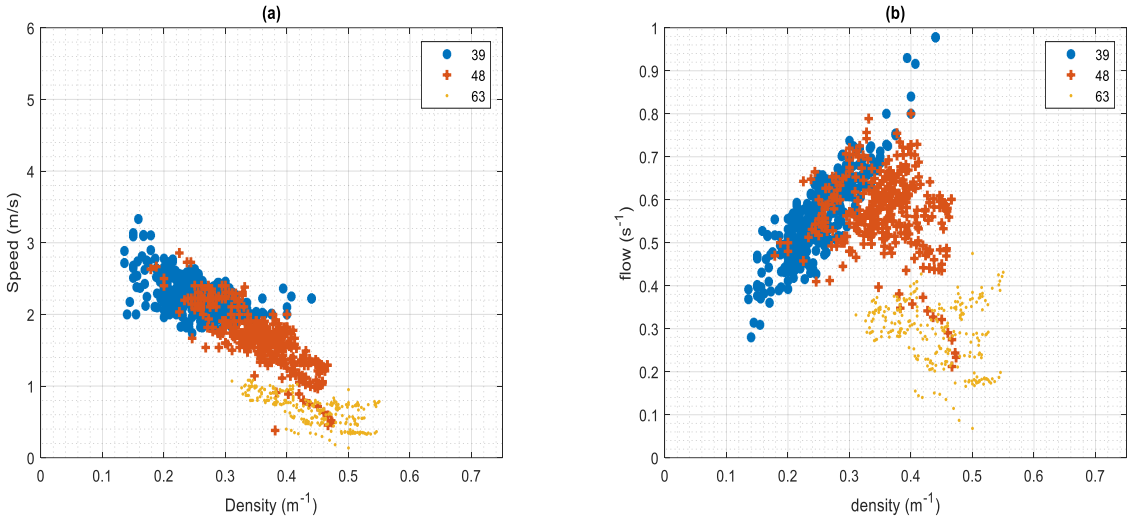

Figure 2 Chinese experiment a) Speed-density relationship; b) Flow-density relationship

3.4.2. Calibration

For each of the studied models, a number of inputs are needed. These inputs can be categorized into three groups. The first category includes the inputs that are extracted directly from the datasets, such as the time-space and the time-speed profiles of the leading vehicle and the starting location and speed of the following vehicle. The second category includes the parameters that are calibrated using all of the trips, as they are more representative of the road facility and the fundamental diagram that governs it rather than the trip itself. Subsequently, these parameters are assigned a single value across all of the bicycle-following events in order to maintain and represent the homogeneity of the road facility. Namely, the concerned parameters are the free-flow speed u_f and the spacing at jam density s_j (inverse of k_j), which are shared among the three models along with the roadway capacity q_c and the speed-at-capacity u_c, which are needed to generate a

simulated trajectory in the case of the proposed model formulation. Those parameters were estimated using a heuristic automated tool (SPD-CAL) that is used for the calibration of steady-state traffic stream models using the macroscopic data shown in Figure 1 and Figure 2. SPD-CAL conducts an optimization operation with the orthogonal error serving as the objective function (Rakha et al., 2010; Michel Van Aerde et al., 1995b). The reasons for which the data related to the two experiments was combined are twofold: First, the Chinese experiment shows a clear lack of data in the free-flow regime. Second, the two datasets seem to overlap almost perfectly as shown in Figure 3, which presents the calibration results of the fundamental diagram of the facility.

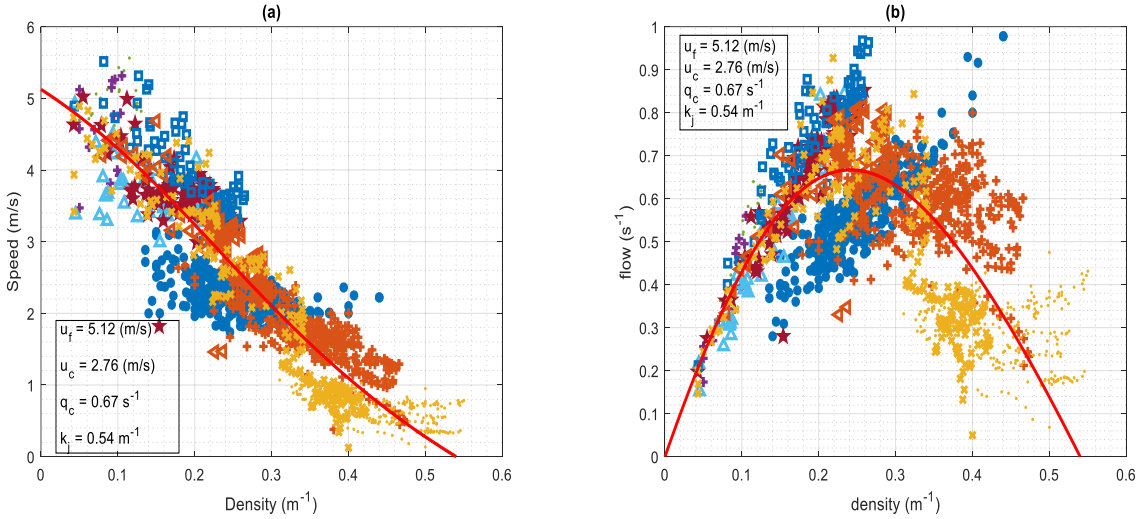

Figure 3 Calibration of the fundamental diagram a) Speed-density relationship; b) Flow-density relationship

Next, the calibration procedure is complemented by the calibration of the remaining variables. At a first glance, the calibration of the proposed model might seem complex due to the sheer number of variables involved. However, most of these parameters have fixed values that are either constant or dependent on certain characteristics of the road and/or the bicycle. For instance, knowing that the experiments were run on a dry and flat asphalt road, the values of the grade G, the rolling coefficient C_{rr}, and the friction coefficient μ were set to 0, 0.004, and 0.8 respectively. For the remaining variables, the following assumptions are made:

- The cyclist is an untrained male (P_{ftp}=2.04 W/kg),
- The bicycle weighs 8 kg,
- The proportion of the total mass on the rear axle equals 0.60,
- The aerodynamics coefficients are such that $C_d A_f$ = 0.4,
- The desired deceleration level d_{des} is equal to 1.5 m/s^2,
- The total efficiency factor $\eta_{eff}\eta_{gears}$ = 0.62.

To highlight the practicality and ease of implementation of the model, we present a simplified formulation of the bicycle dynamics model in which the different parameters were substituted with their respective values in Equation 20. Unless a potential user is interested in

modeling a very specific scenario with a high level of detail, the presented version of the dynamics model is adequate for testing the average user after implementing the model formulation in Equation 13, as it is representative of a standard typical scenario.

$$a_{max} = \min\left(1.26\frac{m_{cyclist}}{(m_{cyclist}+8).v_n}, 4.7\right) - \frac{0.003v_n^2 + 0.04}{(m_{cyclist}+8)} \quad (20)$$

Considering a cyclist weight of 75 kg, each of the considered models would require the calibration of three additional parameters. In that context, the values (g_1, g_2, g_3) for the proposed model, (τ, T, b_{max}) for the NDM model, and (a, T, b) for the IDM model are obtained for each cyclist trajectory through an optimization operation that aims to minimize the error between empirical and simulated data. For each pair of successive trajectories (leader/follower), the simulated trajectory of the follower was initialized with the empirical speed and spacing for each of the three models. Next, the calibration procedure of each model was conducted heuristically with the objective of finding the set of parameters resulting in the smallest error values. In that context, the absolute spacing error, presented in Equation 21, was chosen to serve as the error objective function given that this was one of the errors used to compare the NDM and IDM models in a previous publication (Kurtc et al., 2020). Subsequently, the performance of each model is quantified through the comparison of the simulated spacing data s^{sim} against the empirical observations s^{obs}.

$$f_{abs} = \frac{\sum_{i=1}^{n}\left(s_i^{sim} - s_i^{obs}\right)^2}{\sum_{i=1}^{n}\left(s_i^{obs}\right)^2} \quad (21)$$

The choice to optimize each model with regards to the absolute spacing error is reasonable given that the optimization operation was done on an event-by-event basis. We opted to calibrate each model separately for each event rather than for the dataset as a whole. Even though that increased the computation time, a more fair comparison of the results is made possible as each model was allowed to propose its best possible fit for each trajectory. Hence, the different model outputs are reflective of the strength points of each model. The use of the denominator in the error objective function is justified by the need to account for the trip duration variability across the different events. By dividing the absolute error with a variable that is sensitive to the aforementioned variability; its effects on the chosen error metric are minimized.

Furthermore, given the relatively long duration of the events specific to the Chinese experiment, we have opted to calibrate the three models using the initial 75% of each trajectory for calibration purposes. The remaining portion of the trajectory (25%) is used to validate the models and quantify their predictive power. Such a procedure was not possible for the German data, for which the integrality of the trajectory is used, due to the very short trips involved.

3.4.3. Results

Having access to the calibrated parameters, the simulated trajectories were obtained for the different events of the two datasets. The characteristics of the calibration errors related to the German and Chinese experiments are presented in Table 3. For the German data, lower error values

are observed for the IDM and the NDM models when compared to the FR model. However, the trend is reversed when the Chinese data is considered. In fact, the FR and NDM models are shown to outperform the IDM model, with the FR model results slightly better than those of the NDM. The observed discrepancies between the results of the two datasets could be attributed to the short trip durations in the German experiments in which the trajectories are collected over just a 20-meter section (in comparison to the 146-meter trajectories of the Chinese experiment).

Table 3 Characteristics of the calibration errors for the FR, IDM and NDM models

	German Dataset			Chinese Dataset		
	FR	**IDM**	**NDM**	**FR**	**IDM**	**NDM**
Mean	0.0063	0.0025	0.0033	0.043	0.058	0.044
Median	0.0024	0.0004	0.0005	0.029	0.040	0.030
Std Dev	0.0096	0.0077	0.0100	0.064	0.076	0.052

Further error metrics for the IDM, NDM and FR models are shown in Table 4, which presents the key distribution parameters for the error objective function of the Chinese trajectory data. For instance, when the full trajectories are considered, the table demonstrates that the proposed model along with the NDM model offer almost identical percentiles and that they are slightly better in terms of fitting the observed data than the IDM model. That statement is further supported by Figure 4, which plots the empirical cumulative distribution functions corresponding to the three models. Specifically, Figure 4.c demonstrates that the cumulative distribution functions of the FR model and the NDM models are almost identical at every data point of the error axis. Next, the distribution functions corresponding to the German experimental data are plotted in Figure 5. While the plot makes it clear that the FR model underperforms the other two models, the small magnitude of the errors involved does not undermine the performance of the model or its suitability for modeling bicycle following behavior.

Table 4 Distribution characteristics of the error function

		25% percentile	Median	75% percentile	95% percentile
Calibration	**FR**	0.017	0.029	0.047	0.125
	IDM	0.023	0.040	0.067	0.172
	NDM	0.017	0.030	0.053	0.130
Validation	**FR**	0.028	0.054	0.118	0.396
	IDM	0.026	0.054	0.120	0.505
	NDM	0.025	0.048	0.108	0.463
Full Trajectory	**FR**	0.023	0.036	0.062	0.158
	IDM	0.027	0.044	0.076	0.194
	NDM	0.022	0.036	0.063	0.154

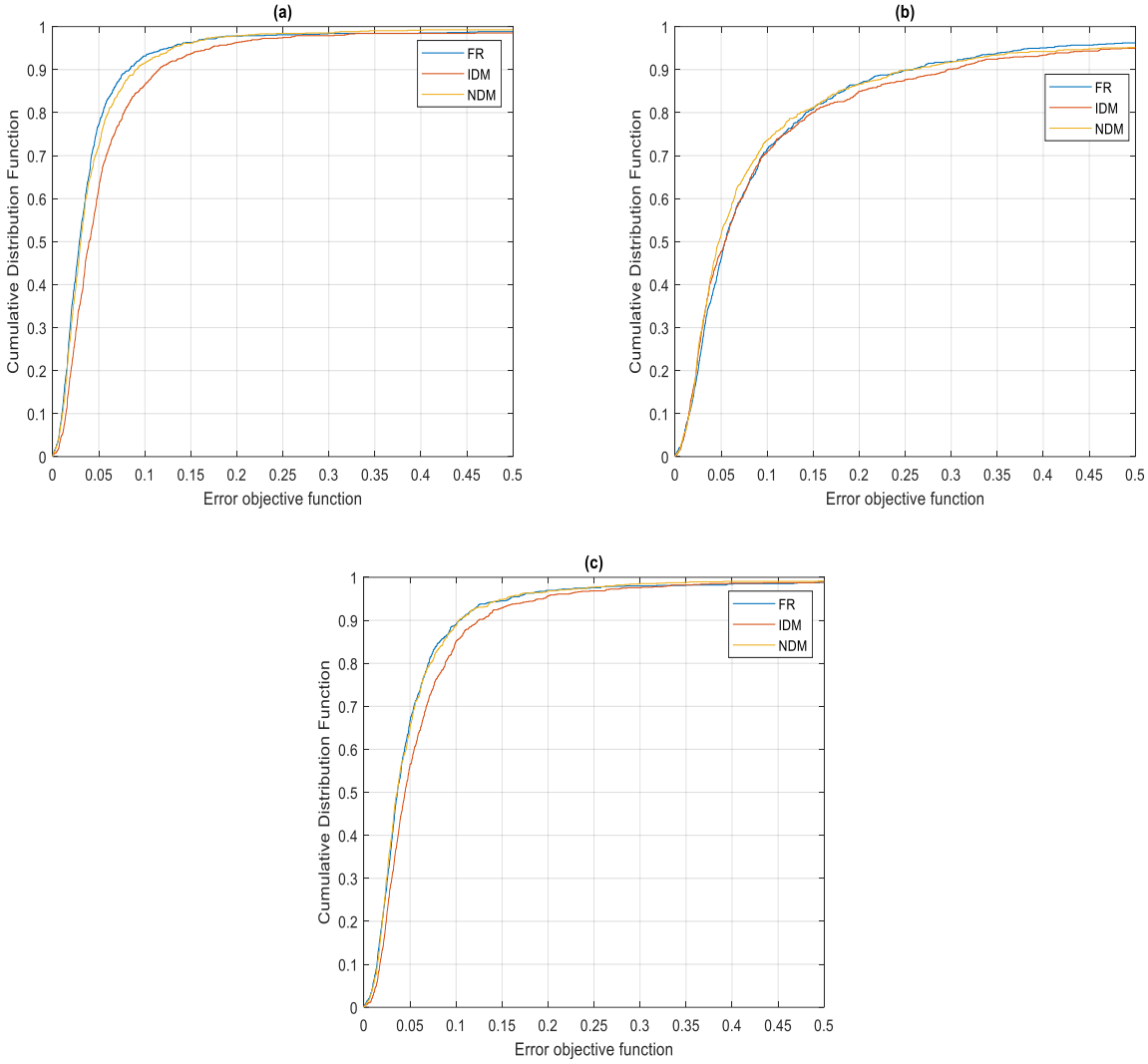

Figure 4 Cumulative distribution function of the error of the Chinese dataset using: a) the first 75% of the trajectory (calibration trajectory); b) the last 25% of the trajectory (validation trajectory); c) the full trajectory

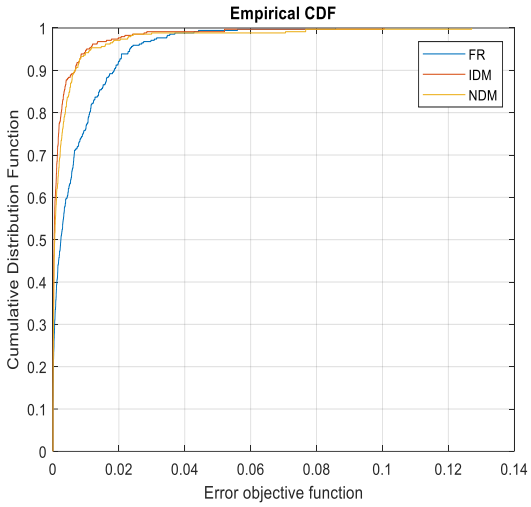

Figure 5 Cumulative distribution function of the error of the German dataset

To better statistically quantify the difference in performance between the different models, the rank of each model was determined for each event based on the calculated error objective function. In doing so, it was found that the FR model ranked first as it outperformed the NDM and the IDM models in approximately 47% of the cases. The NDM model demonstrated a good performance as well as it offered the best fit in 42% of the events. To have a deeper understanding of the results, the performance of the FR model was directly compared with the NDM model. It was found that the two models performed equally well, with each model producing the lowest error in exactly half the events. That is in accordance with the results presented in Table 4 and Figure 4.

While all the models resulted in a good fit to the data without any clear favorite, it is worth noting the main advantage of the proposed model. Specifically, the main advantage of the FR model is its flexibility in capturing different dynamic characteristics specific to both the cyclist and the environment, such as athletic capability, size, gender, weather, and road grade. The robustness of the model is further complemented by its explicit inclusion of parameters that are reflective of the human-in-the-loop element separately from the bicycle dynamics variables. Put simply, the model is able to emulate cyclist behavior variability even when the same physical characteristics and road conditions are considered. To illustrate the previous points, the study proceeded to perform a simple sensitivity analysis in which a 100-meter trip is simulated for different case scenarios. In each of the scenarios, all the model parameters were set to a fixed value except for one. That would allow visualizing its impact on the generated trajectories. The following case scenarios are considered:

- *Scenario 1*: the coefficient of friction of the road, μ is varied between 0.1 and 0.8 in order to model several road conditions ranging from icy to dry as shown in Figure 6.a.
- *Scenario 2*: the functional threshold power is varied between 2.0 W/kg to 6.4 W/kg in order to model the physical capability of the eight cyclist categories ranging from an untrained individual to a world-class athlete (Figure 6.b).

- *Scenario 3*: several road grades were investigated ranging from a 4% downhill to a 4% uphill at 2% increments (Figure 6.c).
- *Scenario 4*: The final scenario investigates the effect of the cyclist gender on the results (Figure 6.d).

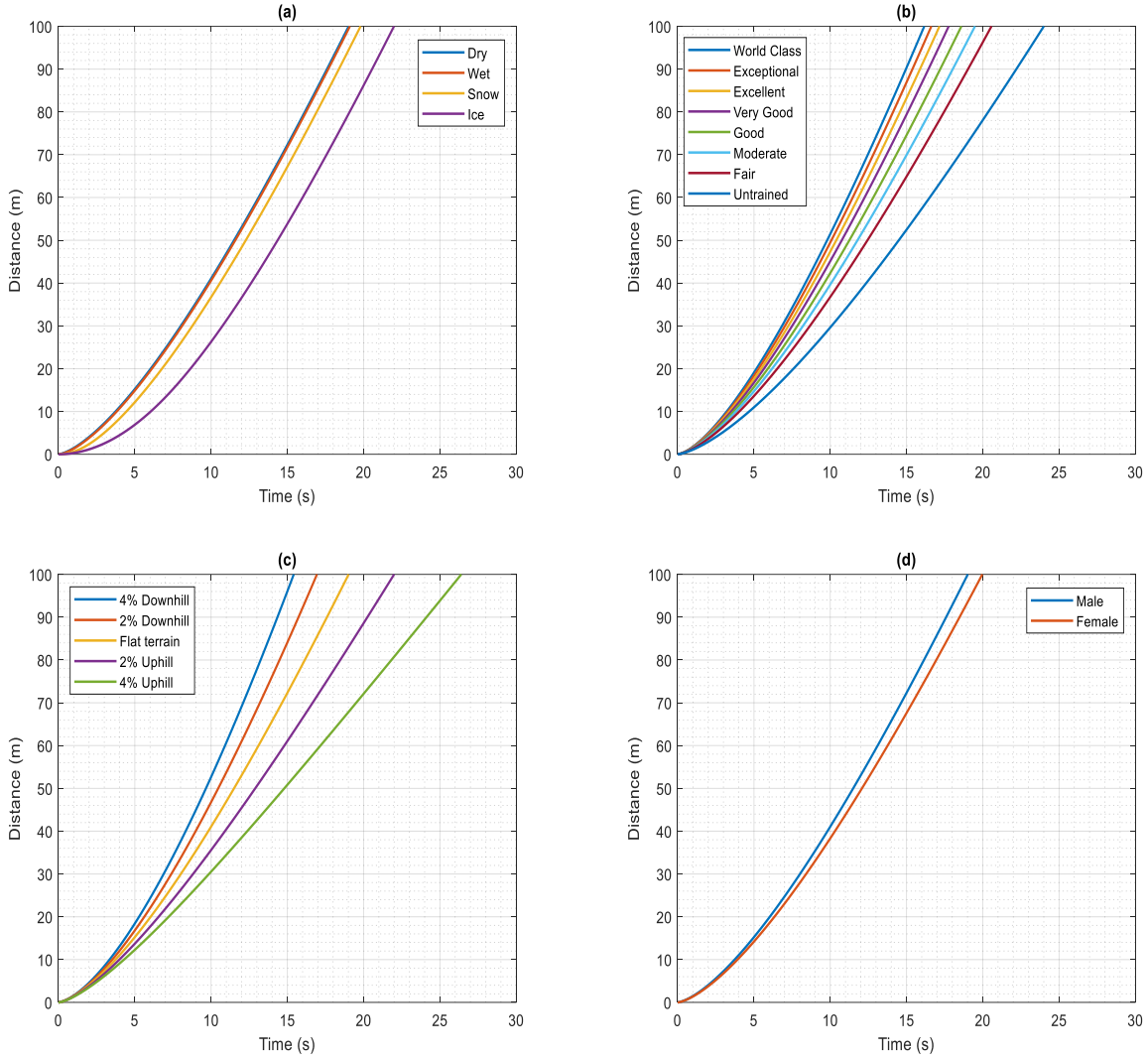

Figure 6 Effect of different model parameters on the simulated trajectories: a) Coefficient of road friction; b) Functional threshold power; c) Road Grade; d) Gender

While evaluating the calibration results, the research team explored the relationships and correlations between the different combinations of optimal parameters (g_1, g_2, g_3). Figure 7.a to Figure 7.c, which plot the variation of g_1, g_2 and g_3 against each other, make it easy to identify certain patterns related to the range of variation of those parameters responsible for modeling cyclist behavior variability. First, it is relatively clear in Figure 7.a and Figure 7.c that there is a significant concentration of g_2 values in the area between 0 and 100. Second, the plots suggest that g_1 is the easiest variable in terms of calibration as the range of the optimized values is quite limited compared to the other two variables. Another observation relates to a potential correlation between

the g_2 and g_3 parameters. The observed patterns in Figure 7.c seem to not be random and suggest the existence of a family of hyperbolic functions that governs the relationship between the two parameters. Determining the latter functions and analytically confirming the observed boundaries would probably result in the reduction of the computational time of the optimal solution in comparable future studies. An analytical investigation of the relationships between the three parameters would constitute an interesting and useful complement to this study.

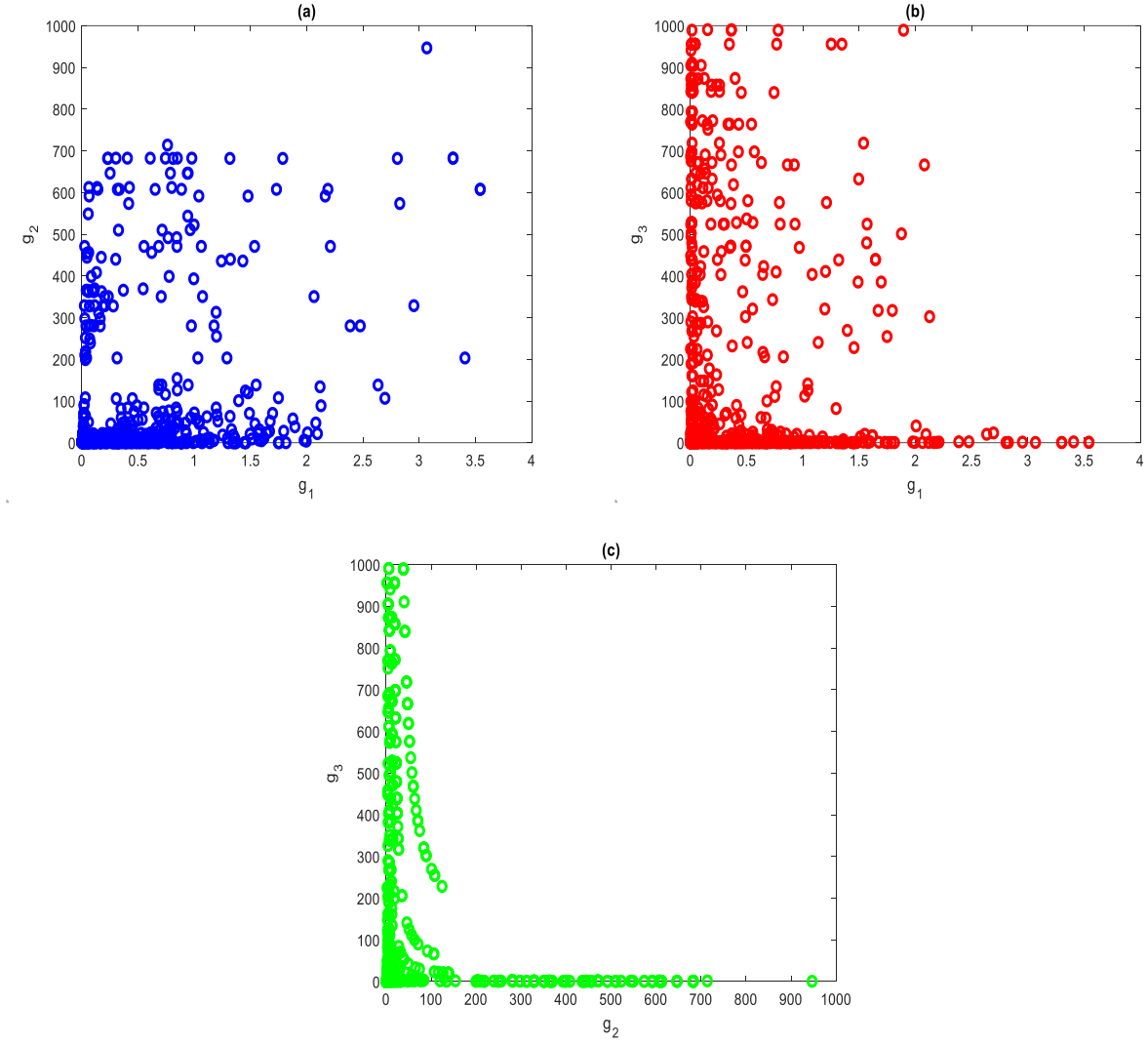

Figure 7 Variation of the FR model parameters against each other: a) g1 vs. g2; b) g1 vs. g3; c) g2 vs. g3

From a qualitative standpoint, Figure 8 presents plots of both the empirical and the simulated time-space trajectories corresponding to the Chinese experimental run in which 63 cyclists were involved. The choice of that specific scenario is not random and is justified by the presence of stop-and-go waves and several traffic perturbations due to the high density level. That would allow for a more comprehensive evaluation of the suitability of the proposed FR model formulation for the simulation of bicycle-following behavior. The figure confirms that the FR

model reflects the overall behavior of the cyclists. Specifically, the simulated trajectories are shown to successfully follow the different patterns in the empirical data and to precisely replicate the empirically observed stop-and-go waves.

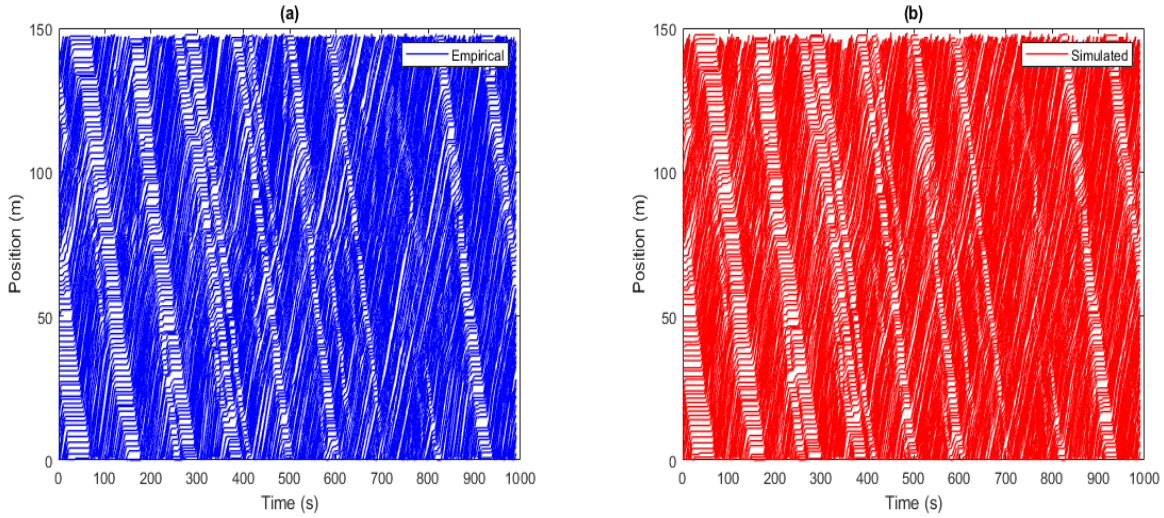

Figure 8 Bicycle trajectories for the Chinese experimental run with 63 cyclists: a) Empirical; b) Simulated

4. DATA COLLECTION METHODOLOGY

Thirty-three participants were recruited via flyers distributed manually, online, and through social media. Flier content included contact information, a summary of the requirements for the study, and an explanation of the monetary compensation for driving the bike and car simulators. Subsequently, prospective participants were screened for eligibility and scheduled to drive in the simulator environment. Participants were required to possess a valid driver's license and were compensated $15 per hour for their participation. In addition, participants were asked about their biking experience. We provided them with water and candy when they felt tired or had headaches while driving with simulators.

Under the supervision of an advisor, a team of undergraduate and graduate student research assistants observed the IRB-approved driving tasks, and questionnaire. Participants were asked to fill out a pre-survey questionnaire, drive for about two hours in different simulated scenarios, and fill out the post-survey questionnaire to find the effect of their experience on driver behavior.

The observer made sure that the participants completely understood the objectives of this project. They instructed the participants to briefly familiarize themselves with the simulator environment and explained the procedure before each scenario. Two Participants were instructed to drive bike and car simulators at the same time. When each scenario was run, one participant had to follow the other vehicle in the study. All the scenarios were designed to investigate changes in bicyclist behavior = toward vehicle traffic. The participants started driving in a base scenario with no vehicle traffic to compare their driving behavior with other high traffic condition scenarios. Participants then drove seven different in-vehicle scenarios – including:

- Scenario 1-1: Bicycle only (traffic scenario independent) - without traffic
- Scenario 1-2: Bicycle only (traffic scenario independent) - with traffic
- Scenario 2: Car moving straight (Bicycle ahead of Car, Bicycle in path, same direction velocity vector)
- Scenario 3: Car moving straight (Bicycle ahead of Car, Bicycle in path stationary)
- Scenario 4: Car moving straight (Bicycle behind Car, Bicycle in path, same direction velocity vector)
- Scenario 5: Car moving straight (Bicycle behind Car, Bicycle in path stationary)
- Scenario 6: Car moving turning right (Bicycle ahead of Car, Bicycle in path, same direction velocity vector)

A simple real-world network consisting of a straight two-way, two-lane route and two signalized intersections with four phases and a 110 second cycle length was designed for both participants driving the scenarios with different initial start points. The location of bike and car was defined in the software and the following attributes were considered for the simulation:

- Minimum Weight of bicyclists[1]: 50 kg
- Maximum Weight of bicycle: 7.5 kg
- The tolerance of bicyclist plus bicycle weight: 55 kg ~ 87 kg
- Max brake force[2]: 1000 N
- Front layout[3]: 0%
- Rear layout: 100%
- Estimated acceleration[4]: 3.5 $\frac{m}{s^2}$
- Air friction[5]: 0.4
- Pitch Inertia[6]: 17 $\frac{kg}{m^2}$
- Roll Inertia: 13 $\frac{kg}{m^2}$
- Yaw Inertia: 10 $\frac{kg}{m^2}$

As shown in Figure 9, the simulated network for bicyclists and car drivers was considered as below:

[1] Weight of the car. Minimum and maximum values are used to simulate the different loads of each vehicle
[2] the maximum force that the brakes can apply on the wheels
[3] Layout of the car drive wheels: front-wheel drive, rear-wheel drive, or four-wheel drive.
[4] The amount of acceleration drivers are using
[5] Friction the coefficient for the car, used to compute the air drag
[6] consists of inertia of the vehicle, Roll Inertia, Pitch Inertia, and Yaw Inertia

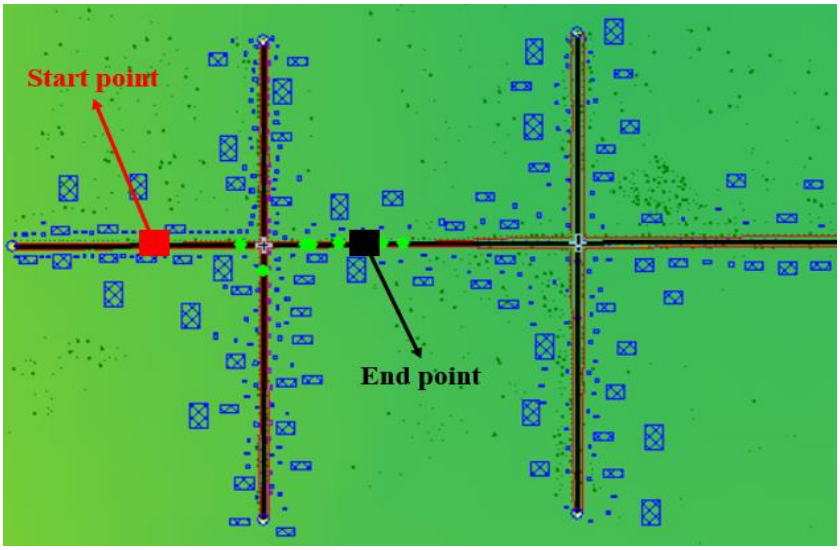

Figure 9 The simulated network

It is worth mentioning that, 25 $\frac{mile}{hour}$ (or 40 $\frac{km}{hour}$) was defined for the cars, and the speed limit of bicyclists was defined as 12 $\frac{mile}{hour}$ (or 20 $\frac{km}{hour}$) .

In the scenario 1-1, only one bicycle was assigned on the network. We tried to investigate the longitudinal motion of bicyclists without vehicle traffic conditions.

In the scenario 1-2, the first scenario with heavy traffic, (500 $\frac{veh}{hour}$) was modeled.

In the second scenario (scenario 2), the bike is ahead of the car, and the bicycle goes straight before the signalized intersection. The bicycle stops before the intersection. The software stops analyzing when the bike arrives at the stop line of the first intersection.

In the third scenario, the location of the bicycle was defined in front of the car. Bicycles and cars were run from 492 ft (150m) before the signalized intersection to 492 ft (150m) after the signalized intersection. The "same direction velocity vector" means "the same direction". Additionally, the bicycle must pass the intersection and both the bike and car must stop after the signalized intersection.

Scenario 4 is the same as the second scenario. In scenario 4, the bicycle is behind the car.

Scenario 5 is the same as the third scenario. In scenario 5, the bicycle is behind the car.

In scenario 6, the car should turn right, the bicycle is ahead of the car, and the bike goes straight until it passes the signalized intersection. We ignored the left turn in scenario 6. The conflict between the bike when passing the intersection and the car when turning right is investigated in this scenario.

During each driving scenario, participants were instructed to drive as they typically would on a real road for approximately 5 min and comply with the speed limit. The daytime scenery closely matched driving situations in the Baltimore metropolitan area and was designed to create a sense of real-world driving for each participant. Traffic flow and density were designed similarly in all seven scenarios. The driving experience in each scenario progresses in urban downtown routes. The bike and car simulators were integrated together for this project. When both simulators

are integrated, the car simulator participant can watch the scenario on the car simulator's screen. Therefore, both participants can follow each other and they can be informed about the location of one another during the simulation. As shown in Figure 10, two participants can follow each other in the same scenario.

Figure 10 Integration of bike and car simulators

The questionnaires asked about demographic information and real driving behavior before the driving simulator experience (pre-survey), and driving behavior after driving the simulator (post-survey). Observers gave participants the option of completing the questionnaire on their own or with the assistance of the observer. The simulation was displayed on three, 40-inch LCD screens. Participants sat within the simulator's driver compartment, which provided a view of the roadway and dashboard instruments, including a speedometer (Figure 10). Naturalistic engine sounds, road noises, and sounds of passing traffic were provided to simulate the real world. Simulated vehicles with varying speed and volume were randomly programmed with assigned low traffic volume to represent off-peak conditions in the area. The special collision sound and a message consisting of "Collision" word were designed for scenarios where the participant collides with other vehicles or bicyclists. Different information about the driver's behavior including speed, throttle, brake, steering velocity, offset from road center, and lane change was also calculated. For example, offset from the road center, which was reported as the deviated distance from the road center toward the right or left side, was calculated and saved as an indicator of impaired driving performance. Greater within-lane deviation indicated poorer driving precision.

Average driving speed when participants exited from the bike lane was calculated based on the speed of the vehicle and computed as the degree to which drivers changed their speed for each scenario. Lane change frequency was used as an indicator and defined as the number of times the driver changed lanes. The brake force and throttle, which are indicators of distraction, were compared for each scenario. The severity with which participants hit the brakes demonstrated inattention to the road and taking the mind off the road.

Descriptive statistics were also obtained on pre-survey questionnaire data regarding participant characteristics. Some 43.8% of participants were male and 56.2% were female. The

age group of participants was: 42.4% between 18 to 25 years old; 18.2% between 26 to 35 years old; 18.2% between 36 to 45 years old; 18.2% between 46 to 65 years old; and 3% in more than 65 years old.

Additionally, the ethnicity (Figure 11), educational status (Figure 12), condition of employment (Figure 13), annual household income (Figure 14), were collected.

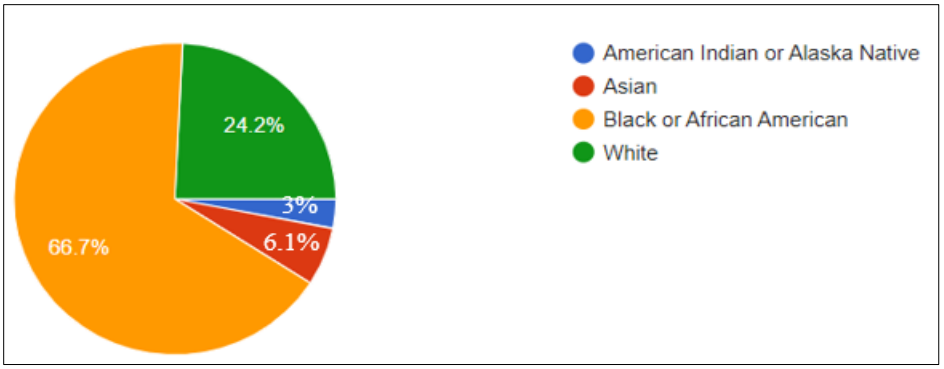

Figure 11 Ethnicity of the participants

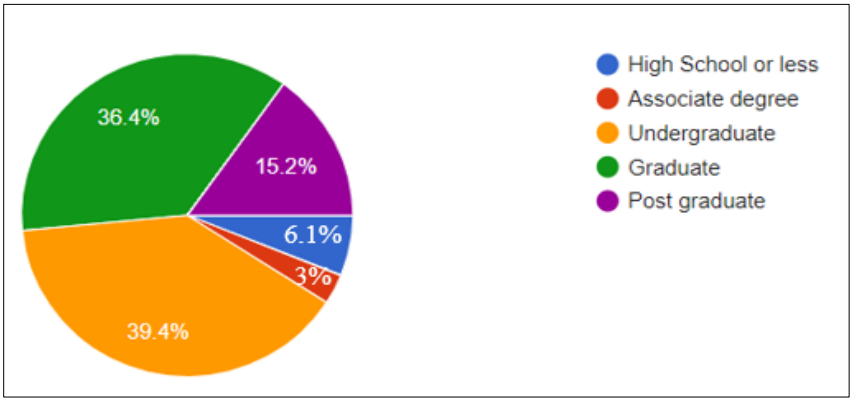

Figure 12 Educational status of participants

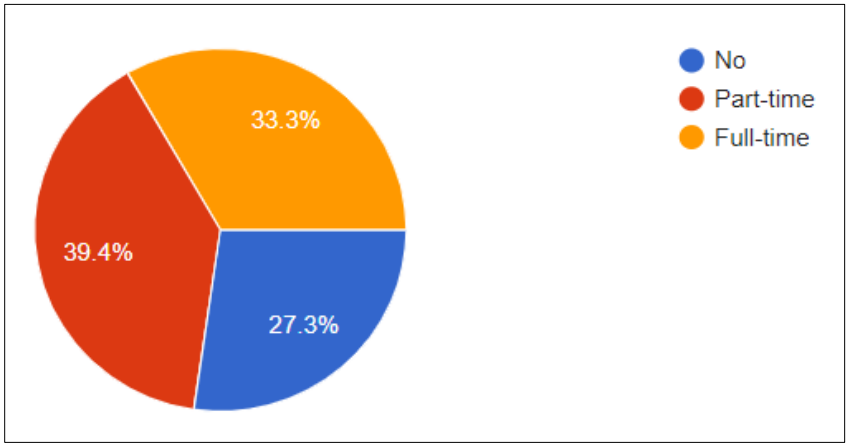

Figure 13 The participant's employment condition

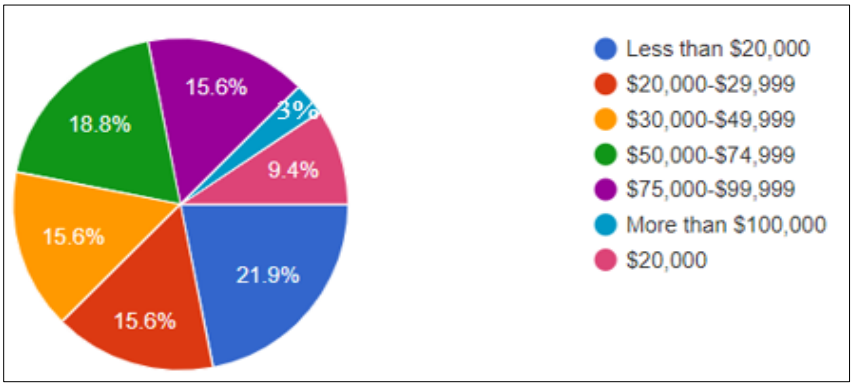

Figure 14 The participant's annual household income

Participants were classified to different sessions, each consisting of two participants with one riding the bike simulator and the other driving the car simulator. They then switched, and the participant who rode the bike simulator drove the car simulator and vice versa. Afterwards, we asked each participant to express his/her opinions regarding their perceived safety by selecting a number between 1 and 5. The descriptions of each value are shown in Table 5.

Table 5 Description of the safety of bike lane from participants' point of view

Number	1	2	3	4	5
Description	Pretty unsafe	unsafe	Not safe not unsafe	safe	Pretty safe

We asked the participants to consider the weather conditions and the number of other vehicles around the bike when judging the safety of the bike lane. A simple average was calculated for 33 obtained results. Table 6 shows the results of bike riders, and Table 7 shows the result of car drivers.

Table 6 Bike rider's opinion about the safety of the road (Average percentage - %)

Scenario	Pretty unsafe (1)	Unsafe (2)	Not safe and not unsafe (3)	Safe (4)	Pretty safe (5)
Scenario 1-1	0	21.2	21.2	24.2	33.3
Scenario 1-2	6.1	36.4	33.3	18.2	6.1
Scenario 2	0	27.3	24.2	39.4	9.1
Scenario 3	9.1	21.2	36.4	24.2	9.1
Scenario 4	0	39.4	24.2	30.3	6.1
Scenario 5	9.1	30.3	27.3	30.3	3
Scenario 6	9.1	27.3	33.3	24.2	6.1

Table 7 Car driver's opinion about the safety of the road (Average percentage - %)

Scenario	Pretty unsafe (1)	Unsafe (2)	Not safe and not unsafe (3)	Safe (4)	Pretty safe (5)
Scenario 1-1	0	9.1	24.2	36.4	30.3
Scenario 1-2	0	21.2	45.5	21.2	12.1
Scenario 2	0	15.2	27.3	48.5	9.1
Scenario 3	0	9.1	48.5	33.3	9.1
Scenario 4	0	15.2	33.3	36.4	15.2
Scenario 5	0	15.2	39.4	39.4	6.1
Scenario 6	3	15.2	33.3	42.4	6.1

In a post-survey questionnaire, six solutions proposed to improve the safety of bike lane were designed. Participants could choose up to three solutions. The bike lane was designed without any barriers or separate markings with a carriageway. The bike lane marking was designed in the software as shown in Figure 15. Bike route signs were located every 100m along the road.

Figure 15 The simulated cross section of the shared bike lane

Figure 16 shows the results of post-survey questionnaire:

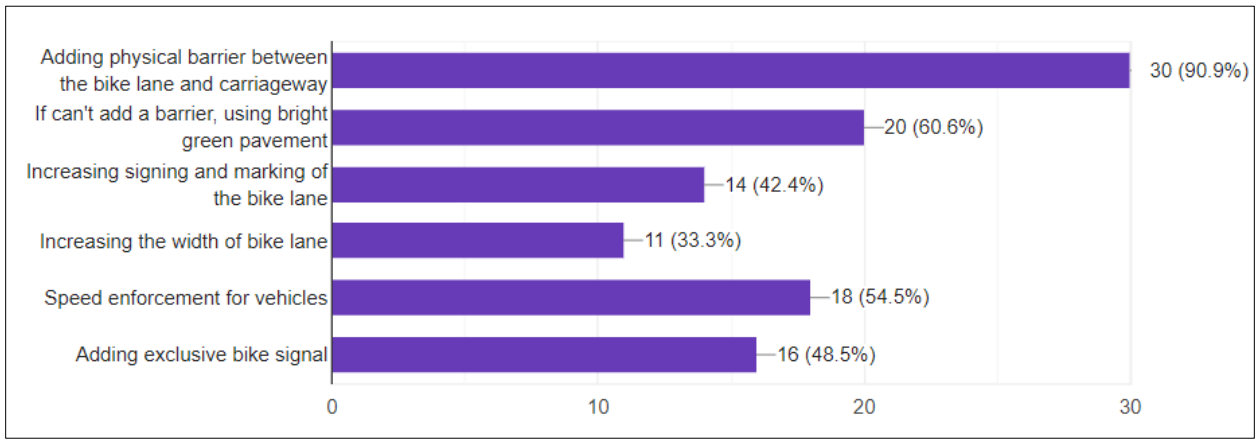

Figure 16 The participants' opinion regarding the improvement of the designed bike lane

As shown in Table 5 and Table 6, the safety of the designed bike lane was diminished when high traffic volume (500 veh/hour) was assigned on the network. As shown in Figure 16, adding physical barrier between the bike lane and carriageway (declared by 30 participants), using bright green pavement (declared by 20 participants), and providing speed enforcement (speeds less than 40 km/hour – declared by 18 participants) were three frequently-selected safety promotion solutions among participants.

5. VALIDATION OF FR CAR-FOLLOWING MODEL

5.1. Validation

In order to analyze the Fodholun-Rakha (FR) car-following model, the values of the following equations were obtained., the following variables are introduced:

n= the index of the lead vehicle

n+1= the index of the subject (following) vehicle

$X_{n+1} = position\ of\ the\ subject\ (following)\ vehicle$

$U_{n+1} = speed\ of\ the\ subject\ (following)\ vehicle,$

$U_n = speed\ of\ the\ lead\ vehicle$

$a_{n+1} = acceleration\ of\ the\ subject\ vehicle$

$u_f = the\ vehicle's\ desired\ speed\ (also\ known\ as\ the\ roadway\ free - flow\ speed)$=11.17m/se

$d_{desired} =\ a\ desired\ comfortable\ vehicle\ deceleration\ level\ (typically\ taken\ to\ be - 3\ m/s2)$

$S_{n+1} =\ the\ vehicle\ spacing\ from\ the\ back\ bumper\ of\ the\ subject\ vehicle\ to\ the\ back\ bumper\ of\ the\ lead\ vehicle$

$S_j = the\ vehicle\ spacing\ at\ a\ speed\ of\ zero\ (i.e., the\ jam\ density\ spacing)$

τ= $the\ driver's\ perception - reaction\ time$. The driver's perception-reaction time varies as a function of the roadway parameters ($u_f = 11.17\frac{m}{se}, u_c = 8.3775, q_c = 0.61, k_j = 0.1886$) and the vehicle's speed.

β = the gearshift impacts at low traveling speeds when trucks are accelerating. This factor is set to 1.0 for light duty vehicles.

η = the driveline efficiency (unitless)=0.9

P = the vehicle power (kW) = 381hp ~ (1hp=0.746 kw) = 284.2 kw

ɣ = a constant reduction factor of the vehicle power aiming to represent the throttle level (when the objective is to determine the maximum acceleration that a vehicle is able to achieve, the value of this factor is set equal to 1).

M_{ta} = the mass of the vehicle on the tractive axle (kg) =0.55*2700=1485kg

g = the gravitational acceleration (9.8067 m/s2)

μ = the coefficient of road adhesion or the coefficient of friction (unitless) = (air friction coefficient: 0.4)

ρ = the air density at sea level and a temperature of 15◦C (1.2256 kg/m3)

C_d = the vehicle drag coefficient (unitless), typically 0.30

C_h = the altitude correction factor equal to 1–0.000085 h where h is the altitude in meters (unitless)=1

A_f = the vehicle frontal area (m2), typically 0.85 multiplied by the height and width of the vehicle (height= 1.96m , width= 1.72m) □ 0.85*1.96*1.72 = 2.865m^2

C_{r0} = a rolling resistance constant that varies as a function of the pavement type and condition (unitless) =1.25

C_{r1} = the second rolling resistance constant (h/km) = 0.0328

C_{r2} = the third rolling resistance constant (unitless)= 4.575

M = the total vehicle mass (kg) (weight: 2700kg = 6000lb)

G = the roadway grade (unitless), Longitudinal slope

$f_p = the\ driver\ throttle\ input, the\ range\ is\ between\ 0.0\ and\ 1.0.$

The time headway ensures that the subject vehicle, n +1 follows its lead vehicle at a safe spacing in order to avoid a collision under state-state conditions (i.e., when both vehicles are traveling at the same constant velocity and assuming that the subject vehicle's deceleration maneuver starts τ seconds after the lead vehicle decelerates). [$S_{n+1}^{\sim} = s_j + \tau u_{n+1}$]

$$\tau = \frac{1}{k_{j^*} u_c^2}\left[\frac{k_{j^*} u_c^2}{q_c} - u_f + \frac{(u_f - u_c)^2}{u_f(u_f - u_{n+1})}\right] \quad (22)$$

If the lead vehicle is traveling at a higher velocity (non-steady-state conditions) then the desired safe following spacing can be computed by the following equation. This equation allows the driver to drive at a spacing less than the steady-state spacing when the vehicle ahead of it is driving at a higher speed. In equation (23), the following variables are considered:

$c_1 = 0.796, c_2 = 0.169, c_3 = 0.121$

$$S_{n+1}^{\sim} = \left(c_1 + \frac{c_2}{(u_f - u_n)} + c_3 u_n - \frac{u_{n+1}^2 - u_n^2 - \sqrt{(u_{n+1}^2 - u_n^2)^2}}{4d_{des}}, s_j\right) \quad (23)$$

The FR model includes two terms. The first term is the vehicle acceleration term, while the second term is the vehicle deceleration term. Both terms ensure that the vehicle does not collide with its lead vehicle.

$$a_{n+1} = f_p a_{max} + \frac{[u_{n+1}^2 - u_n^2 + \sqrt{(u_{n+1}^2 - u_n^2)^2}]^2}{16(d_{desired} + gG) * (s_{n+1} - s_j)^2} \quad (24)$$

$$f_p = e^{-aX_{n+1}}(1 - X_{n+1}^b e^{b(1-X_{n+1})})^d \quad (25)$$

$$X_{n+1} = \frac{\tilde{s_{n+1}}}{s_{n+1}} * \frac{u_{n+1}}{\tilde{u_{n+1}}} \quad (26)$$

$\tilde{S_{n+1}}$= the desired spacing for the current speed. This variable is acquired from equation (27):

$$\tilde{S_{n+1}} = s_j + \tau u_{n+1} \quad (27)$$

$\tilde{u_{n+1}}$ = the desired speed for the current spacing. This variable is calculated from equation (28).

$$U_{n+1}^{VA} = \frac{0.555 + S_{n+1} - \sqrt{(-0.556 - S_{n+1})^2 - 0.484 * (11.17 * S_{n+1} - 9.06)}}{0.242}$$

$$U_{n+1}^{VA} = \frac{0.555+S_{n+1}-\sqrt{(-0.556-S_{n+1})^2-(5.406*S_{n+1}-4.385)}}{0.242} \quad (28)$$

The acceleration, position, and speed of the user-vehicle in each time stamp is obtained by equations (31-33). In each time stamp, the Euler's method is followed to update the new speed and new position for the next time stamp. Based on Euler's method, the new position and speed are obtained by equations (29-30):

$$\mathrm{v}(t_2)=\mathrm{v}(t_1)+\mathrm{a}(t_1)*(t_2-t_1) \quad (29)$$
$$\mathrm{x}(t_2)=\mathrm{x}(t_1)+\mathrm{v}(t_1)*(t_2-t_1) \quad (30)$$

Variables like "a, b, and d" are model parameters that are calibrated to a specific driver and model the driver input to the gas pedal. The required parameters for FR model are the acceleration parameters: a, b, d, $d_{desired}$.

$$a_{max} = \frac{F_{n+1} - R_{n+1}}{M} \quad (31)$$

$$F_{n+1} = min\ (3600 * \frac{\eta \gamma \beta P}{u_{n+1}}, M_{ta} g \mu) \quad (32)$$

$$R_{n+1} = \frac{\rho C_d C_h A_f g u_{n+1}^2}{2} + MgC_{r0}(C_{r1}u_{n+1} + C_{r2}) + MgG \quad (33)$$

FR car-following model was calibrated for the scenarios 2, 3, 4, 5, 6. The user vehicle ($or\ following\ vehicle$) and front vehicle (lead vehicle) were investigated in each scenario. The "bike as the front vehicle" was excluded from the calibration analysis, meaning that the participants who follow the bike as the front (lead) vehicle was completely excluded. Table 8 shows the number of correct participants in each scenario for calibrating the FR car-following model. It is worth mentioning that 33 participants were recruited to drive the car simulator and ride the bike simulator in each scenario.

Table 8 Number of reliable participants after removing bike as the front vehicle

Scenario	Number of the correct participants
2	20
3	15
4	18
5	18
6	12

Equations (22-33) were rewritten as a MATLAB code. A reliable sample consisting of 100 values of (a,b,d) was determined to analyze the FR car-following model. The speed plots were drawn for each participant in each scenario. The obtained speed values from MATLAB code were compared to the collected speed values by the car simulator. Eventually, Root-mean-square (RMSE) was obtained for each pair of (a,b,d) for each participant in each scenario. RMSE is the standard deviation of the residuals (prediction errors). Residuals are a measure of how far from the regression line data points are; RMSE is a measure of how spread out these residuals are. In other words, it tells how concentrated the data is around the line of best fit. RMSE is calculated by equation (34):

$$RMSE = \sqrt{\frac{(\sum_{i=1}^{N}(x_{f_i} - x_{o_i})^2}{N}} \quad (34)$$

In equation (34), $(x_{f_i} - x_{o_i})$ is the difference of forecasts (expected values or unknown results; the obtained speed values from MATLAB code) from observed values (known results; the collected speed values by the car simulator), and N is the sample size.

5.2. Discussion

As shown in Table 8, a total 83 reliable participants were obtained to validate the FR car-following model. In each scenario, the speed-time chart obtained by MATLAB code (consisting of equations 22-33) and the speed collected by the car simulator were drawn. It is worth noting that the time intervals for each participant may be different from one another since the values recorded when the bicycle was the front vehicle were excluded from the data analysis. Diverse time intervals were therefore seen for each participant when the front (lead) vehicle was not a bicycle. As mentioned before, a consistent sample including 100 (a,b,d) values was selected to run the FR car-following model for each participant in each scenario. Each (a,b,d) pair was utilized to run the MATLAB code. Position, speed, and acceleration were then obtained. After finding position, speed, and acceleration values, equation 34 was used to calculate the RMSE. In total, 100 RMSEs were obtained for each participant in each scenario. Respectively, 2000, 1500, 1800, 1800, and 1200 RMSEs were obtained in scenarios 2, 3, 4, 5, 6.

The smallest RMSE was selected for each participant in each scenario. Finally, 20, 15, 18, 18, and 12 smallest RMSEs were selected for statistical analysis. Subsections 4.2.1 to 4.2.5 explain the smallest RMSE values in scenarios 2 to 6. Scenario 1 was designed to evaluate the performance

of bicycles on the road. In scenario 1, no interaction between the car and the bike was applied. Nevertheless, this scenario is excluded from the RMSE computational analysis.

5.2.1. Scenario 2

The second scenario stated that the bike is ahead of the car, and that the bike stops before the signalized intersection. Table 9 shows the obtained results of the smallest RMSEs for each participant.

Table 9 Smallest RMSEs in Scenario 2

Participant ID #	Smallest RMSE (x)	Normal distribution
1201	7.9	0.0442
1202	8.9	0.0492
1204	11.0	0.0578
1209	9.9	0.0539
1212	13.8	0.0608
1216	29.3	0.0028
1218	4.0	0.0227
1220	7.2	0.0402
1221	9.2	0.0508
1223	15.1	0.0586
1224	19.1	0.0404
1228	14.9	0.0589
1230	13.6	0.0610
1231	3.0	0.0182
1235	20.9	0.0304
1236	21.8	0.0255
1239	12.0	0.0601
1243	9.9	0.0540
1245	4.9	0.0272
1247	18.2	0.0453

As shown in Table 9, the RMSE of participant 1231 (RMSE=3) was selected as the smallest RMSE. Mean (=13.15), variance (=42.61), and standard deviation (=6.52) were acquired for Table 9. The bell-shaped standard normal distribution chart for Table 9 is shown in Figure 17.

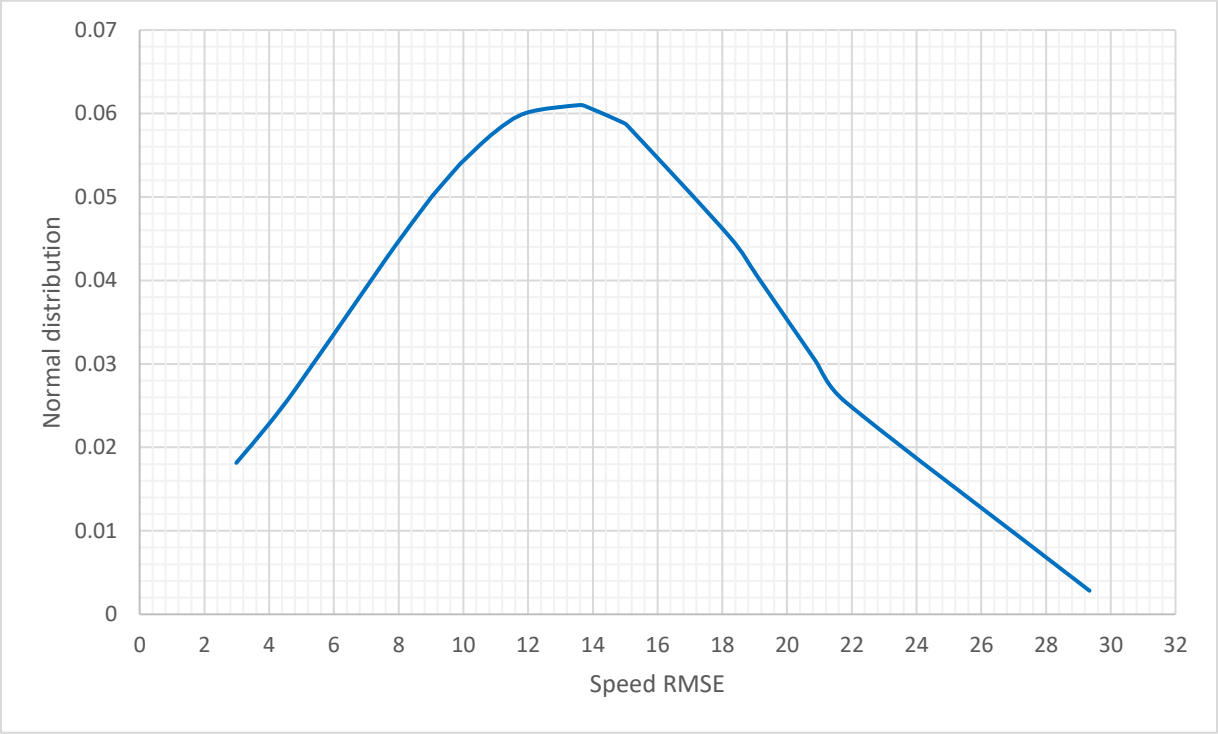

Figure 17 Standard normal distribution chart in scenario 2

The speed trajectory for participant #1231 is shown in Figure 18.

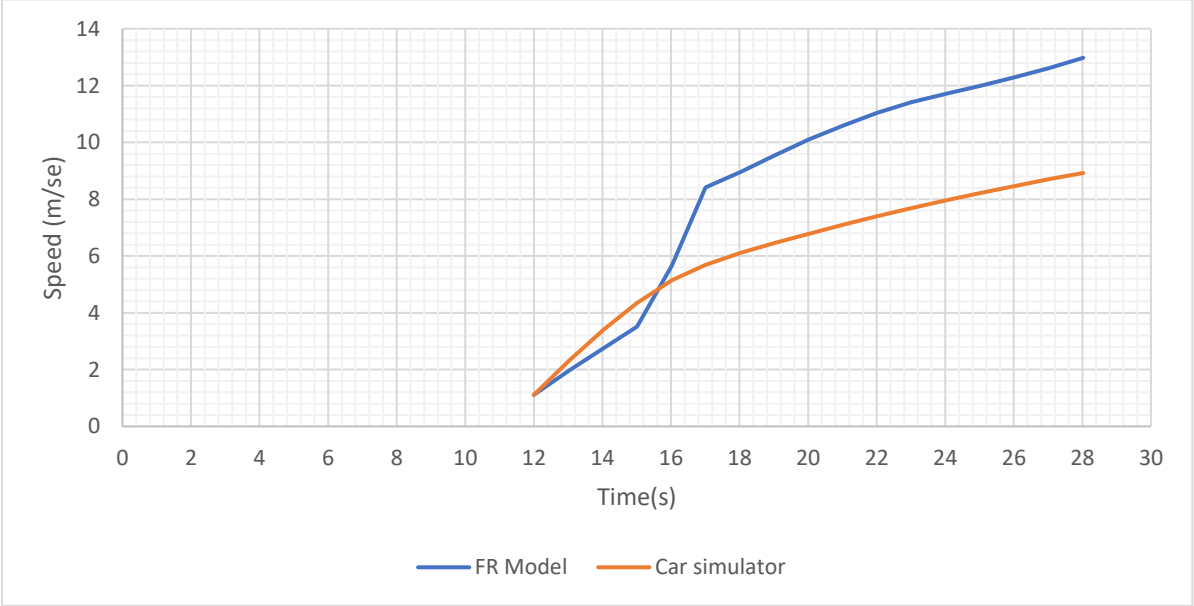

Figure 18 Speed trajectory (RMSE=3) in scenario 2

Figure 18 shows that the obtained speed changes by FR car-following model (MATLAB code) were greater than the values of collected speeds by car simulator. The FR model's speeds experienced a considerable jump after the 16th event. Furthermore, mean (=8.63), variance

(=4.79), and standard deviation (=2.19) were obtained for the smallest RMSE in scenario 2. Figure 19 shows the acceleration trajectory for the smallest RMSE in scenario 2.

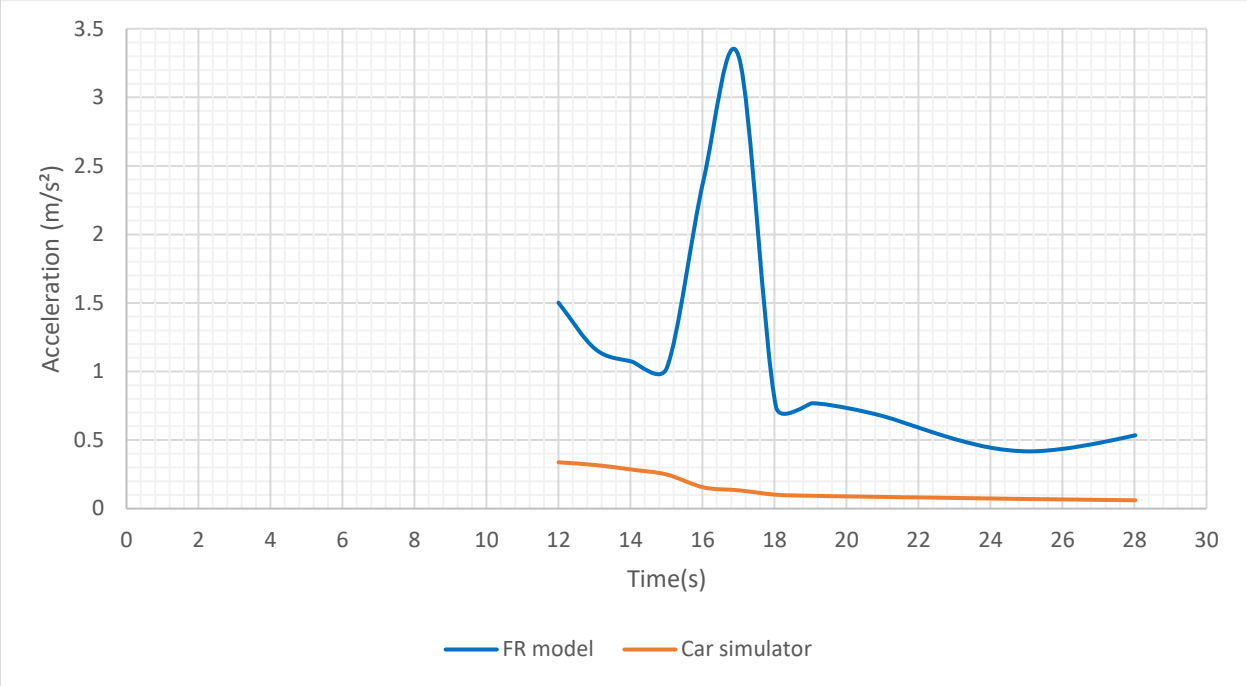

Figure 19 Acceleration trajectory of the smallest RMSE in scenario 2

5.2.2. Scenario 3

In the third scenario, the bike was positioned in front of the car. Bikes and cars were run from 492 ft (150m) before the signalized intersection to 492 ft (150m) after the signalized intersection. The bike had to pass the intersection, and both the bike and the car had to stop after the signalized intersection. Table 10 shows the obtained results of the smallest RMSEs for each participant in the third scenario. As shown in Table 10, the RMSE of participant 1246 (RMSE=3.6) was selected as the smallest RMSE. Mean (=12.32), variance (=51.62), and standard deviation (=7.18) were procured for Table 10. The bell-shaped standard normal distribution chart for Table 10 is shown in Figure 20.

Table 10 Smallest RMSEs in Scenario 3

Participant ID #	Smallest RMSE (x)	Normal distribution
1203	4.6	0.0313
1204	17.9	0.0411
1206	19.2	0.0351
1209	11.4	0.0551
1220	6.3	0.0389
1224	17.3	0.0437
1228	11.4	0.0551
1230	6.6	0.0406
1236	6.5	0.0398
1239	5.3	0.0344
1242	13.8	0.0544
1243	31.5	0.0016
1244	15.0	0.0517
1246	3.6	0.0267
1247	9.7	0.0521

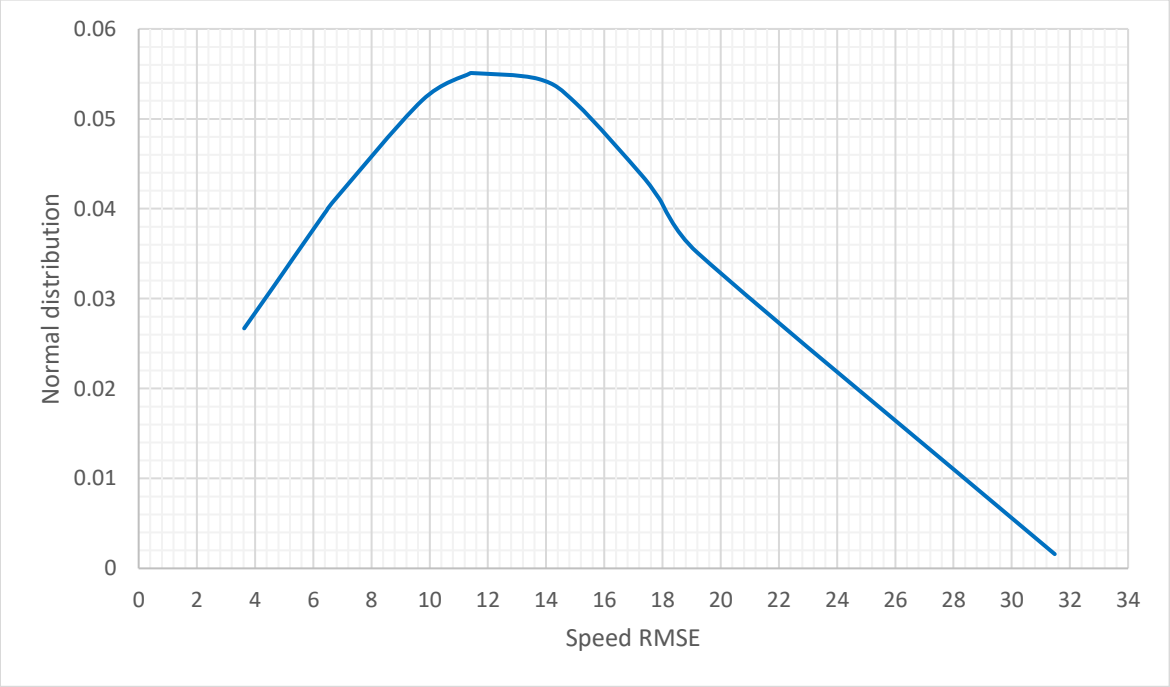

Figure 20 Standard normal distribution chart in scenario 3

The speed trajectory for participant #1246 is shown in Figure 21.

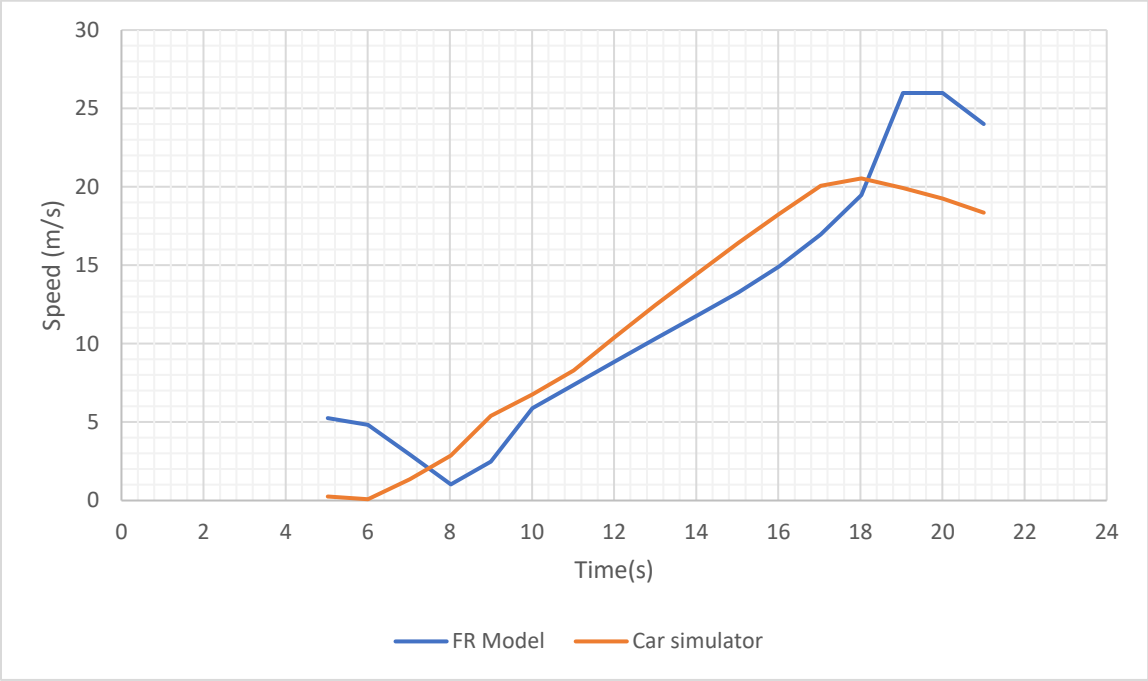

Figure 21 Speed trajectory (RMSE=3.6) in scenario 3

As shown in Figure 21, the speed values obtained by the FR model is less than the speed values by collected by the car simulator after the 7th event. The FR speed chart experienced a sharp jump in the 17th event and were greater than speed values collected by the car simulator. Additionally, mean (=11.84), variance (=4.47), and standard deviation (=2.17) were obtained for the smallest RMSE in scenario 3. Figure 22 shows the acceleration trajectory for the smallest RMSE in scenario 3.

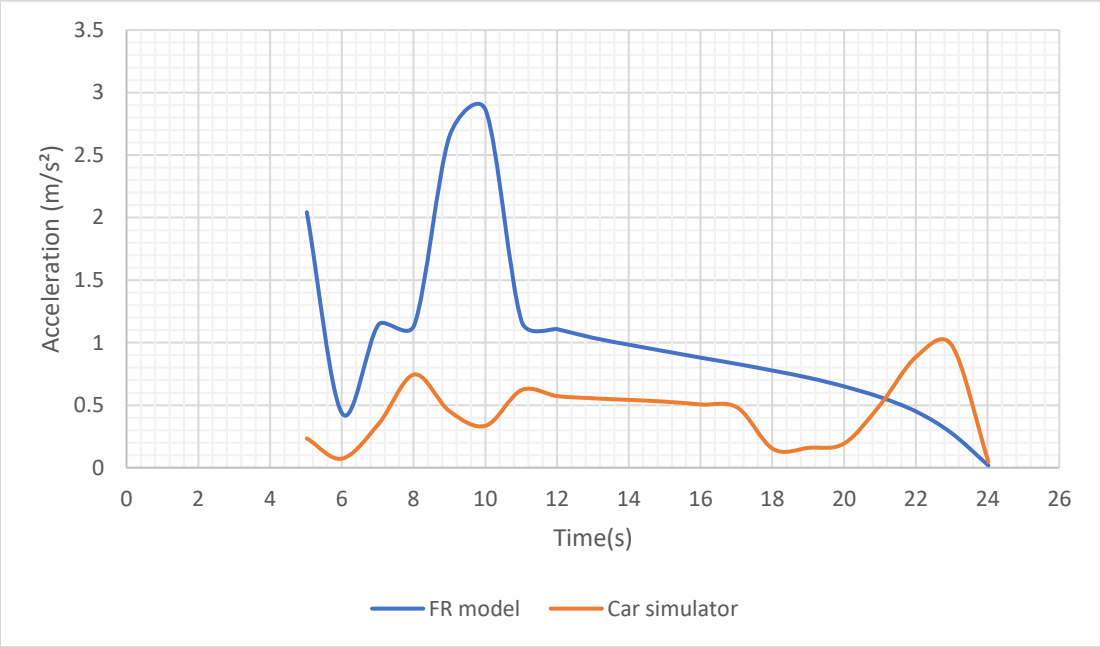

Figure 22 Acceleration trajectory of the smallest RMSE in scenario 3

5.2.3. Scenario 4

Scenario 4 declared that the bike is behind the car and that the bike must stop before the signalized intersection. Table 11 shows the obtained results of the smallest RMSEs for each participant in the fourth scenario. As shown in Table 11, the RMSE of participant 1236 (RMSE=1.3) was selected as the smallest RMSE. Mean (=7.73), variance (=24.22), and standard deviation (=4.92) were obtained for Table 11. The bell-shaped standard normal distribution chart for Table 11 is shown in Figure 23.

Table 11 Smallest RMSEs in Scenario 4

Participant ID #	Smallest RMSE (x)	Normal distribution
1201	5.5	0.0734
1206	22.6	0.0008
1210	3.9	0.0598
1212	8.2	0.0807
1218	6.3	0.0778
1220	5.9	0.0753
1221	5.6	0.0735
1222	8.0	0.0809
1223	14.6	0.0304
1224	10.1	0.0721
1233	3.6	0.0567
1236	1.3	0.0346
1242	9.2	0.0773
1244	7.6	0.0810
1245	4.5	0.0655
1246	3.0	0.0513
1247	2.7	0.0480
1250	8.5	0.0802

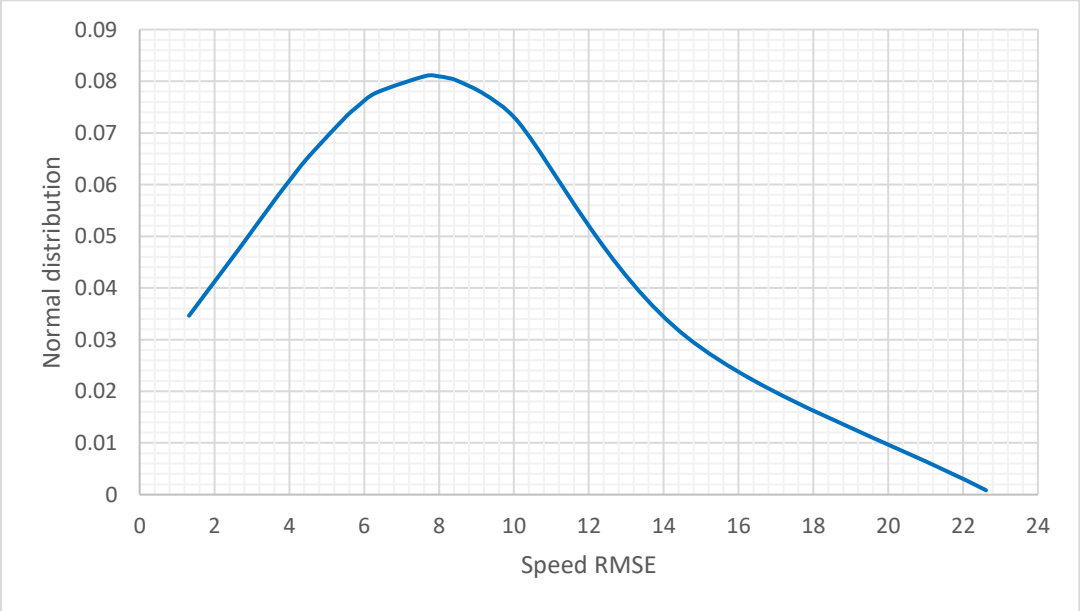

Figure 23 Standard normal distribution chart in scenario 4

The speed trajectory for participant #1236 is shown in Figure 24.

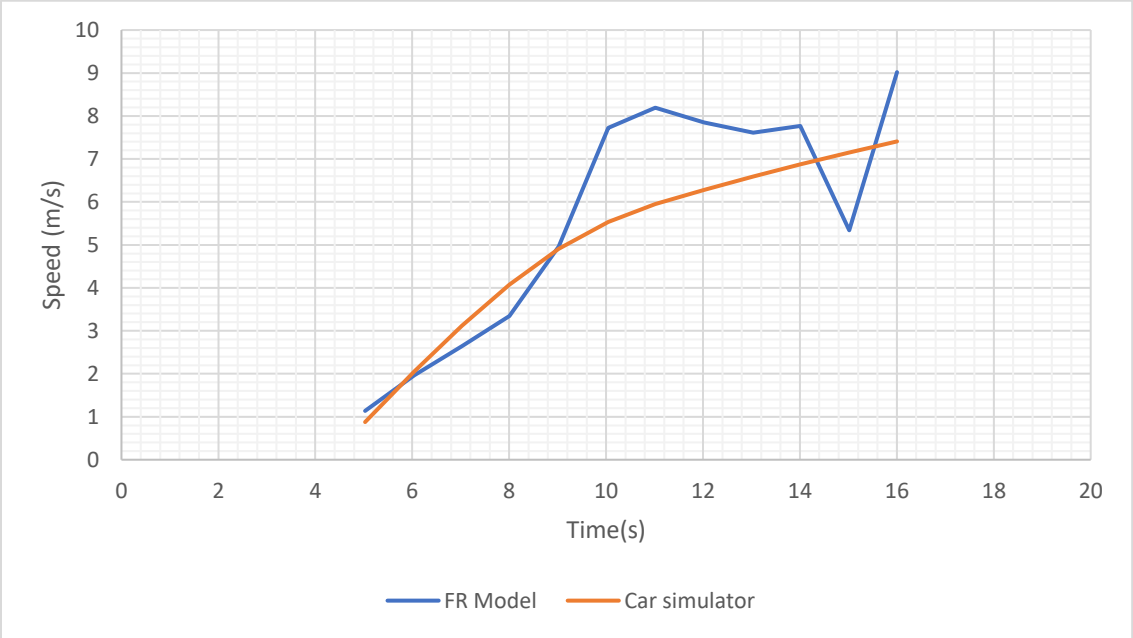

Figure 24 Speed trajectory (RMSE=1.3) in scenario 4

As shown in Figure 24, the speed values collected by the FR model were less than those collected by the car simulator from the 6th to 9th events, and in the 15th event. Speed values collected by the FR model also experienced an ascending slope from the 9th to 14th event, and the speed trajectory collected by the car simulator experienced a mild ascending slope from the 5th to 16th event. Moreover, mean (=5.6), variance (=1.55), and standard deviation (=1.24) were obtained for the smallest RMSE in scenario 4. Figure 25 shows the acceleration trajectory for the smallest RMSE in scenario 4.

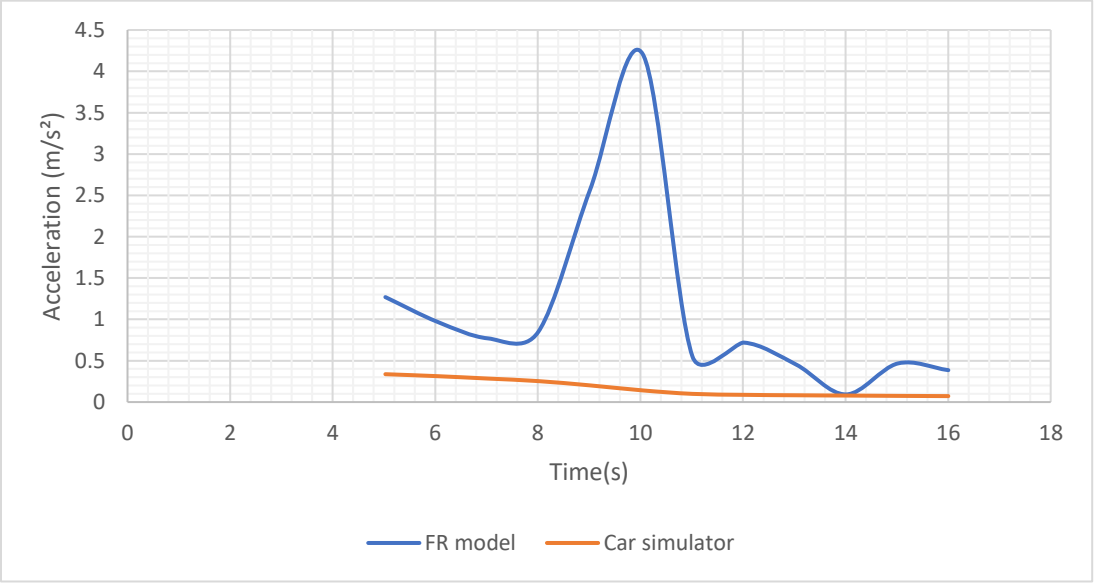

Figure 25 Acceleration trajectory of the smallest RMSE in scenario 4

5.2.4. Scenario 5

Scenario 5 is nearly identical to scenario 3, however the bike is positioned behind the car. Table 12 shows the obtained results of the smallest RMSEs for each participant in scenario 5. As shown in Table 12, the RMSE of participant 1231 (RMSE=1.9) was selected as the smallest RMSE. Mean (=6.61), variance (=10.04), and standard deviation (=3.17) were gained for Table 12. The bell-shaped standard normal distribution chart for Table 12 is shown in Figure 26.

Table 12 Smallest RMSEs in Scenario 5

Participant ID #	Smallest RMSE (x)	Normal distribution
1201	5.3	0.1108
1202	7.5	0.1119
1203	5.1	0.1091
1205	5.1	0.1087
1209	13.6	0.0124
1218	6.1	0.1171
1220	3.6	0.0823
1222	3.9	0.0317
1223	2.1	0.0525
1231	1.9	0.0488
1233	8.5	0.0975
1235	6.3	0.1176
1239	7.3	0.1140
1242	5.8	0.1160
1243	5.3	0.1113
1244	8.8	0.0928
1245	7.4	0.1134
1247	13.4	0.0139

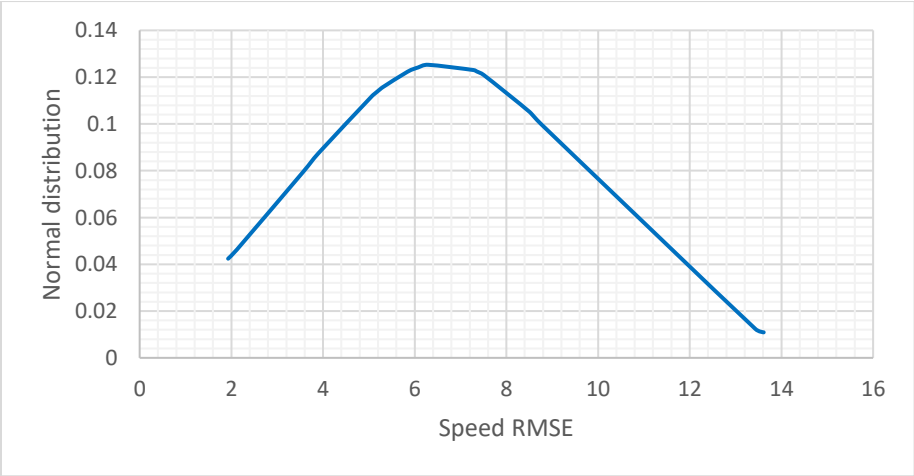

Figure 26 Standard normal distribution chart in scenario 5

The speed trajectory for participant #1231 is shown in Figure 27.

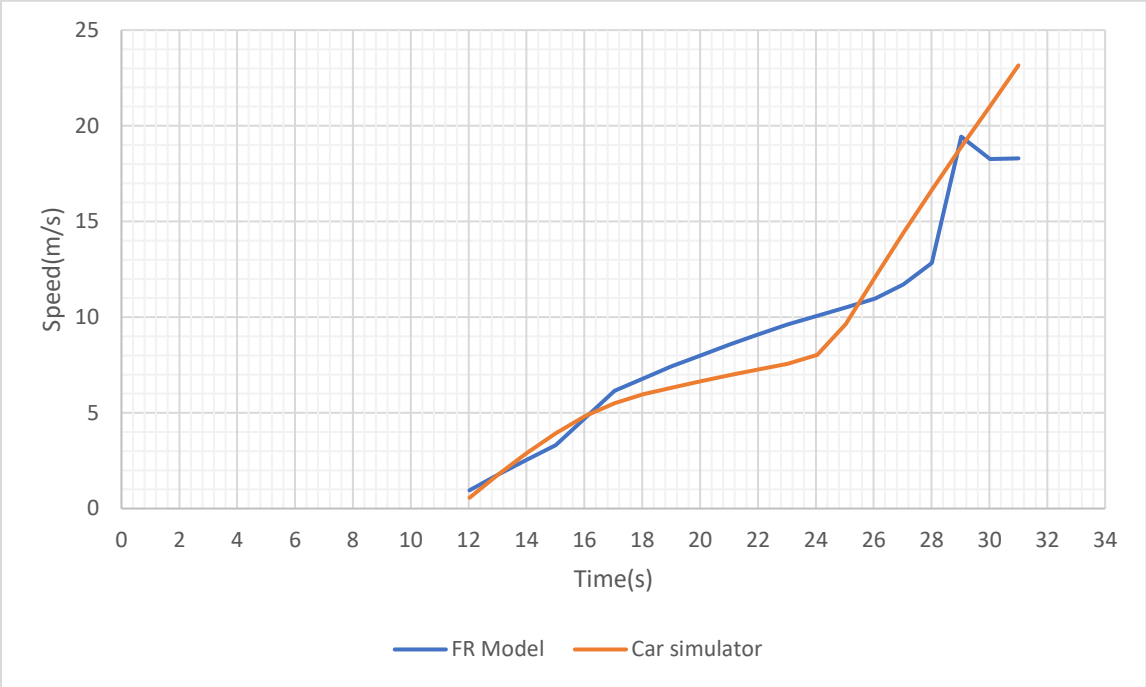

Figure 27 Speed trajectory (RMSE=1.9) in scenario 5

As shown in Figure 27, the speeds obtained by the FR model are less than those collected by the car simulator in the 12th to 16th events, and the 25th to 31st events. Both trajectories experienced a mild ascending slope from events 16 to 25. Mean (=9.1), variance (=1.31), and standard deviation (=1.14) were obtained for the smallest RMSE in scenario 5. Goodness of fit for participant 1231 was calculated as 0.997, showing how well sample data resembles a normal distribution. Figure 28 shows the acceleration trajectory for the smallest RMSE in scenario 5.

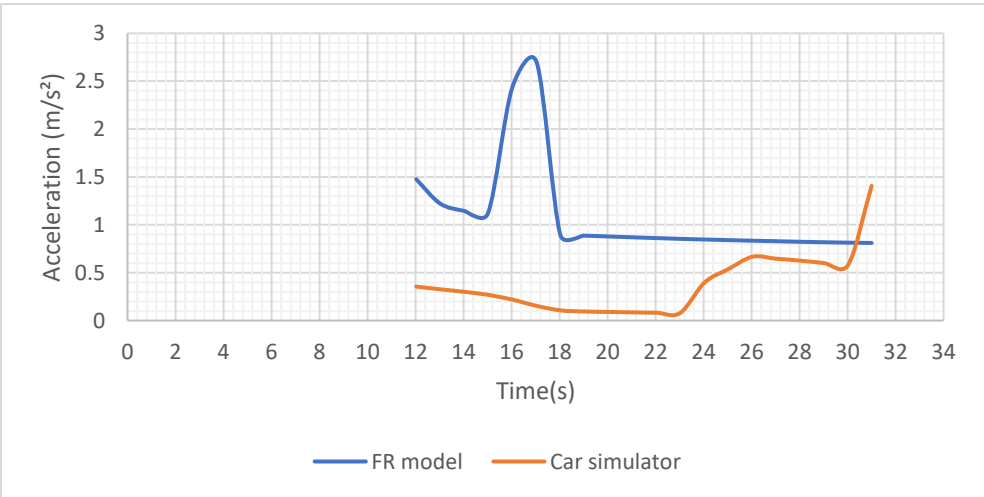

Figure 28 Acceleration trajectory of the smallest RMSE in scenario 5

5.2.5. Scenario 6

Scenario 6 states that the car must turn right in the intersection, the bike is ahead of the car, and the bike must go straight until it passes the signalized intersection. This scenario was designed to investigate the performance of car drivers when interacting with bicyclists at signalized intersections. In the sixth scenario, bicyclists started riding straight and the car driver started to turn right from west bound to south bound. A conflict was seen at the middle of the intersection between car drivers and bicyclists, although most participants respected bicyclists' right-of-way in the conflict area. The confliction area is shown in Figure 29.

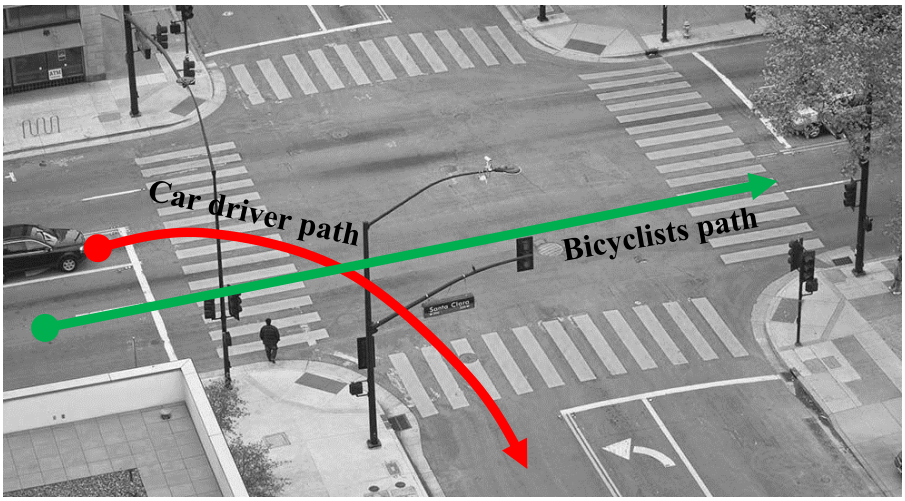

Figure 29 Conflict area

Table 13 shows the obtained results of the smallest RMSEs for each participant in scenario 6. As shown in Table 13, the RMSE of participant 1239 (RMSE=2.4) was selected as the smallest RMSE. Mean (=9.3), variance (=35.98), and standard deviation (=5.99) were acquired for Table 13. The bell-shaped standard normal distribution chart for Table 13 is shown in Figure 30.

Table 13 Smallest RMSEs in Scenario 6

Participant ID #	Smallest RMSE (x)	Normal distribution
1201	5.2	0.0526
1209	15.7	0.0378
1216	12.2	0.0594
1218	4.0	0.0452
1220	16.0	0.0358
1223	17.3	0.0276
1229	4.0	0.0449
1233	5.8	0.0560
1235	6.0	0.0573
1239	2.4	0.0342
1242	3.2	0.0397
1247	18.5	0.0205

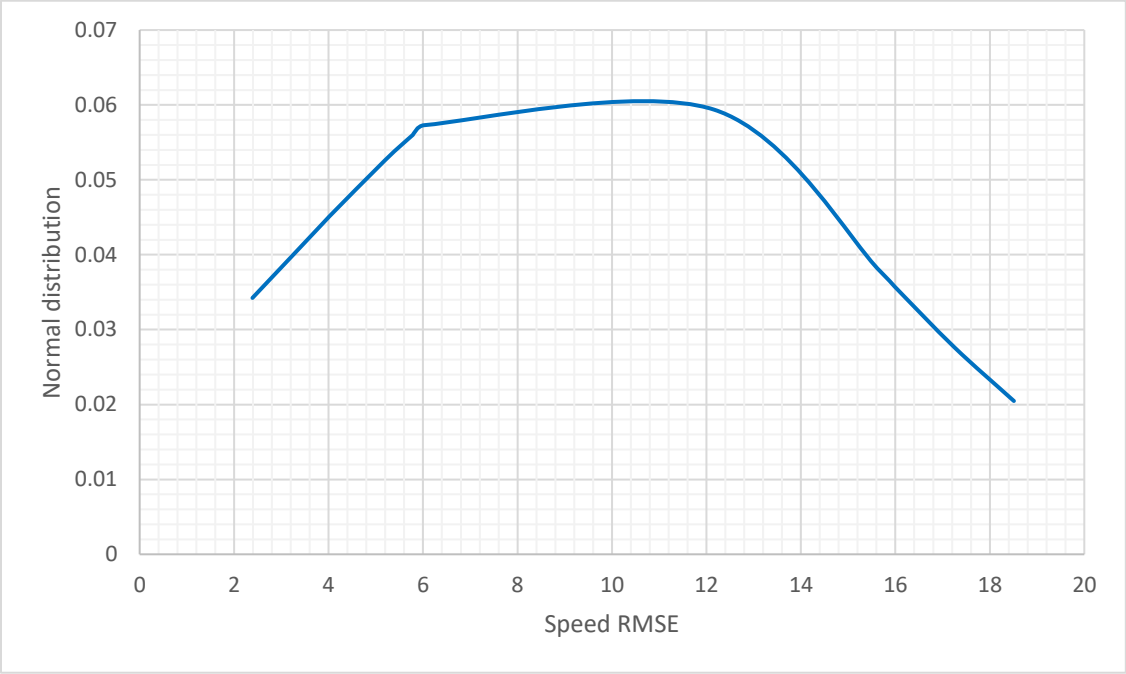

Figure 30 Standard normal distribution chart in scenario 6

The speed trajectory for participant #1239 is shown in Figure 31.

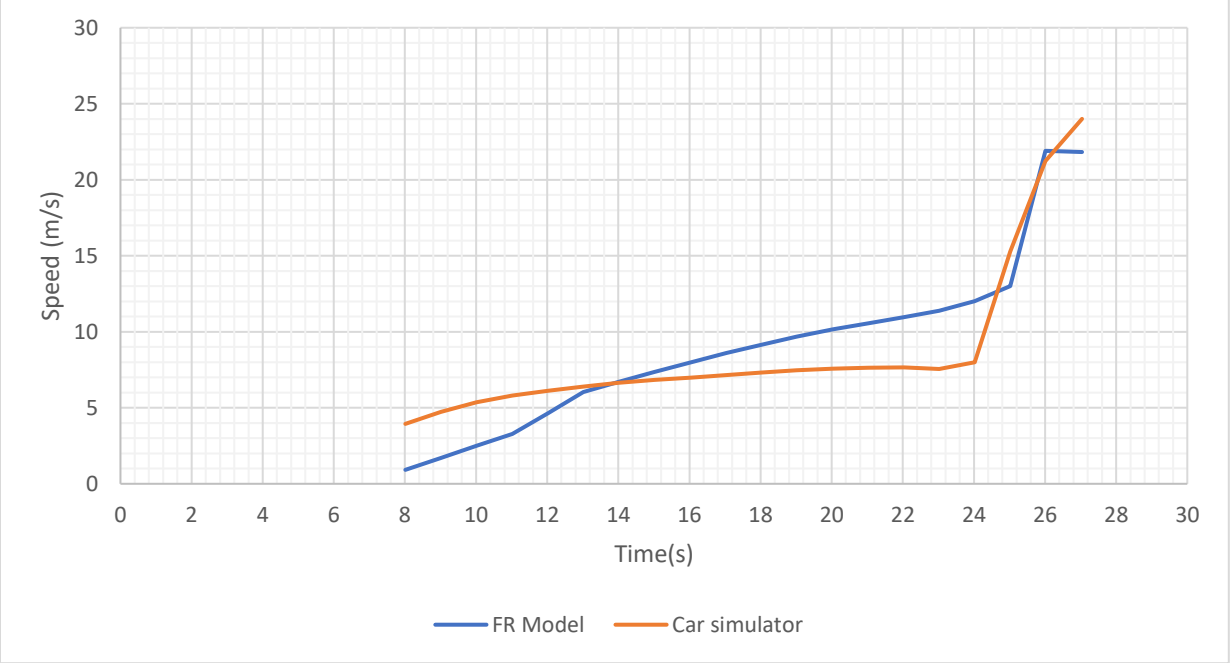

Figure 31 Speed trajectory (RMSE=2.4) in scenario 6

Figure 31 shows that the FR model speed values are less than the car simulator speed values in the8th to 13th and 25th to 27thevents. The FR model speed values experienced an ascending mild slope from the 13th to 25th events, while the car simulator speed values experienced a nearly

constant slope in this time interval. The mean (=9.01), variance (=4.12), and standard deviation (=2.03) were obtained for the smallest RMSE in scenario 6. Figure 32 shows the acceleration trajectory for the smallest RMSE in scenario 6.

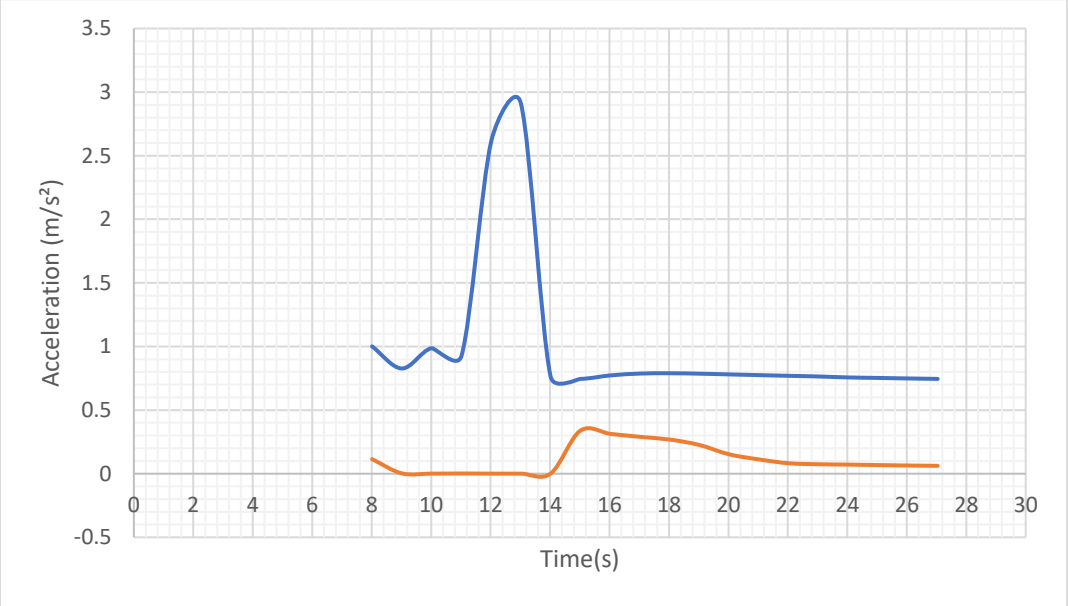

Figure 32 Acceleration trajectory of the smallest RMSE in scenario 6

5.3. Optimal "a, b, and d" model parameters (the driver input to the gas pedal)

The smallest RSMEs in each scenario identified to detect the optimum model parameters. These three values are parameters that are calibrated to a specific driver and model the driver input to the gas pedal. The smallest RMSE in each scenario was scrutinized, and the optimum model parameters for participants #1231 in scenario 2, #1246 in scenario 3, #1236 in scenario 4, #1231 in scenario 5, and #1239 in scenario 6 were specified. Table 14 shows the optimum model parameters.

Table 14 Optimal model parameters (a,b,d)

Scenario	RMSE	Optimal model parameters		
		a	b	d
2	3.0	1.796533695	0.292836385	0.400371922
3	3.6	1.357236292	0.083090091	0.254186277
4	1.3	0.982307127	0.255301632	0.389939398
5	1.9	1.529238754	0.0391814	0.223062249
6	2.4	1.110173497	0.059169787	0.234473687

6. VALIDATION OF FR BICYCLE-FOLLOWING MODEL

In a similar fashion to the previous section, we propose here to validate the FR bicycle-following model using the bicycle simulator data. To achieve that, a certain number of inputs is needed. These parameters are fixed for the different trajectories to maintain the homogeneity of driver behavior and road facilities across all events. They include the free-flow speed (u_f), which was set to the speed limit of the roadway for bicycles at 5.55 m/s along with other variables related to the roadway, such as the speed-at-capacity ($u_c = 3.88$ m/s), the roadway capacity ($q_c = 0.67 bic/s$), and the jam density ($k_j = 0.45\ bic/m$). Additionally, certain parameters that are specific to the bicyclist and the bicycle are defined. These include their respective weights taken equal to 75 kg and 7.5 kg. Other parameter definitions are as follows: η_{eff} is the efficiency of the bicycle chain (0.95 unitless); η_{gear} is the gear efficiency (0.65 unitless); m_{ta} is the mass of the vehicle on the tractive axle (60% of the total mass of the bicyclist and the bicycle in kg); g is the gravitational acceleration (9.8067 m/s^2); μ is the coefficient of road adhesion or the coefficient of friction (0.8 unitless); ρ is the air density at sea level and a temperature of 15°C (1.2256 kg/m^3); C_d is the vehicle drag coefficient (unitless), typically 0.80; A_f is the vehicle frontal area (m^2), typically 0.5 multiplied by the height and width of the bicyclist and bicycle system; C_{rr} is a rolling resistance constant that varies as a function of the pavement type and condition (0.004 unitless); and the desired deceleration level d_{des} is equal to 1.5 m/s^2. Finally, the cyclist is assumed to be an untrained male resulting in P_{ftp} being equal to 2.04 W/kg.

The remaining input variables (g_1, g_2, g_3) consist of model-specific parameters that require calibration depending on the researcher's objectives. Since this study aims to validate the FR bicycle-following model by evaluating its performance to match the collected bicycle simulator data, the different parameters need to be calibrated such that the resulting simulated behavior of the bicycle matches its observed behavior as closely as possible. The calibration procedure of the different parameters of each model was conducted heuristically taking the speed RMSE as the error objective function (the same function used to calibrate the car-following model in the previous section). A total of 233 trajectories dispersed over the seven defined scenarios were selected for the calibration procedure. Furthermore, it is noteworthy that we opted to calibrate the model separately for each trajectory rather than for the dataset as a whole. Even though that exponentially increased the computation time, the model was allowed to propose its best possible fit for each of the 233 events. Finally, the calibration procedure was conducted heuristically using a feasible region comprising a total of 200000 value combinations for the optimized parameters (g_1, g_2, g_3).

Having access to the calibrated parameters, the optimal simulated speed profiles were obtained for each bicycle trajectory. The corresponding speed outputs ensure the smallest RMSE between the FR model's predictions and the observed data over its whole timespan. The detailed results are presented in Table 15 along with metrics about the mean, median, and standard deviation for each of the considered scenarios as well as the aggregated data. Quantitatively speaking, the magnitude of the resulting RMSE values confirm the success of the FR model in

terms of replicating the observed behavior. In fact, the observed RMSE values never exceeded 0.18 across all trajectories with a mean of 0.036 and a standard deviation of 0.07.

Table 15 RMSE values for the different scenarios

Participant	***Scenario***						
	1-a	*1-b*	*2*	*3*	*4*	*5*	*6*
Participant 1201	0.017	0.012	0.022	0.016	0.027	0.015	0.013
Participant 1202	0.056	0.022	0.029	0.032	0.022	0.033	0.049
participant 1203	0.025	0.096	0.024	0.021	0.057	0.021	0.036
Participant 1204	0.179	0.034	0.044	0.039	0.043	0.024	0.085
Participant 1205	0.025	0.029	0.027	0.019	0.018	0.067	0.027
Participant 1206	0.014	0.035	0.027	0.016	0.040	0.021	0.016
Participant 1209	0.036	0.029	0.021	0.017	0.045	0.022	0.023
Participant 1210	0.025	0.023	0.043	0.019	0.025	0.020	0.037
Participant 1212	0.018	0.036	0.055	0.022	0.048	0.027	0.031
Participant 1216	0.033	0.054	0.057	0.038	0.056	0.037	0.053
Participant 1218	0.015	0.019	0.027	0.022	0.019	0.026	0.016
Participant 1220	0.053	0.168	0.109	0.017	0.028	0.015	0.060
Participant 1221	0.017	0.015	0.026	0.017	0.017	0.015	0.017
Participant 1222	0.044	0.036	0.045	0.014	0.043	0.012	0.055
Participant 1223	0.022	0.012	0.031	0.039	0.058	0.039	0.021
Participant 1224	0.042	0.021	0.031	0.053	0.032	0.038	0.030
Participant 1228	0.040	0.038	0.047	0.032	0.036	0.040	0.032
Participant 1229	0.024	0.015	0.031	0.022	0.184	0.020	0.010
Participant 1230	0.019	0.017	0.022	0.023	0.022	0.015	0.026
Participant 1231	0.012	0.016	0.024	0.010	0.027	0.020	0.019
Participant 1233	0.043	0.017	0.031	0.038	0.033	0.013	0.035
Participant 1235	0.018	0.017	0.024	0.014	0.014	0.023	0.012
Participant 1236	0.016	0.169	0.043	0.009	0.026	0.009	0.027
Participant 1239	0.047	0.062	0.042	0.082	0.045	0.090	0.025
Participant 1241	0.015	0.020	0.023	0.023	0.026	0.019	0.029
Participant 1242	0.032	0.022	0.020	0.018	0.025	0.032	0.026
Participant 1243	0.036	0.064	0.021	0.057	0.087	0.014	0.025
Participant 1244	0.006	0.036	0.043	0.031	0.022	0.020	0.025
Participant 1245	0.008	0.015	0.017	0.014	0.072	0.013	0.019
Participant 1246	0.036	0.020	0.030	0.019	0.022	0.023	0.015
Participant 1247	0.022	0.017	0.030	0.012	0.022	0.016	0.013
Mean	***0.032***	***0.038***	***0.034***	***0.026***	***0.040***	***0.026***	***0.029***
Median	***0.025***	***0.022***	***0.030***	***0.021***	***0.028***	***0.021***	***0.026***
Std Dev	***0.030***	***0.039***	***0.017***	***0.016***	***0.032***	***0.017***	***0.016***

To illustrate the results, the probability distribution of the speed RMSE of the different trajectories is plotted in Figure 33. The figure demonstrates the FR model's good performance in terms of fitting the observed data. That is demonstrated by the fact that its RMSE distribution is geared towards the lower end of the speed errors (between 0 and 0.03).

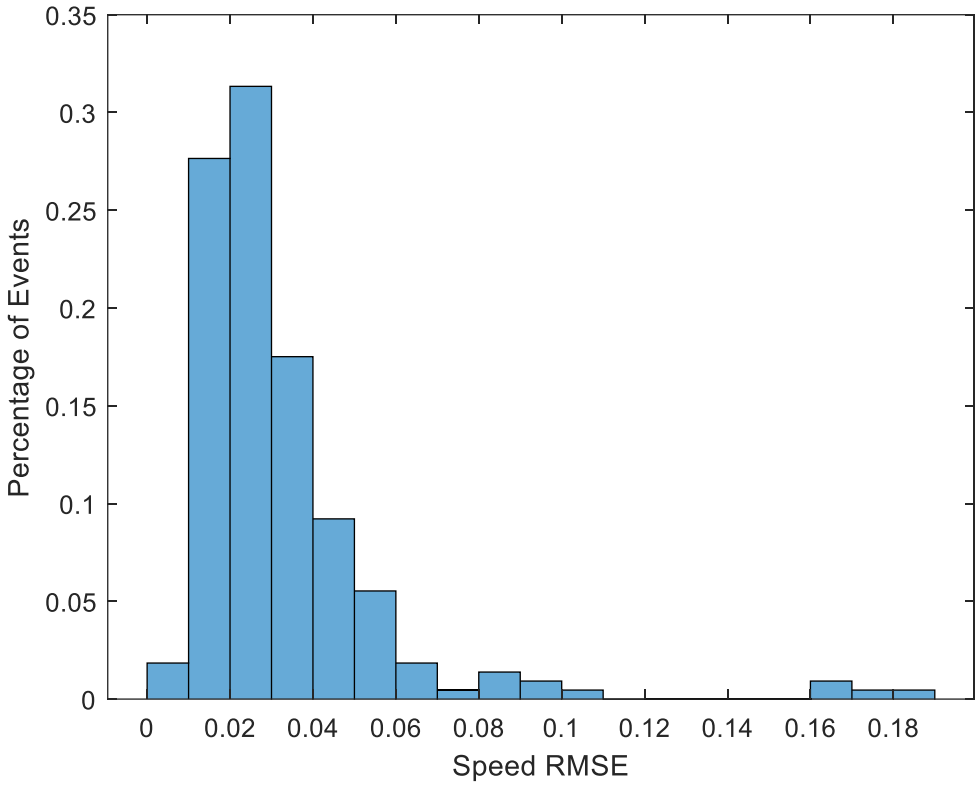

Figure 33 Probability distribution of the speed RMSE for the different models

In order to examine the performance of the different models qualitatively, the resulting simulated speeds are presented for some sample trajectories. In fact, Figure 34 to Figure 39 plots the variation of the observed and simulated speed profiles for seven different events over time (one from each scenario). For each event, the results from the FR model is drawn in order to compare its predictions with the observed bicycle simulator behavior. The figures confirm that the empirical behavior was well-captured in all the presented events. That is further confirmed by looking at the time-space diagrams of Figure 40 and Figure 41, which illustrate the overlap between the simulated and empirical trajectories. In all these figures, the observed trajectory is plotted in blue while the simulated trajectory is drawn in red.

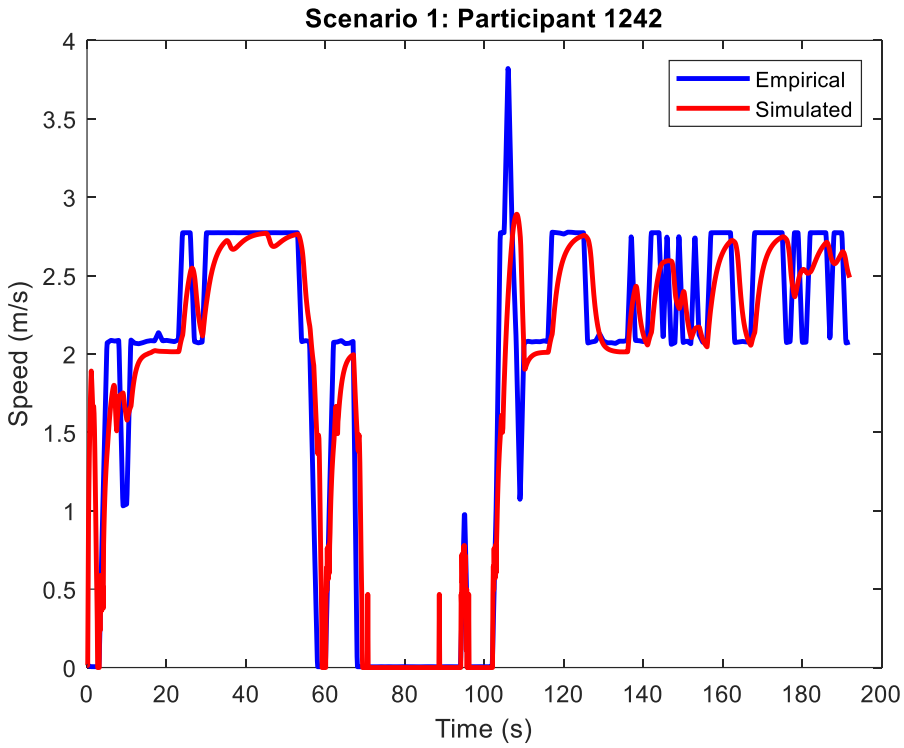

Figure 34 Speed profile: Scenario 1.a, Participant 1242

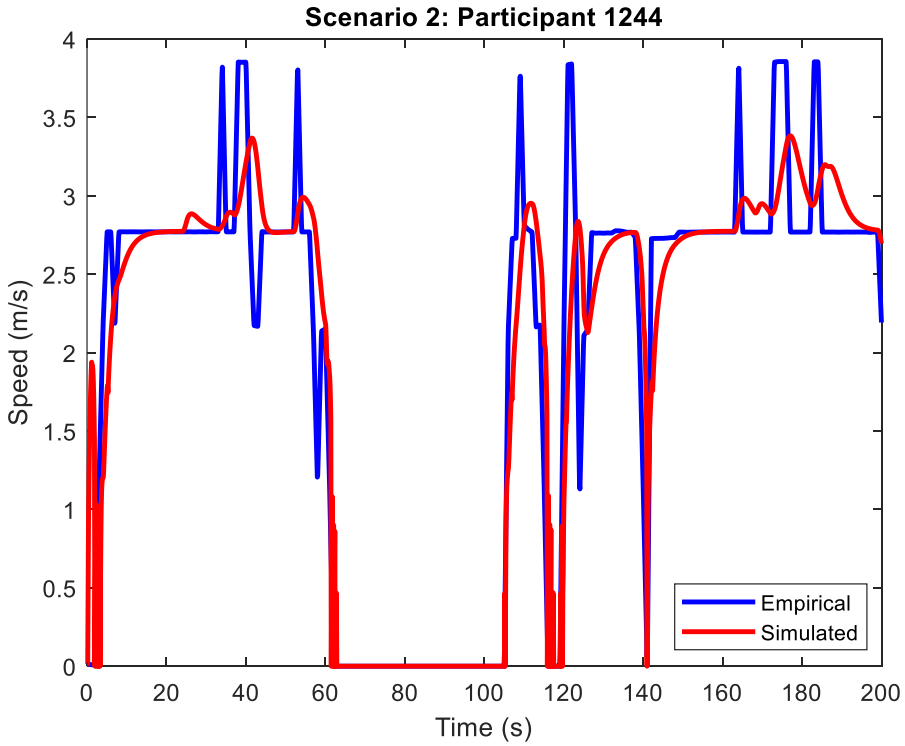

Figure 35 Speed profile: Scenario 2, Participant 1244

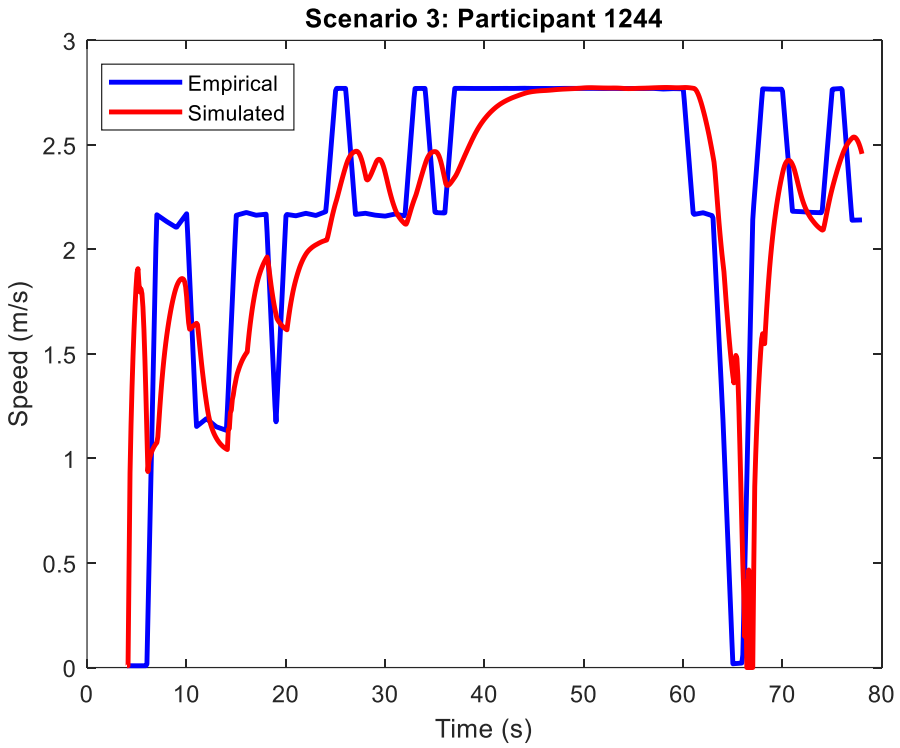

Figure 36 Speed profile: Scenario 3, Participant 1244

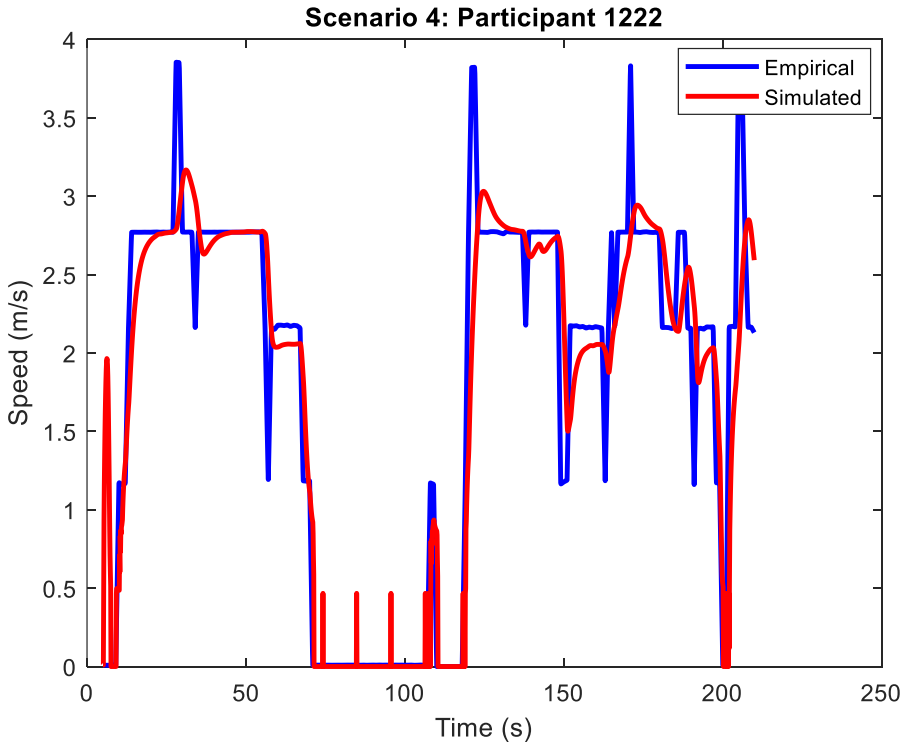

Figure 37 Speed profile: Scenario 4, Participant 1222

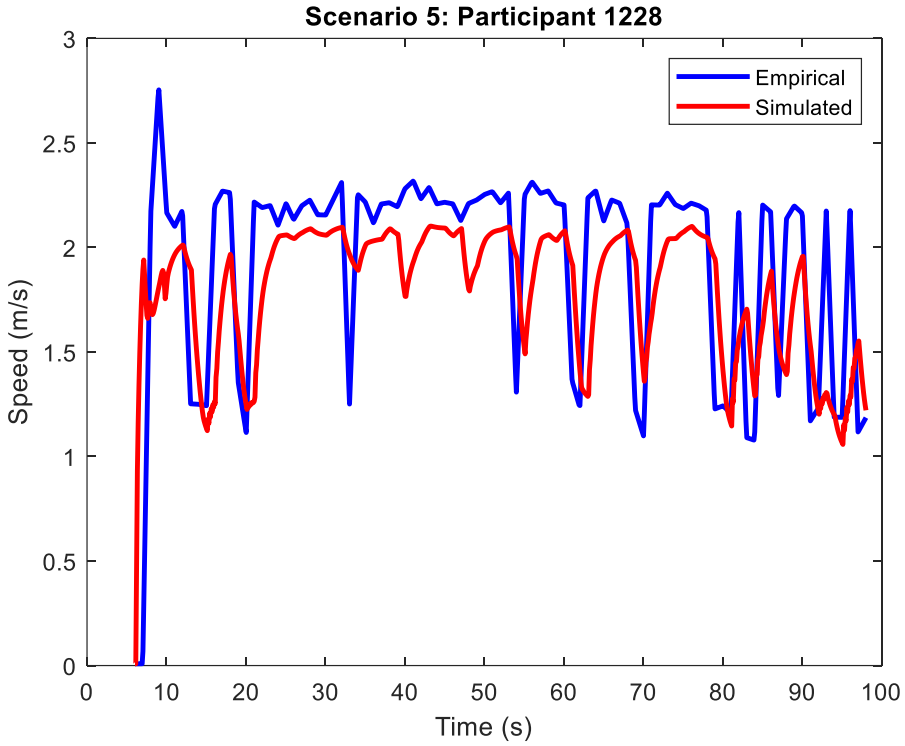

Figure 38 Speed profile: Scenario 5, Participant 1228

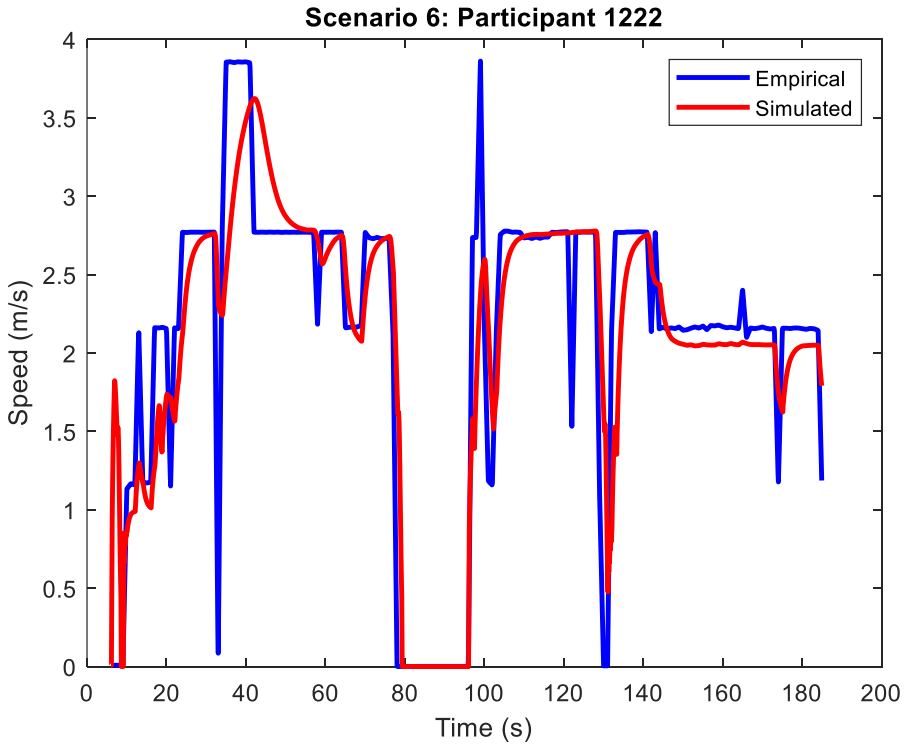

Figure 39 Speed profile: Scenario 6, Participant 1222

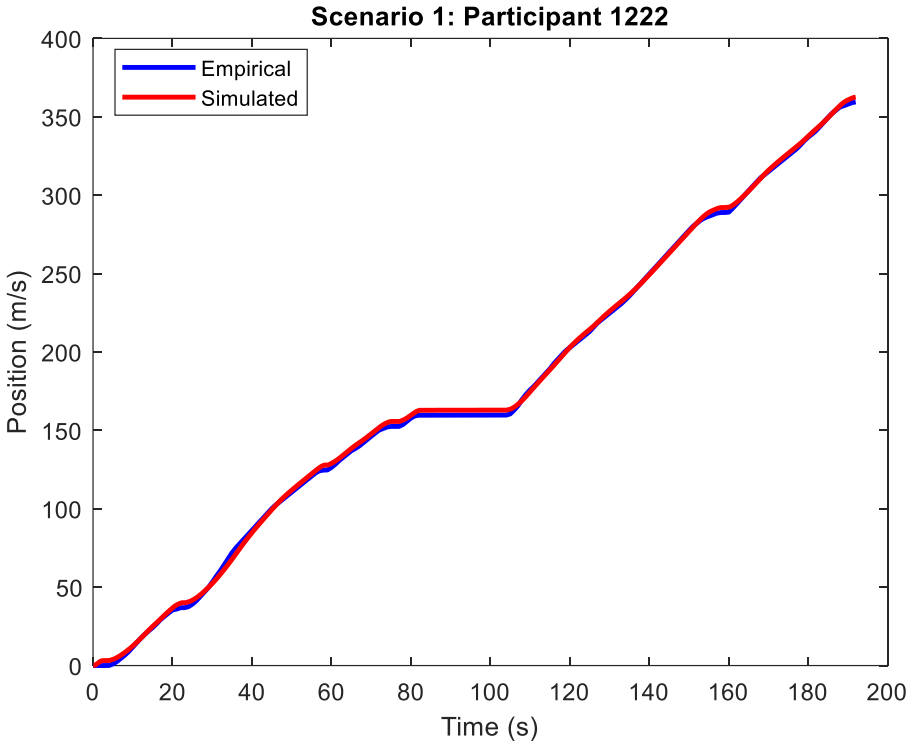

Figure 40 Time-space diagram: Scenario 1, Participant 1222

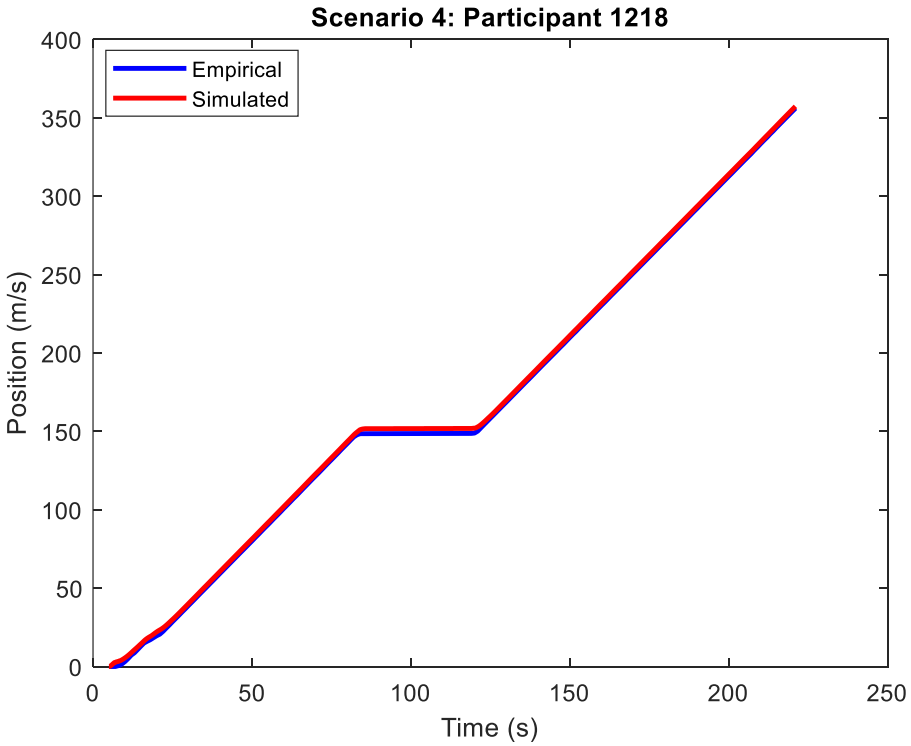

Figure 41 Time-space diagram: Scenario 4, Participant 1218

7. CONCLUSION

The research presented in this report extended the FR car-following model by making it suitable for the simulation of the longitudinal motion of bicycles. The extension was achieved through the re-parameterization of vehicle-related input variables along with the integration of new parameters such that the characteristics and fundamentals of the bicycle/bicyclist system are fully captured. The proposed model is the first point-mass dynamics-based model for the description of the following behavior of bicycles in both constrained and unconstrained conditions. The main benefit of the model lies in its robustness and its ability to model bicyclist behavior variability. The proposed model is the only existing model that is sensitive to bicyclists' physical characteristics and roadway surface conditions.

Initially, the study used experimental ring-road data to validate the proposed model by comparing its performance with two other state-of-the-art bicycle following models. The research findings demonstrate that the FR model is successful in replicating empirical bicyclist behavior and that the techniques used in car-following theory could be used, with minor modifications, to model bicyclist longitudinal motion modeling, thus eliminating the need to develop bicycle-specific models. However, the research team is aware that the data collected from the ring-road experiments is not representative of bicycle behavior on urban roads as certain important factors that impact bicyclists in real traffic situations are ignored.

To address that, the research team collected experimental cycling data using advanced car and bicycle simulators. Thirty-three participants were invited to ride the bike simulator and drive the car simulator simultaneously. Both simulators were integrated together, and each driver could see the location of the other participant in the simulation time interval. Six scenarios were developed. Scenario 1 was designed to investigate the performance of bikes on the road. Scenarios 2 through 6 were designed to evaluate the behavior of both participants (bicyclist and car driver) when both simulators are integrated, especially the interaction time intervals between bicyclists and other road users on the simulated network. The resulting data was collected for both the bicycle simulator and the car simulator, allowing the research team to investigate the performance of both variants of the FR model (for cars and bicycles) using the collected dataset.

The FR car-following model was validated based on data collected from 33 participants in each scenario. Root Mean Square Error (RMSE) was used as an efficient indicator of the ability of a car-following model to replicate empirical behavior from a statistical perspective. A reliable sample including 100 (a,b,d) pairs was selected to find the RMSE and optimum model parameters. In total, 83 reliable trajectories were determined and the RMSE values were calculated. The FR model was rewritten in MATLAB software (Equations 22-33) to find the speed, position, and acceleration values. First and foremost, the speed values from MATLAB code (FR model) were obtained, then the speed values for each participant were compared with the collected speeds from the car simulator. RMSE values were determined, and the smallest RMSE among 100 RMSEs for each participant in each scenario was specified. Additionally, the speed and acceleration trajectories for the smallest RMSE were drawn. Eventually, the optimal model parameters (a,b,d) values were identified.

Next, the FR bicycle-following model was validated using the bicycle simulator data. A total of 233 trajectories from the 33 participants was used to evaluate the ability of the model to match the observed behavior. The calibration of the model was conducted heuristically to determine the optimal model parameters among a total of 200000 parameter combinations. The results confirm without doubt the ability of the FR bicycle-following model to mimic the observed behavior in the bicycle simulator data. This is demonstrated by the low RMSE values as well as the illustrated speed profiles and time-space diagrams, which confirm the ability of the proposed model to follow the different patterns observed in the collected data.

This research effort was initiated for the purpose of developing a variant of the FR car-following model that is suitable to model bicycle longitudinal motion behavior. It also served to validate the model by using experimental data collected from an advanced bicycle and car simulator to incorporate factors that shape bicyclists' behavior, such as the bicyclists' physical condition and their interactions with other road users. Based on the findings presented in this report, the stated objectives have been achieved successfully.

8. REFERENCES

1. Fadhloun, K. and H. Rakha, A novel vehicle dynamics and human behavior car-following model. International Journal of Transportation Science and Technology. International Journal of Transportation Science and Technology, 2020. 9(1): p. 14-28.
2. Pucher, J. and R. Buehler, Why Canadians cycle more than Americans: a comparative analysis of bicycling trends and policies. Transportation Policy, 2006. 13(3): p. 265-279.
3. People for bikes participation study. https://www.peopleforbikes.org/reports/us-bicycling-participation-report , 2020.
5. Liu, Y., et al., Simulation of riding a full suspension bicycle for analyzing comfort and pedaling force. 6th Asia-Pacific Congress on Sports Technology (APCST), 2013. 60: p. 84-90.
6. Nazemi, M., et al., Studying bicyclists' perceived level of safety using a bicycle simulator combined with immersive virtual reality. Accident Analysis and Prevention, 2021: p. 943-954.
7. Jiang, R., et al., Traffic dynamics of bicycle flow: experiment and modeling. Transportation Science 2017. 51(3): p. 998-1008.
8. Gavrilidou, A., et al., Modelling cyclist queue formation using a two-layer framework for operational cycling behavior. Transportation Research Part C, 2019: p. 468-484.
9. Goddard, T., et al., Unsafe bicyclist overtaking behavior in a simulated driving task: The role of implicit and explicit attitudes. Accident Analysis and Prevention, 2020: p. 595-606.
10. Jin, S., et al., An improved multi-value cellular automata model for heterogeneous bicycle traffic flow. Physics Letters A, 2015: p. 2409-2416.
11. Guo, N., R. Jiang, and S. Wong, Bicycle flow dynamics on wide roads: Experiment and modeling. arXiv: Adaptation and self-organizing systems, 2019.
12. Twaddle, H. Development of tactical and operational behavior models for bicyclists based on automated video data analysis. in Technische Universitat Munchen. 2017. Munchen.

13. Twaddle, H., T. Schendzielorz, and O. Fakler. Bicycles in urban areas: Review of existing methods for modeling behavior. in Transportation Research Board 93rd Annual Meeting. 2014. Washington, D.C.
14. Thigpen, C., et al., Who is ready to bicycle? Categorizing and mapping bicyclists with behavior change concepts. Transport Policy, 2019. 82(0967-070X): p. 11-17.
15. Thigpen, C., Who is ready to bicycle? Categorizing and mapping bicyclists with behavior change concepts. Transport Policy 82, 2019: p. 11-17.
16. Chuang, K.H., The use of a quasi-naturalistic riding method to investigate bicyclists' behaviors when motorists pass. Accident Analysis & Prevention, 2013. 56: p. 32-41.
17. Piatkowski, D.P., W. Marshall, and A. Johnson, Identifying behavioral norms among bicyclists in mixed-traffic conditions. Transportation Research Part F: Traffic Psychology and Behaviour, 2017. 46: p. 137-148.
18. Piatkowski, D.P., Identifying behavioral norms among bicyclists in mixed-traffic conditions. Transportation Research Part F: Traffic Psychology and Behavior 46, 2017: p. 137-148.
19. Nygårdhs, S., et al., Bicyclists' adaptation strategies when interacting with text messages in urban environments. Cognition, Technology & Work, 2018. 20(3): p. 377-388.
20. Lee, O., et al., Modelling cyclists' comfort zones from obstacle avoidance manoeuvres. Accident Analysis and Prevention 144, 2020.
21. Joo, S., Oh, C., A novel method to monitor bicycling environments. Transportation Research Part A., 2013: p. 1-13.
22. Twaddle, H., et al. Use of automated video analysis for the evaluation of bicycle movement and interaction. in Video Surveillance and Transportation Imaging Applications, IS&T/SPIE Electronic Imaging. 2014. San Fransisco, California.
23. Luo, Y., et al., Modeling the interactions between car and bicycle in heterogeneous traffic. Journal of Advanced Transportation, 2013. 49.
25. Apasnore, P., K. Ismail, and A. Kassim, Bicycle-vehicle interactions at mid-sections of mixed traffic streets: Examining passing distance and bicycle comfort perception. Accident Analysis & Prevention, 2017. 106: p. 141-148.
26. Klieger, J. and I. Savage, Motor-vehicle drivers' behavioral response to increased bicycle traffic. Journal of Safety Research, 2020. 74: p. 97-102.
27. Silva, C., K. Clifton, and R. Moeckel, Observational method and coding framework for analyzing the functionality of unprotected bicycle lanes. Transportation Research Procedia, 2019. 41: p. 559-571.
28. Guiso. Traffic simulation in the FIAT Research Driving Simulator: Development and perspectives. in DSC'95, Sophia Antipolis, France. 1995.
29. Curtis, N., Ultimate Buyers Guide to Turbo Trainers. 2014, turbobiketrainer.com/. TurboBikeTrainer.com.
30. Shin, J. and C. Lee, Reaction force estimation using control force of motion system for bicycle simulator. international conference on motion and vibration control, 2002. 6.1: p. 603-608.
32. Abagnale, C., et al., Design and Development of an Innovative E-Bike. Energy Procedia, 2016. 101: p. 774-781.
33. Arunachalam, M. and R. Rajesh, A typical approach in conceptual and embodiment design of foldable bicycle. International Journal of Computer Applications, 2014. 87(19).

34. Beckmann-Dobrev, B., S. Kind, and R. Stark, Hybrid Simulators for Product Service-Systems – Innovation Potential Demonstrated on Urban Bike Mobility. Procedia CIRP, 2015. 36: p. 78-82.
35. Dahmen, T., et al., Validation of a Model and a Simulator for Road Cycling on Real Tracks. In: Sports Engineering. 2011. 14(2-4): p. 95-110.
36. Escalona, J., A. Kłodowski, and S. Muñoz, Validation of multibody modeling and simulation using an instrumented bicycle: from the computer to the road. Multibody System Dynamics, 2018. 43.
37. Englund, C., M. Nilsson, and A. Voronov, Application of data mining techniques to model visual distraction of bicyclists. Expert Systems with Applications, 2016. 52: p. 99-107.
38. Ginters et al., SKOPJE bicycle inter-modality simulator – E-environment through simulation and ticketing. European Modeling and Simulation Symposium, 2014.
39. He, Q.C., et al., Key techniques in interactive bicycle simulator. 2005. 39: p. 1422-1426.
40. He, Q.-c., X. Fan, and D. Ma, Full Bicycle Dynamic Model for Interactive Bicycle Simulator. J. Comput. Inf. Sci. Eng., 2005. 5: p. 373-380.
41. Jamin, A., et al. A Novel Multiscale Cross-Entropy Method Applied to Navigation Data Acquired with a BS. 41st Annual International Conference of the IEEE Engineering in Medicine and Biology Society (EMBC). 2019.
42. Jeong, S.H., et al. The Development of a New Training System for Improving Equilibrium Sense Using a Virtual Bicycle Simulator. in IEEE Engineering in Medicine and Biology 27th Annual Conference. 2005.
43. Kakutani, K. and J. Furusho, Developement of an Integrated PerformanceSimulator for a Power-assited Bicycle. IEEJ Transactions on Industry Applications, 2003. 123(11): p. 1330-1338.
44. Kim, S.-u., K. Lee, and K.-c. Koo, Toward an Evaluation Model of User Experiences on Virtual Reality Indoor Bikes. European Scientific Journal, 2017. 1(Special Edition): p. 22-36.
45. Kooijman, J.D.G., A.L. Schwab, and J.P. Meijaard, Experimental validation of a model of an uncontrolled bicycle. Multibody Syst Dyn, 2008. 19: p. 115–132.
46. Kwon, D.S., et al. KAIST Interactive Bicycle Simulator. in International Conference on Robotics & Automation 2001. Seoul, Korea.
47. Lee, O., et al. Description of a model based bicycle simulator. 6th Annual International Cycling Safety Conference. 2017. Davis, California, USA.
48. Schwab, A. and A.M. Recuero. Design and experimental validation of a haptic steering interface for the control input of a bicycle simulator. in Proceedings of ECCOMAS Multibody Dynamics Conference. 2013. Citeseer.
49. Snapika, K., et al., Bicycle Simulator. International Journal of Pure and Applied Mathematics, 2018. 118(24).
50. Shin, J.C. and C.W. Lee, Reaction force estimation using control force of motion system for bicycle simulator. The Proceedings of the International Conference on Motion and Vibration Control. 6.1: p. 603-608.
51. Shoman, M. and H. Imine. Modeling and simulation of bicycle dynamics. 8th Transport Research Arena TRA 2020. 2020. Helsinki, Finland: TRA 2020
52. Yap, H.J., et al., Design and development of 6-DOF system for virtual bicycle. Movement, Health and Exericise, 2016. 5(2): p. 31-39.
53. Mitchell, C., https://www.investopedia.com/terms/v/virtual-reality.asp. 2020.

54. Bogacz, M., et al., Comparison of Cycling Behavior between Keyboard-Controlled and Instrumented Bicycle Experiments in Virtual Reality. Transportation Research Record, 2020. 2674(7): p. 244-257.
55. Bottone, M., R. Smith, and N. Thacker, Oculus Bike: An Interactive Virtual Reality Bicycle Simulator. 2015.
56. Carraro, G.U., et al. The peloton bicycling simulator. in Proceedings of the third symposium on Virtual reality modeling language. 1998.
57. Kikuchi, T. and K. Kobayashi, Development of cylindrical magnetorheological fluid brake for virtual cycling system. 2011 IEEE International Conference on Robotics and Biomimetics, 2011: p. 2547-2552.
58. Chen, C.K., et al., Study of interactive BS. in application of virtual reality. Journal of the Chinese society of mechanical engineers, 2007. 28(6): p. 633-640.
59. Dahmen, T. and D. Saupe. Simulation and optimization of race-bike training on real tracks. in 14th annual Congress of the European College of Sport Science. 2009. Oslo,Norway.
60. Gao, X., Sun, H. X., Jia, Q. X., Song, J. Z., & Zhao, F., Design and implementation of bicycle simulator. Journal of System Simulation, 2005. 17(5): p. 1163-1167.
61. Hernández–Melgarejo, G., et al., Mechatronic design and implementation of a bicycle virtual reality system. ISA Transactions, 2020. 97: p. 336-351.
62. Herpers, R., et al. FIVIS–a bicycle simulation system. in World Congress on Medical Physics and Biomedical Engineering. 2009. Munich, Germany: Springer.
63. Horne, D., M. Ghodrat Abadi, and D.S. Hurwitz, Bicycling Simulator Calibration: Proposed Framework. Transportation Research Record, 2018. 2672(37): p. 11-18.
64. Jia, Q.X., et al., Research and implement of human-computer interaction system of gymnastic bicycle simulator. Journal of Beijing University of Posts and Telecommunications (2006. 29: p. 83-87.
65. Kakutani, K. and J. Furusho, Developement of an Integrated Performance Simulator for a Power-assited Bicycle. Ieej Transactions on Industry Applications, 2004. 123: p. 1330-1338.
66. Katsigiannis, S., R. Willis, and N. Ramzan, A QoE and Simulator Sickness Evaluation of a Smart-Exercise-Bike Virtual Reality System via User Feedback and Physiological Signals. IEEE Transactions on Consumer Electronics, 2019. 65(1): p. 119-127.
67. Keler, A., et al. A bicycle simulator for the evaluation of traffic control strategies in urban environments. in DSC 2020-19th Driving Simulation & Virtual Reality Conference. 2020.
68. Al-Kefagy, M. and S. Pokrajac, E-BS a virtual reality application that evaluates user interfaces in an urban traffic environment. 2019.
69. Nazemi, M., et al., Studying cyclists' behavior in a non-naturalistic experiment utilizing cycling simulator with immersive virtual reality. Arbeitsberichte Verkehrs-und Raumplanung, 2018. 1383.
70. Ouden, J.D. Inventory of bicycle motion for the design of a bicycle simulator. in Delft University of Technology. 2011.
71. Padmini, S., et al. Development of virtual simulator for paddle powered vehicle. in The 11th National Conference on Mathematical Techniques and Applications. 2019. AIP Publishing.
72. Rakhmatov, R., et al. Virtual Reality Bicycle with Data-Driven Vibrotactile Responses from Road Surface Textures. in 2018 IEEE Games, Entertainment, Media Conference (GEM). 2018.

73. Schramka, F., et al., Development of virtual reality cycling simulator. Arbeitsberichte Verkehrs-und Raumplanung, 2017. 1244.
74. Schulzyk, O., et al., A real bicycle simulator in a virtual reality environment: the FIVIS project. Springer-Verlag Berlin Heidelberg, 2009. 22: p. 2628–2631.
75. Shoman, M.M. and H. Imine, Bicycle Simulator Improvement and Validation. IEEE Access, 2021. 9: p. 55063-55076.
76. Tang, Y., et al. Loughborough University Institutional Repository The development of a virtual cycling simulator. in International Conference on Technologies for E-Learning and Digital Entertainment. 2018.
77. Ullmann, D., et al., BikeVR: a virtual reality bicycle simulator towards sustainable urban space and traffic planning. Proceedings of the Conference on Mensch und Computer, 2020.
78. Yap, H.J., et al., Design and development of a spatial immersive track cycling simulator. Malaysian Journal of Movement, Health & Exercise, 2018. 7(2): p. 39-52.
79. Grover, A., Bicycle Accident Statistics in the United States. 2020.
80. Brown, H., C. Sun, and Z. Qing, Investigation of Alternative Bicycle Pavement Markings with the Use of a Bicycle Simulator. Transportation Research Record, 2017. 2662(1): p. 143-151.
81. Ghodrat abadi, M., et al., Factors impacting bicyclist lateral position and velocity in proximity to commercial vehicle loading zones: Application of a bicycling simulator. Accident Analysis & Prevention, 2019. 125: p. 29-39.
82. Kaß, C., et al. A Methodological Approach to Determine the Benefits of External HMI During Interactions Between Cyclists and Automated Vehicles: A Bicycle Simulator Study. in HCI in Mobility, Transport, and Automotive Systems. Driving Behavior, Urban and Smart Mobility. 2020. Cham: Springer International Publishing.
83. Lindström, D., et al. Designing HMIs for an active safety system on bicycles. in Proceedings of the 11th International Conference on Automotive User Interfaces and Interactive Vehicular Applications: Adjunct Proceedings. 2019. Utrecht, Netherlands: Association for Computing Machinery.
84. Matviienko, A., et al. Augmenting bicycles and helmets with multimodal warnings for children. in 20th International Conference on Human-Computer Interaction with Mobile Devices and Services. 2018. Association for Computing Machinery.
85. Nazemi, M., Unravelling bicyclists' perceived safety using a bicycle simulator combined with immersive virtual reality and a physiological sensor. 2020, Doctor of Science Dissertation: Zurich.
86. O'Hern, S., J. Oxley, and M. Stevenson, Validation of a bicycle simulator for road safety research. Accident Analysis & Prevention, 2017. 100: p. 53-58.
87. O'Hern, S., J. Oxley, and M. Stevenson, A simulator examination of bicycle lane width. Advances in Transportation Studies, 2018(1): p. 137-148.
88. Powell, J., Hardware design for an electro-mechanical bicycle simulator in an immersive virtual reality environment. 2017, Master of Science Dissertation.
89. Sawitzky, T.V., T. Grauschopf, and A. Riener. The Next Stage of Road Traffic Education: A Mixed Reality Bicycle Simulator to Improve Cyclist Safety. 2020.
90. Suzuki, M. Development of Bicycling Simulator for Analysis of Traffic Safety and Flow. in WCTR Conference. 2013.

91. Tsuboi, H., S. Toyama, and T. Nakajima. Enhancing Bicycle Safety Through Immersive Experiences Using Virtual Reality Technologies. in Augmented Cognition: Intelligent Technologies. 2018. Cham: Springer International Publishing.
92. Warner, J., et al., A Simulator-based Analysis of Engineering Treatments for Right-hook Bicycle Crashes at Signalized Intersections. Accident Analysis & Prevention, 2017. 104: p. 46-57.
93. Yamaguchi. et al. Development of Bicycle Simulator with Tilt Angle Control Tilt Angle. in 2018 IEEE 42nd Annual Computer Software and Applications Conference (COMPSAC). 2018.
94. Cynecki, M.J., Making the way for pedestrians and bicycles: Realizing the environmental, health and economic benefits. Transportation Research Board, 3, 2012.
95. Ragland, D.R. Roadway/urban design and pedestrian/bicyclist safety: basic principles and applications. in Safety Sustainability and Future Urban Transport. 2012. New Delhi: Eicher Goodearth Pvt Ltd.
96. JacoBS.en, P.L., F. Racioppi, and H. Rutter, who owns the roads? How motorized traffic discourages walking and bicycling. Injury Prevention, 2009. 15: p. 369-373.
99. Kim, N.G., D.W. Kim, and T.K. Kwon. Development of a Virtual Reality Bicycle Simulator for Rehabilitation Training of Postural Balance. 2006. Springer-Verlag Berlin Heidelberg.
100. Almeida, R.d.S.e., et al., Exploring non-conventional Sensorimotor Devices in a Virtual Bicycle Simulator. Journal on Interactive Systems, 2020. 11(1): p. 45-56.
101. Caro, S. and S. Bernardi. The role of various sensory cues in self-speed perception: a bicycle riding simulator preliminary study. 2015.
102. Dialynas, G., R. Happee, and A.L. Schwab, Design and hardware selection for a bicycle simulator. Mech. Sci., 2019. 10(1): p. 1-10.
103. Herpers et al., Multimedia Sensory Cue Processing in the FIVIS Simulation Environment. 2011: p. 217-233.
104. Rittenbruch, M., et al. An Exploratory Physical Computing Toolkit for Rapid Exploration and Co-Design of On-Bicycle Notification Interfaces. in Proceedings of the 2020 ACM Designing Interactive Systems Conference. 2020. Eindhoven, Netherlands: Association for Computing Machiner.
105. V. Kurtc and M. Treiber, "Simulating bicycle traffic by the intelligent-driver model-Reproducing the traffic-wave characteristics oBS.erved in a bicycle-following experiment," Journal of Traffic and Transportation Engineering (English Edition), pp. 19-29, 2020.
106. S. Xue, C. Feliciani, X. Shi and R. Jiang, "Understanding the single-file dynamics of bicycle traffic from the perspective of car-following models," Journal of Statistical Mechanics: Theory and Experiment, pp. https://iopscience.iop.org/article/10.1088/1742-5468/ab7c66, 2020.
107. M. Abdelaziz and C. Gang, "Adapting Car Traffic Models and Concepts to Bicycle Traffic," in Celebrating 50 Years of Traffic Flow Theory, Portland Oregon, United States, 2014.

Andresen, E., Chraibi, M., Seyfried, A., & Huber, F. (2014). *Basic Driving Dynamics of Cyclists*, Berlin, Heidelberg.

<CAS_Readiness_of_the_road_network_April_2017.pdf>.
Chandler, R. E., Herman, R., & Montroll, E. W. (1958). Traffic dynamics: studies in car following. *Operations research, 6*(2), 165-184.
Drew, D. R. (1968). Traffic flow theory and control.
Fritzsche, H.-T. (1994). A model for traffic simulation. *Traffic Engineering+ Control, 35*(5), 317-321.
Gazis, D., Herman, R., & Rothery, R. (1961). Nonlinear follow-the-lead models of traffic flow. *Operations research, 9(4)*, 545-567.
Gazis, D. C., Herman, R., & Rothery, R. W. (1961). Nonlinear follow-the-leader models of traffic flow. *Operations research, 9*(4), 545-567.
https://zwiftinsider.com/rider-categorization-based-on-ftp-how-do-you-rank/. (2016). Retrieved 07/16, 2020
Jiang, R., Wu, Q., & Zhu, Z. (2001). Full velocity difference model for a car-following theory. *Physical Review E, 64*(1), 017101.
Kurtc, V., & Treiber, M. (2020). Simulating bicycle traffic by the intelligent-driver model-Reproducing the traffic-wave characteristics observed in a bicycle-following experiment. *Journal of Traffic and Transportation Engineering (English Edition)*. doi: https://doi.org/10.1016/j.jtte.2019.03.005
Newell, G. F. (2002). A simplified car-following theory: a lower order model. *Transportation Research Part B: Methodological, 36*(3), 195-205.
Olstam, J. J., & Tapani, A. (2004). Comparison of Car-following models.
Pipes, L. A. (1953). An operational analysis of traffic dynamics. *Journal of Applied Physics, 24*, 274-287.
Pipes, L. A. (1967). Car-following models and the fundamental diagram of road traffic. *Transportation Research, 1*, 21-29.
Rakha, H. (2009). Validation of Van Aerde's simplified steadystate car-following and traffic stream model. *Transportation letters, 1*(3), 227.
Rakha, H., & Arafeh, M. (2010). Calibrating Steady-State Traffic Stream and Car-Following Models Using Loop Detector Data. *Transportation Science, 44*(2), 151-168. doi: 10.1287/trsc.1090.0297
Rakha, H., Lucic, I., Demarchi, S. H., Setti, J. R., & Van Aerde, M. (2001). Vehicle dynamics model for predicting maximum truck acceleration levels. *Journal of Transportation Engineering, 127*(5), 418-425.
Rakha, H., Pasumarthy, P., & Adjerid, S. (2009). A simplified behavioral vehicle longitudinal motion model. *Transportation Letters: The International Journal of Transportation Research, 1*(2), 95-110.
Rakha, H., Pasumarthy, P., and Adjerid, S. . (2009). A Simplified Behavioral Vehicle Longitudinal Motion Model. *Transportation Letters: The International Journal of Transportation Research, Vol. 1(2), pp. 95-110.*
Rakha, H., & Sidky, A. (2004). *Blacksburg instrumented city traffic signal data acquisition system.* Paper presented at the Proceedings - 7th International IEEE Conference on Intelligent Transportation Systems, ITSC 2004, Washington, DC, United States.
Soden, P., & Adeyefa, B. J. J. o. B. (1979). Forces applied to a bicycle during normal cycling. *12*(7), 527-541.
Treiber, M., Hennecke, A., & Helbing, D. (2000). Congested traffic states in empirical observations and microscopic simulations. *Physical Review E, 62*(2), 1805.

Van Aerde, M. (1995). *Single regime speed-flow-density relationship for congested and uncongested highways.* Paper presented at the 74th TRB Annual Conference, Washington DC.

Van Aerde, M., & Rakha, H. (1995a). *Multivariate calibration of single regime speed-flow-density relationships.* Paper presented at the Proceedings of the 6th 1995 Vehicle Navigation and Information Systems Conference, Seattle, WA, USA.

Van Aerde, M., & Rakha, H. (1995b). *Multivariate calibration of single regime speed-flow-density relationships [road traffic management].* Paper presented at the Vehicle Navigation and Information Systems Conference, 1995. Proceedings. In conjunction with the Pacific Rim TransTech Conference. 6th International VNIS.'A Ride into the Future'.

Wu, N., & Rakha, H. (2009). Derivation of Van Aerde Traffic Stream Model from Tandem-Queuing Theory. *Transportation Research Record: Journal of the Transportation Research Board, 2124*(1), 18-27.